12-2007

Design of an active orthotic device for joint management.

Steven Clayton Anderson
University of Louisville

DESIGN OF AN ACTIVE ORTHOTIC DEVICE FOR JOINT MANAGEMENT

By

Steven Clayton Anderson
B.S., University of Louisville, 2005

A Thesis
Submitted to the Faculty of the
University of Louisville
J. B. Speed School of Engineering
in Partial Fulfillment of the Requirements
for the Professional Degree

MASTER OF ENGINEERING

Department of Mechanical Engineering

December 2007

DESIGN OF AN ACTIVE ORTHOTIC DEVICE FOR JOINT MANAGEMENT

Submitted by:_____
Steven Clayton Anderson

A Thesis Approved On

_____
(Date)

by the Following Reading and Examination Committee:

_____
Peter M. Quesada, Thesis Director

_____
William P. Hnat

_____
John H. Lilly

ACKNOWLEDGEMENTS

ABSTRACT

Existing treatment programs and procedures are incapable of addressing the complications encountered with patients who experience spasticity and hypertonia related joint contractures. Current passive therapy procedures and devices are only capable of managing the extent of joint contractures on patients with chronic and acute onset severe neurological disorders.

The project was conceived as a means to develop an active device that is capable of adapting to the state of the joint to mange the extent of contractures and to permit consideration for the prevalence of spastic activity episodes and hypertonia. The project focused on the design of the physical prototype and the controller software in order to regulate the operation of such a device. Additionally, the signal conditioning and sensor package was developed as determined to be appropriate for the requirements of the device.

The operation of the device was verified in the bench-top environment in the laboratory and on human subjects in order to qualify, verify, and tune the position tracking capability of the device, spastic activity detection and rejection capability of the device, and the operation of patient controlled devices. The overall operation of the device was evaluated on a group of human subjects. Using simulated contractures and spastic activity episodes, the validity of the preliminary deterministic test data was confirmed as was the appropriate operation of the device. The end prototype devices are capable of responding to a spastic activity episode by maintaining a constant load in addition to mimicking the passive extension behavior of conventional commercial devices.

TABLE OF CONTENTS

LIST OF TABLES

LIST OF FIGURES

I. INTRODUCTION

Use of various treatment procedures has developed through several forms to address complications with patient mobility related to joint contractures. Most recently, the use of Low Load Prolonged Stretch derived through flexible orthotic devices has been shown to be effective in the management of joint contractures associated with the onset of spastic activity episodes and episodes of elevated muscle tone (Light, Nuzik et al. 1984; MacKay-Lyons 1989; Steffen and Mollinger 1995; Nuismer, Ekes et al. 1998). These types of contractures are often associated with acute onset diseases such as cerebro-vascular accidents and traumatic brain injuries in addition to the more chronic persistent diseases such as cerebral palsy and muscular dystrophy (Roper 1987; Yarkony and Sahgal 1987; Dylan, Sherman et al. 1998; Braun and Botte 1999; Vattanasilp, Ada et al. 2000). As a consequence the degree and frequency of the episodes and subsequent contracted joints have degraded the quality of life and the functional capacity of the affected patients (Grover, Gellman et al. 1996). Consequently, the use of current passive and available treatment techniques does not mitigate the state of the joint during onset of the spastic activity episodes (Blanton and Grissom 2002).

A. Contractures

1. Overview of Contractures

Affecting patients with acute onset diseases and chronic persistent disorders relating to neurological function, spasticity and hypertonia are neuromuscular disorders that have frequently led to contracted muscles and a reduced range of joint motion. Typically, the contractures are driven by a reduced control over or impairment of the

inhibitory pathways of the flexor muscle groups, which lead to an imbalance in antagonistic muscle function and a persistent state of elevated muscular tone in the affected flexor groups (Roper 1987; Dylan, Sherman et al. 1998).

Consequently, the reduced range of motion and elevated tone result in varying degrees of functional loss and pain for the affected patient which precipitate increased energy expenditure and pain for the patient (Ferido and Habel 1988; Grover, Gellman et al. 1996; Gracies, Elovic et al. 1997; Nuismer, Ekes et al. 1998). In the majority of cases, the functional loss incurred has resulted in a substantial and significant impediment to daily living and normal activity, with research in a study that showed 84% of 75 patients examined as part of a case study (Yarkony and Sahgal 1987). For patients with hemophilia, the loss of function was documented to impair the ability of the subjects to dress and feed themselves and to perform basic tasks utilizing the elbow away from the body (Gilbert and Radomisli 1999).

For several patients, the degree of the neurological disorder is great enough to leave the patient in a non-ambulatory state (Grover, Gellman et al. 1996). The lack of motion and prolonged bed rest has been shown to increase muscle deterioration (Kitahara, Hamaoka et al. 2003) and increase the prevalence and severity of the experience contractures at the affected joint.

The acute onset disorders affected by contractures include traumatic brain injury, cerebral vascular accident, spinal cord injury, quadriplegia, and cortical lesions amongst other neurological disorders (Yarkony and Sahgal 1987; Ferido and Habel 1988; MacKay-Lyons 1989; Dylan, Sherman et al. 1998; Braun and Botte 1999; Vattanasilp, Ada et al. 2000). Among the more chronic disorders, those affected by the onset of joint

contractures include cerebral palsy, muscular dystrophy, and Parkinson's disease (Flett, Stern et al. 1999). Of importance to note is that not all joint contractures occur as a result of the impaired function of the inhibitory pathways and a residual imbalance of antagonistic function. Several fixed joint contractures and long standing contractures have been caused by physical impairment or injury where the muscular tissue has been damaged through fibrosis or hemophilia (Fernandex-Palazzi and Battistella 1999; Flett, Stern et al. 1999; Blanton and Grissom 2002). Such contractures do not generally show improvement with the treatment procedures used with the dynamic contractures associated with hypertonia and spasticity.

2. Management of Contractures

As a means of managing existing developed dynamic contractures, several treatment procedures have been developed. Existing treatments classify into surgical and non-surgical techniques with the surgical techniques including the physical lengthening of the muscle. In addition, the option exists to not treat the development of the contracture and permit the further deterioration at the joint.

In the treatment of contractures, the first mechanism of managing the contracture is the option of no treatment at all. This process occurs for the patients who have yet to seek treatment or for whom treatment is not possible due to limiting geographical or socio-economic factors. The victim becomes further impaired over the duration of time through which no treatment is applied as the contracture becomes further defined and compounded. This progression results in an increase in the pain for the victim as well as an increased dependency upon others as independent function diminishes along with the quality of life experienced.

Non-surgical techniques include the temporary selective chemical neuropathy, passive and active muscle stretching, and the use of orthotic devices to increase the patient's range of motion. However, the surgical procedures carry the associated risks of over-lengthening of the muscle, development of infection, and residual scarring amongst other sequelae, especially in the treatment of young patients (Flett, Stern et al. 1999). Non-surgical techniques are often preferred over surgical techniques in dynamic contractures due to the high risks associated with the latter. Selective chemical neuropathy has proven effective in reducing the effects of spasticity with the use of phenol or alcohol injections.

However, recovery is transient and subject to irreversible nerve damage, skin necrosis, permanent muscle damage and fibrosis. Alternatively, botulinum toxin A, a potent biological agent, has been proven with localized injection, to reduce the effects of elevated muscle tone through the paralysis of the nerve fibers within the tissue. Though the process has been demonstrated without significant side effects, the recovery process is slow as new nerve tissue develops within the muscle, with recovery time extending to three to six months.

3. Current Passive Practices

Existing orthotic devices and methods used in practice today to manage joint contractures have developed in several forms. However, their basic principle of operation is essentially the same through successively stretching the joint through an iteration of joint range of motion. The intention of existing procedures is to stretch the muscle beyond its existing length in order to provide for an improved range of motion. Developed non-invasive techniques include intermittent brief high load and passive

stretching, serial casting, and orthotic devices with elastic members to provide a restoring load at the coincident joint.

4. Passive Stretching

In long term care facilities and in physical therapy, isolated passive stretching has been used to manage mild contractures and hypertonia (Stap and Woodfin 1986; Tardieu, Lespargot et al. 1988; Mosley 1997). As indicated, the patient spends a period of time with a therapist stretching the passive elastic tissue of the muscles at the joint successively in order to drive the joint to a heightened state of flexibility and an increased range of motion. Such a treatment routine reflects a creep consideration of muscle tissue where limited range of motion and heightened stiffness is attributed to the limited motion of the joint (Mosley 1997). However, due to the low occurrence of treatment relative to non-treatment periods, the effects of passive stretching is limited if spastic activity occurs without management between treatment routines permitting the joint to stabilize at a further reduced range of motion and requiring an increase in therapy duration (Gilbert and Radomisli 1999).

As a subset of this routine, continuous passive motion has been shown to be effective in increasing the range of motion through a continuous driving of the joint through a prescribed motion set (Stap and Woodfin 1986). For more severe contractures, high load brief stretch, similar in form to the isolated passive stretching, has been used to drive an increase in the range of motion of the patient (Light, Nuzik et al. 1984). However, the therapist stretches the muscle beyond the extent of the passive elastic tissue in the joint and stretch the contractile tissue in attempt to generate a higher restoring force in the joint. Great care is taken not to increase the level of patient discomfort during this

procedure because the degree of stretching is greater than that found in isolated passive stretching. Consequently, the duration of the therapy carries the same significant drawbacks as the isolated passive stretching routine due to the high differential between the duration of non-treatment time against treatment time.

5. Serial Casting

As a more long term treatment mechanism, serial casting has been applied to the management of dynamic and some fixed contractures with success in achieving an increase in the range of motion of the patient (Booth, Doyle et al. 1983; Otis, Root et al. 1985; Moseley 1997; Corry, Cosgrove et al. 1998; Flett, Stern et al. 1999; Pohl, Ruckriem et al. 2002). In order to drive the extension of the joint, the intended muscle group is stretched first before a plaster or fiberglass cast is applied to maintain the new extended position. Through the prolonged loading of the joint, the affected muscle joint adapts to the new extended length to become the new neutral length of the joint. Through a successive iteration of cast application or cast wedging of the joint in incrementally improved joint positions, the patient range of motion is subsequently increased stepwise towards the desired range of motion. The use of serial casting has even been shown to be effective for fixed contractures for knee joints (Fernandex-Palazzi and Battistella 1999).

In improving the application of serial casting, the drive has been focused on an increased casting frequency to reduce the onset and prevalence of pressure ulcers (Fernandex-Palazzi and Battistella 1999; Pohl, Ruckriem et al. 2002), reducing the use of plaster drop out casts and increasing the use of fiberglass casting procedures (Pohl, Ruckriem et al. 2002). However, due to the concealed nature of the treatment practice, the relatively low frequency of castings in comparison to what could be achieved with an

active orthosis, and the heterogeneity in patient competency, several consequences exist in the determination of the patient's pain threshold and overall tolerance to pain. Poor competency coupled with cognitive impairment will predispose the treatment to the development of pressure ulcers, regardless of attempts to pad bony promenades of the exoskeletal frame (Moseley 1997).

Additionally, the potential for the development of pressure ulcers exists undetected beneath the surface of the casting driving the discomfort and deterioration of the tissue of the patient. Of importance to note is that regardless of casting frequency, or patient competency, the effects of serial casting has been shown to be significantly diminished if applied six months or more beyond the onset of the joint contractures. Another significant drawback to serial casting is the transient state of the results post treatment as the treated joints have been shown to drive back to a degree of a contracted state (Moseley 1997; Corry, Cosgrove et al. 1998; Flett, Stern et al. 1999).

6. Low Load Prolonged Stretch

Low Load Prolonged Stretch was developed as a means to counter the issues affecting passive stretch and serial casting procedures (Light, Nuzik et al. 1984; MacKay-Lyons 1989; Steffen and Mollinger 1995; Nuismer, Ekes et al. 1998). In a similar manner to serial casting, the neutral position of the joint is incrementally increased through a procedure of setting the joint in an orthotic device or through an increase in surface traction developed loading. Most orthotic devices consist of elastic elements either in the form of an elastic element at the coincident joint between two rigid sidebars or two elastic side bars coincident about a rigid joint (McPherson, Becker et al. 1985; Anderson, Snow et al. 1988; Jansen, Windau et al. 1996; Prosser 1996; Grissom and

Blanton 2001; Blanton and Grissom 2002). Through the displacement of the joint beyond the neutral position, a restoring load is generated on the device through the deflection of the elastic elements as the joint attempts to return to the developed neutral position.

The open configuration of the device and the softer nature of the orthotic devices with respect to serial casting permits improvements in device adjustment through clinical evaluation of fit in order attenuate the development of pressure ulcers. The use of an orthotic device significantly improves the non-treatment versus treatment duration differential to improve the management of the onset of spastic activity episodes than passive stretching (Light, Nuzik et al. 1984). Though the devices permit some degree of movement during a spastic activity episode, the motion range is limited through the increasing restoring load developed by the elastic elements of existing orthotic devices. This increased restoring load, which is significant in comparison to that experienced at the set position of the joint, increases the level of patient discomfort. Additionally, the duration of treatment is affected in order to attenuate the development of pressure ulcers. However, any changes to the stiffness of the device or the removal of the device require a clinician to perform appropriately, eliminating the influence of the patient in the control over their treatment routine.

B. Muscular Atrophy

For healthy ambulatory individuals, prolonged unloading of the joint has resulted in a diminished functional capacity as demonstrated through prolonged bed rest (Widrick, Trappe et al. 2002) and microgravity conditions (Akima, Kawakami et al. 2000; Fitts, Riley et al. 2000). In as little as twenty-one days, the level of upper extremity strength as

determined through grip strength endurance and elbow extension torques has been shown to be significantly decreased (Kitahara, Hamaoka et al. 2003). In cerebral palsy patients, fibrosis of the muscle tissue has set in after only four days of unloading through prolonged bed rest (Flett, Stern et al. 1999). Cellular change has been observed to occur in as little as 24 hours after unloading (Williams, Tardieu). Additional experimentation on both the upper and lower extremities has derived similar conclusions for both the upper and lower extremities. Of significance, however, is that the bulk of the patients who experience spasticity and hypertonia driven joint contractures, especially in the lower extremities, are non-ambulatory and unloading has already resulted in a significant reduction in strength and endurance. During the period of treatment, the unloading experienced through the use of an orthosis would not result in a significant change in the ambulatory state nor the unloaded state of the patient.

C. Fit Considerations

For devices that are capable of generating a high degree of loading at a skin device interface, the risk for tissue damage or discomfort to the patient exists that would lead to an increase in the period of disuse by the patient. The risk associated with pressure ulcer development exists for both low load prolonged stretch orthoses and serial castings. However, the prevalence of pressure ulcer development had been reduced through the increased frequency (Pohl, Ruckriem et al. 2002) in casting changes in serial casting leading to the development of the need for an increase in device adjustability. Similarly in Low Load Prolonged Stretch, an increase in the adjustment frequency of the orthoses would reduce the risk of pressure ulcer development. Additionally, for ankle-foot orthoses, a case study review demonstrated that each of the fit issues observed by the

clinicians leading to discomfort for the patient was strap or device size dependent and did not result in the disuse of an orthosis after correction (Grissom and Blanton 2001; Blanton and Grissom 2002).

Through careful fit practices and appropriate adjustability of the device, the application of the device can be devised such as to accommodate the heterogeneity of the population as far as treatment progression and resolve the development of pressure ulcers. For the development of pressure ulcers due to a spastic activity episode, the importance of a device capable of adapting to the current state of a patient joint in order to reduce the risks imposed on a patient and improve treatment duration.

D. Objective

Incorporating pneumatic muscle actuators into the devices used for extended application of Low Load Prolonged Stretch permits the orthotic device to exhibit an active elastic behavior to achieve a similar response as available with current devices to manage the extent of the contracted joint. However, the use of pneumatic muscle actuators permits the development of an active elastic behavior that is capable of adapting to the current state of the joint depending on whether the device is required to manage the contracture or manage the spastic activity presently active within the joint. The device additionally would be capable of providing a heightened degree of control and adaptability over patient care and comfort.

E. Pneumatic Muscle Actuators

1. Overview

The predecessor of the Pneumatic Muscle Actuator (PMA) was conceived as the McKibben Muscle in the early 1950's(Schulte 1961; Caldwell, Medrano-Cerda et al. 1993). Though they were originally developed for use in the field of prosthetics, the continued development of the pneumatic actuators of this type was discontinued due to the difficulty and the complexity required to control the actuators at that time and their general lack of precision in position and force tracking(McKerrow 1991, Caldwell, Medrano-Cerda et al. 1995). Alternatively, the use of electrical motors of the form of dc motors and stepper motors in this field was followed due to their perceived ease of control.

However, with the development of the Rubbertuator by Bridgestone, the use of commercially available pneumatic muscles became more prevalent. The use continued in industrial applications where a high degree of force was required. As such, the use of PMA's was demonstrated through the nuclear energy industry where the isolation and load generation of the pneumatic muscle was ideally suited to the contained structures of the reactor vessel. A renewed interest in the implementation of the PMA systems has developed as position tracking and PMA modeling has improved.

2. Construction

The primary construction features of a PMA are common across industrial and custom produced models. The actuator is primarily a two layer device consisting of an inner elastic liner typically made from either isobutyl or latex rubber and an outer layer comprised of a counter-woven helical mesh (Caldwell, Medrano-Cerda et al. 1993; Caldwell, Razak et al. 1993; Chou and Hannaford 1994; Caldwell, Medrano-Cerda et al. 1995; Repperger, Phillips et al. 1997; Repperger, Johnson et al. 1999). At each end of

the device are end plugs that encapsulate the two layers to prevent separation. One plug has a through hole in order to permit the charging of the PMA. An arrangement of a typical PMA is shown in Figure 1.
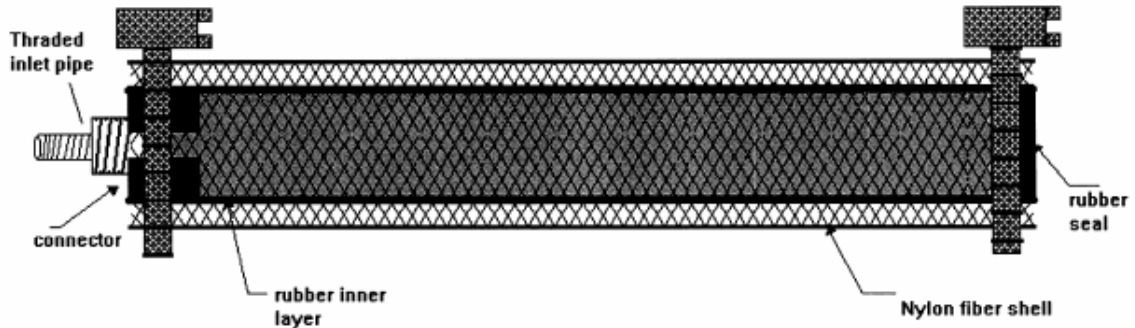
FIGURE 1 – Typical Arrangement of a Pneumatic Muscle Actuator

This inner layer provides the compliant mechanism of the operation device that expands and contracts depending on the pressure within the layer. The outer layer is typically comprised of a nylon interwoven mesh. The primary function of the nylon mesh is to govern the mechanics of the actuator and to carry and distribute the load due to the pressure within the actuator. This function is permitted through the high longitudinal stiffness of the mesh fibers that slide with respect to one another as the elastic liner contracts and expands resulting in an actuator that accordingly extends and contracts in length.

The load carrying capability of the woven mesh additionally permits the safe operation of the device up to 7.5 bar before rupture of the elastic liner occurs(Caldwell, Medrano-Cerda et al. 1995) (Gabrielle). In the event of a tubing rupture, the failure is considered to be a soft failure as the potential blowout is contained by the interwoven mesh (Repperger, Johnson et al. 1999). A safe failure mechanism is essential for modern

applications of the actuators as a biological assist device on the extremities of the human body.

3. Mechanics

The mechanics of the PMA are decidedly nonlinear (Caldwell, Medrano-Cerda et al. 1995). Not only is the operation of the PMA dependent upon the internally applied pressure, but also on the relative position of the actuator in reference to its slack length and the configured initial helix angle of the actuator at the slack length. However, the function of the PMA has been viewed as closed system where the principles of virtual work governed the initial modeling of the actuator. As a rule, any increase in the internally applied pressure results in the travel of the PMA to the lowest possible energy state given the new energy condition and a given amount of force that must be applied by the system of the actuator on the external environment (Gabrielle).

Through an increase in pressure of the actuator, the radial diameter of the actuator increases. This increase in the radial diameter must be accounted for in the travel of the fibers of the interwoven mesh that mush slide against one another in order to extend to the new diameter of the actuator. The increase in the mesh diameter results in a decrease in the interwoven fiber angle and a coordinated decrease in the overall length of the actuator. This mechanism depends upon the assumptions that the fibers are considered inextensible and of a finite length (Zhou 2004). The arrangement of the fiber mesh is shown in Figure 2 (Caldwell 2000).
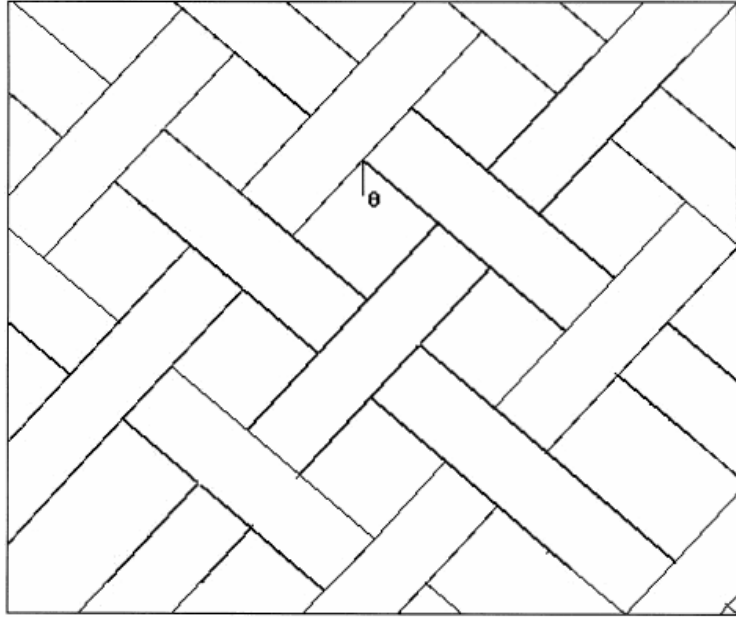
FIGURE 2 – Interwoven Fiber Mesh Arrangement

The contraction of the muscle provides the mechanisms by which work is performed on the external environment. The first mechanism is an extensile change in length in the actuator that changes the physical geometry of the actuator and results in an increase in pressure as the volume decreases which acts as a passive tensile resistive force generation similar to a spring type element. The other mechanism by which work is expended on the external environment is through a change in the internal pressure which as has been shown is similar to an active tensile force generation. Through the use of an affixed mass onto the end of a suspended PMA, the work expended upon the environment in an isotonic load scenario is the work required to raise the mass. For an isometric load scenario where the length of the PMA is fixed beyond the desired length as dictated by the lowest energy state, the PMA will exert a tensile load that may be measured in line with the PMA.

Of note is that a PMA is capable of compressive force generation, yet only when the operating length is shorter than the desired length as dictated by the lowest state of

potential energy (add – Zhou 2004). In this circumstance, the PMA becomes a 1D beam that is deflected from its desired shape and expends a force on the system relative to the energy difference in the operating state from the desired state.

4. Advantages

The advantages of the use of pneumatic muscles have been demonstrated through research into the use and application. One of the primary benefits is the significantly high power to weight ratio typical of 1000 W/kg and their high power to volume ratio typical of 1 W/cm^3 (Chou and Hannaford 1994). This feature results in a the development of a significant driving force with little added mass to the overall system to offset or lag the dynamics of the system and with little required space as compared to the other systems including hydraulic, electric and electro-mechanical systems. As shown before, PMA affords a safe failure mode and with relatively low working pressures at less than 8 bar. In addition, the PMA is capable of a non-linear load generation that increases as the deformation from the optimum length changes. In some circumstances the availability of the driving potential can be a problem, especially in outdoor or open settings, however with PMA systems, the driving medium of air can be of ample supply (Repperger 2004).

In comparison, the use of hydraulics has several drawbacks that would limit is use against PMAs(Caldwell, Medrano-Cerda et al. 1995). The upfront technology capital cost is significantly higher than that of PMAs which can frequently be built at minimal cost. Overall, the use of hydraulics is a dirty system with the higher working pressures and higher potential for catastrophic damage when used in biological assist devices. The systems themselves are plagued by a significant amount of associated components

required to operate and control them and the overall response rates of hydraulic actuators are slower and offer a poorer degree of control than those of PMAs. In addition the weight added by the use of hydraulic actuators is significant and offsets any benefit of applicable power as the system dynamics become significantly altered for the biological assist devices.

The use of electrical motors such as dc and stepper motors and the use of electro-mechanical components that developed in the initial washout of the PMA research provides its own set of drawbacks towards biological assist devices(Caldwell, Medrano-Cerda et al. 1995, Lilly 2004, Repperger 2004). The low power to weight ratio require a significant large size of motor in order to provide the required power. The added weight has been considered to be awkward and hazardous for the use in stand alone portable devices where the motor would apply undesired out-of-plane torques on the patient joint and lead to premature fatigue. The control and function of the electrical equipment is less compliant with respect to PMAs as a stepper motor would lock a joint rigidly in the event of a spastic activity episode at a joint, rather than permit soft deflection of the device under the increasing load on the device. Thus the use of electrical equipment in a biological assist type device would prove detrimental to the health and safety of the patient.

5. Application

Previously the use of Pneumatic Muscle Actuators was limited to a few small subset areas that did not require a significant degree of control over the force or the precise position of the intended object. This application was seen through industrial applications requiring high degrees of load generation and approximate position

correlation in heavy industry including whiskey barrel manufacturing and in the Nuclear Energy Industry.

However, with the improvements in the geometric modeling of PMAs and the position control algorithms, their use as actuators has evolved to cover robotic applications including manipulation rehabilitation continuous passive motion (CPM) arms and biomimetic arms (Caldwell, Medrano-Cerda et al. 1993; Noritsugu and Tanaka 1997). Improvements to the geometric and force prediction modeling have evolved from the simple virtual work calculations to incorporating the interweave angles and relative PMA length into PMA mechanics(Caldwell, Medrano-Cerda et al. 1993; Caldwell, Razak et al. 1993) (Caldwell 2000), including the effects of interlayer friction between the nylon mesh and the inner elastic liner and liner thickness (Chou,Hannaford – 1996), and radial expansion force effects on total system energy, and including the shape distortion effects at the PMA endcaps (Caldwell 2000). These improvements have permitted the evolution of prediction errors from 15-20% to within 1% for position expectation. Work is still under way to improve the effects of force prediction for peak developed forces with enhancements expected due to radial pressure distributions within the PMA (Caldwell 2000).

With respect to the control of PMAs, significant work has been performed in order to adequately control the position of the PMAs. Both open loop and closed loop modeling has been performed. Open loop modeling involved developing an effective stiffness element considering the above listed developments in PMA mechanics in order to provide antagonistic PMA control over the function of an animated puppet arm motion (Gabrielle). The development of closed loop modeling has centered antagonistically

balanced PMAs using robust and adaptive backstepping controllers, sliding mode controllers that provide non-smooth control dependent upon the position of the PMA (add – Carbonell 2001), non-linear feedback control that examined the varied inflation and deflation dynamics of PMAs and utilized sliding gain scheduling for the stiffness to ensure stability (Repperger, Johnson et al. 1999), adaptive discrete PID control (Caldwell, Medrano-Cerda et al. 1995), and fuzzy control logic through fuzzy PD+I controllers and fuzzy sliding mode controllers to yield improved position control and reference tracking (Lilly 2004, Chan, Lilly – 2003).

Additionally, work has been performed to decrease the required bandwidth (cutoff frequency) of the operation of PMAs through the examination of the effects of flow rates through the piping and valves used to control the PMAs and the filler used to charge the PMAs. Of note was that the piping and valve flow impedances were the significant limit to the bandwidth of pneumatic muscle actuators and that through the removal of flow restrictions would improve the bandwidth (add – Davis 2003). The authors also examined various solid, granular, and liquid fillers to note that liquid, as an incompressible substance, provided improvements of up to 400% in bandwidth. The drive to improve bandwidth required for PMA control is dictated through the fast response and position control rates required for advances in robotic technologies.

In addressing the lack of research into the force tracking techniques, biomimicry models were developed to simulate the isometric twitch responses found in humans in PMAs (Repperger 2004). The research included the development of spatial, temporal and spatiotemporal pulse recruitment used to charge the PMA. This work showed that there was promise to the ability of the PMA to track to a certain developed load.

Accordingly, the use of PMAs could be devised to provide prolonged load generation required to counter the passive elastic and active elastic components of a human joint. This application would provide a significant improvement in the management of the prevalence of spastic activity episode related contractures over existing treatment procedures and orthotic devices capable of passive resistance to a joint only. In addition, this application would provide a safe driving mechanism where the intended application is intended as a biological assist device operating next to a live patient. In addition, the small weight increase permissible would improve the portability and improve the duration of use of the device.

<u>F. Prototype Overview</u>

Through the research, a prototype pneumatic muscle actuator driven low load prolonged stretch device (PMA driven LLPS device) and an appropriate control algorithm was developed to control the functionality and the operating state of the device in addition to providing the direct interface with the device. As indicated above with the capacity of pneumatic muscle actuators, the device was developed with a contracture management mode designed to provide the functionality to maintain a desired extended joint position. A spastic activity management mode was developed with the intention to detect the onset and decline of spastic activity episodes and to minimize the discomfort to the patient while still providing resistance to the episode by maintaining a low degree of loading on the joint. Additionally, the compliance of pneumatic muscle actuators permitted the development of a deactivation circuit within the control algorithm which permitted the subject to disengage the functionality of the device in the event of malfunction or extreme discomfort. With the device being centrally a one degree of

19

freedom rotational system, the intended focus of application was limited at this time to the primary hinge joints including the knee and the elbow joints.

G. Evaluation

The performance of the developed device was evaluated through the use of human subjects. Through the use of external submaximal excitation of the nerve fibers within the biceps brachii, a contracted joint was simulated to evaluate the function of the device at passive extension of the joint. Through the use of pulse excitation in addition to the submaximal excitation, the behavior of a spastic activity episode was simulated in order to evaluate the performance of the device in detecting, managing, and rejecting a spastic activity episode. The patient controlled shutoff circuit was also evaluated for functionality in the evacuation of the PMAs and the termination of the execution of the controller.

II.   DESIGN DEVELOPMENT

A. Original Prototype

1. Configuration

A simple prototype used to obtain proof of concept data and intended for the platform development for the implementation of PMA driven LLPS is shown in Figure 3. This device consisted of a four component nylon webbed scaffold placed on the outside of the joint. The side rails were straight members with bolting flanges included to secure the webbed scaffold to the side rails. Proximal and distal segments were secured at the coincident joint through the use of standard SAE fasteners with a washer to permit joint motion. Flanges and bushings were included to house the PMA end caps and to limit out of plane motion.   The device included one single PMA to drive the motion of the prototype placed approximately in the central plane of the device. Padding surrounded the webbed scaffolding and the PMA on each segment of the device with a nylon strap used to secure the device segment to the joint segment.
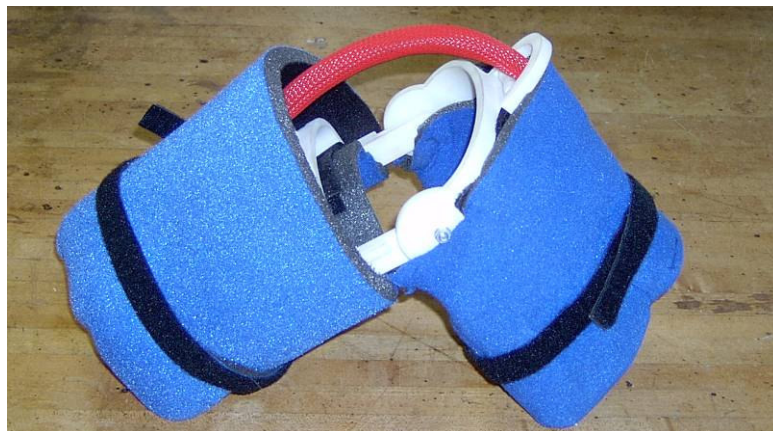
FIGURE 3 – Simple PMA Driven LLPS Device

2. Primary Concerns

However, there were several key considerations in the design of this prototype that provided for poor design development especially in device control and patient-device interfacial loading. The primary concern was with the patient device loading interface where the prototype used a Velcro strap to transfer the loading from the loaded side of the joint to the scaffold elements. This configuration provides for a soft, unreliable load transfer mechanism that includes the low stiffness elements of the strapping, padding, and the cross stiffness of the PMA to collapsing loading before the loading is applied to the physical scaffold.

The location of the PMA proved impractical for the in-situ instrumentation of the joint. In addition to collapsing across the knife edge bushings located at the inboard joint edge into the joint, the PMA would provide an unbalanced loading at the joint. The PMA offsets are different for the proximal and distal segments of the device and the PMA does not act through a constant distance from the joint depending on the deflected state of the joint. This configuration provides for poor correlation of measured joint moment to measured PMA loading due to the non-linear relationship between the two components. The mounting flange structure also provides for a poor implementation of instrumentation due to complications with mounting a load cell to measure the PMA load without presetting the load cell or over-slacking the PMA.

3. Fit Considerations

The scaffold structure proved for a poor fit mechanism with the patient. Due to the location of the scaffold elements on the outside surface of the joint, the device through the loading mechanism exposes the device to the bony promenades located on this side of the joint due to the reduced muscular development required. This type of

22

loading platform would prove to be uncomfortable for a patient over a prolonged period of exposure in addition to the spastic activity episodes. Additionally, the extension of the scaffold elements into the joint provides for a poor fit in the displaced state of the joint as which would be most common during the operation of the device. The joint would have to be located approximately coincident to the device joint, requiring the impingement of the distal segment on the tendons exposed at the lower side of the joint.

The device has a low heterogeneity to the population through the lack of misalignment between the scaffold elements and the side bars to accommodate patients of various sizes and joint types. The development of the scaffold, through its structural configuration, was designed specifically for the knee joint with consideration provided for the misalignment of the proximal and distal segments in the sagittal plane. However this configuration provides poor adaptability to function appropriately at the elbow joint. There is also no consideration to the misalignment required to accommodate the absence of co-linearity found between the proximal and distal segments of the lower extremities. The fit considerations in addition to the loading mechanism would prematurely precipitate the formation of pressure ulcers with a patient and reduce the duration of the treatment to treat the fit related complications.

B. Redesigned Prototype

1. Primary Concerns

The redesigned physical prototype was designed with several of the noted considerations and concerns observed with the original prototype noted in order to improve the overall fit and intended function of the device. The primary objectives included improvements and adjustability within the scaffold architecture and device

strapping in order to improve overall load transfer to and from the patient, improving the internal adjustability of the device to permit flexibility with respect to locating the device to the joints in order to improve device heterogeneity, improving the design of the device to accommodate instrumentation and improving PMA mechanics used to drive the operation of the device. As shown in Figure 4, the redesigned physical prototype illustrates each of features developed as a response to the desired objectives.
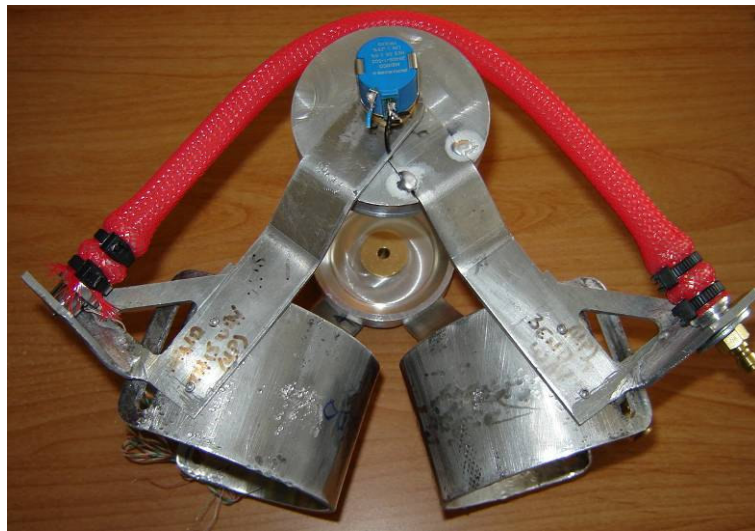
FIGURE 4 – Redesigned Physical Prototype

The webbed scaffolding elements previously located on the outside of the joint was eliminated for the use of circular cuffs located on the inside of the joint at both the proximal and distal segments. This relocation will improve the loading mechanism to the device through direct transfer during contracture management and spastic activity management operations of the device. Rather than transferring the loading through several compliant mechanisms, the loading interface has been integrated into the device to provide for a stiffer configuration. Each of the provided cuffs is offset at an angle with respect to the side rails in order to more comfortably accommodate the heterogeneity in

muscular structure of the proximal and distal segments. For the proximal cuff, the offset angle was preset and fixed at 20 degrees of rotation from the primary axis of the side rail.

The distal cuff has been provided with freedom of rotation to permit the alignment of the joint center with the device center in a more appropriate manner. This feature permits the device to operate for either the knee or the elbow through the provision of the alignment of the cuff. Through the availability of a selection of various cuff sizes, the device can accommodate the heterogeneity in patient size through appropriate selection of cuff size for both the proximal and distal segments.

The construction of the side rails provides an offset at the joint location for the accommodation of the misalignment of the proximal and distal segments in the lower extremities. At the outboard ends of the scaffold side rails, flanges and reinforcing elements have been designed to accommodate the inclusion of two PMAs with one on each side of the device and the direct inclusion of an in-line load cell between one PMA and the flange. Through the location of the offset, a constant radius guide was located at the coincident joint of the device between the proximal and distal segments and inline with the flanges of each segment. The relocation of the PMAs to the outside of the device and the use of a constant radius guide provide for improved PMA mechanics in driving the device and improved patient comfort. A constant radius guide ensures the linear relationship between measured PMA developed load and applied joint moment and ensures the in-plane operation of the PMA and co-linear operation of the load cell.

A threaded brass bushing mechanism was devised in order to provide for the measurement of the device angle between the proximal and distal segments. To secure the bushing to the proximal side rail, a press fit was utilized with tolerances provided for

the free in plane rotation without appreciable in plane translation of the distal segment. A small flange was cemented to the inside surface of each constant radius guide to actuate the wiper arm of the rotary potentiometer. Ensuring that the constant radius guide and the distal segment operated in the same orientation, a offset interference fit was devised that improved the internal clearance with in the joint, as shown in Figure 5. A snap ring feature was used to secure the two side rails and the constant radius guide together and to permit ease of assembly. Because of the aluminum construction of the side rails and the constant radius guide, a nylon ring bushing was included to prevent the galling and damage of either side rail. This construction provided minimal resistance to the functional operation of the device. Through the use of a similar construction for both hinge joints, the device is completely reversible for either the left or right extremities.

FIGURE 5 – Joint Offset Configuration

2. Device and Patient Protection

In order to protect the sensors housed on the device, several features have been intentionally devised in order to maintain the integrity of the entire device. The proximal and distal PMA mounting flanges were designed intentionally large enough to secure the threaded load cell and to protect the sides of the load cell from impact and cross loading.

The use of a constant radius guide eliminated the risk of eccentric loading of the load cell package during normal function of the device. During non-functional operation and manipulation of the device, the padding arrangement and a Velcro strap will secure the PMA in proximity to the constant radius guide. To shield the rotary potentiometer, an aluminum shroud has been constructed that is capable of full enclosure of the sensor while still permitting the reversibility of the device from side to side. Maintaining the comfort and protection of the patient, dense closed cell proprietary foam padding that is machine washable surrounds the key features and edges of the device as well as the interfacial loading surfaces of the cuffs.

3. Load Case Development

The design and development of the side rails was critical to providing the proper stiffness of the device in response to the loading situations. Given the considerations to provide for the device arrangement and patient comfort, the design of the side rails was inherently sensitive to torsional loading of the hinge joint flange. Using a loading array map across the full range of joint motion possible with the device, the critical load case presented to the device would be a potential spastic activity near full extension, during device malfunction, producing the most sensitive loading scenario. A copy of the loading array has been included as an appendix.

For the purpose of analysis, the peak load used in the loading included a developed PMA force of 50 lbs per PMA whereas the fatigue loading case for the dynamic loading scenario was analyzed with a developed PMA force of 25 lbs per PMA. The dynamic loading scenario was developed through the determination of the approximate desired load at which the device was intended to operate during the auxiliary

control mode. The peak load case was developed through the determination of the maximum loading encountered during the process of obtaining passive joint extension data with the device. With respect to a cycle life of 5×10^8 cycles for a full fatigue analysis of the side rail geometry, especially the flanges and the offset, the flanges were designed with a fatigue factor of safety of 1.85.

The scaffold webbing for the flanges and side rail sizes were designed to eliminate the critical features that would have led to the premature failure of the device under the dynamic load case including a poorly designed flange reinforcing web and improperly sized PMA flange dimension. The design of the flanges and webbing permitted the design of the side rails such that a minimum amount of material was required to protrude beyond the primary side rail for the purpose of patient comfort. However, due to the manufacturing process of cold working involved in creating the side rails, the design had to accommodate the loading experienced in manufacturing. Figures 6 and 7 demonstrate the stress distribution and overall deflections of the side rails under the dynamic loading condition. Drafts of each physical component in the assembly have been included as an appendix. Currently there are three full developed prototypes of the developed design.
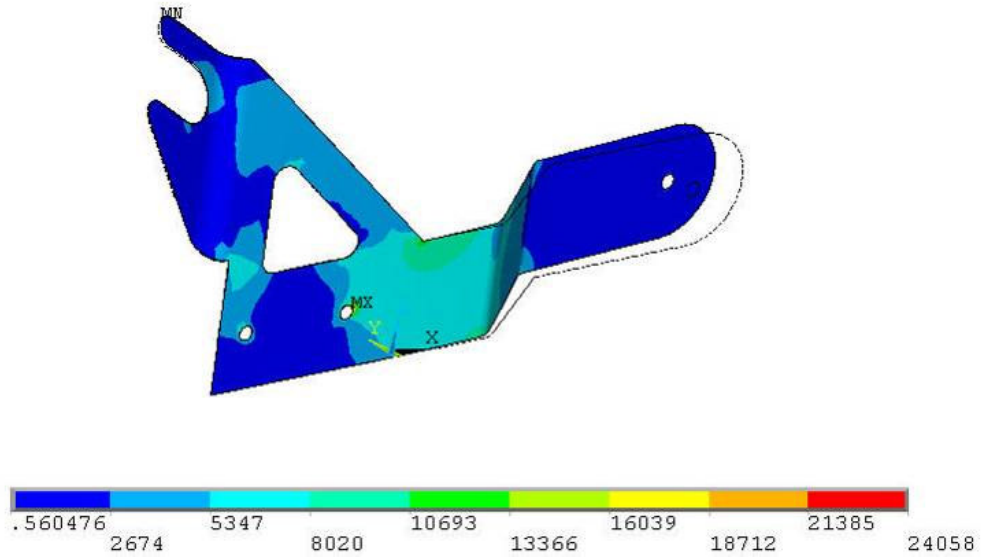
FIGURE 6 – Side Rail Stress Distribution
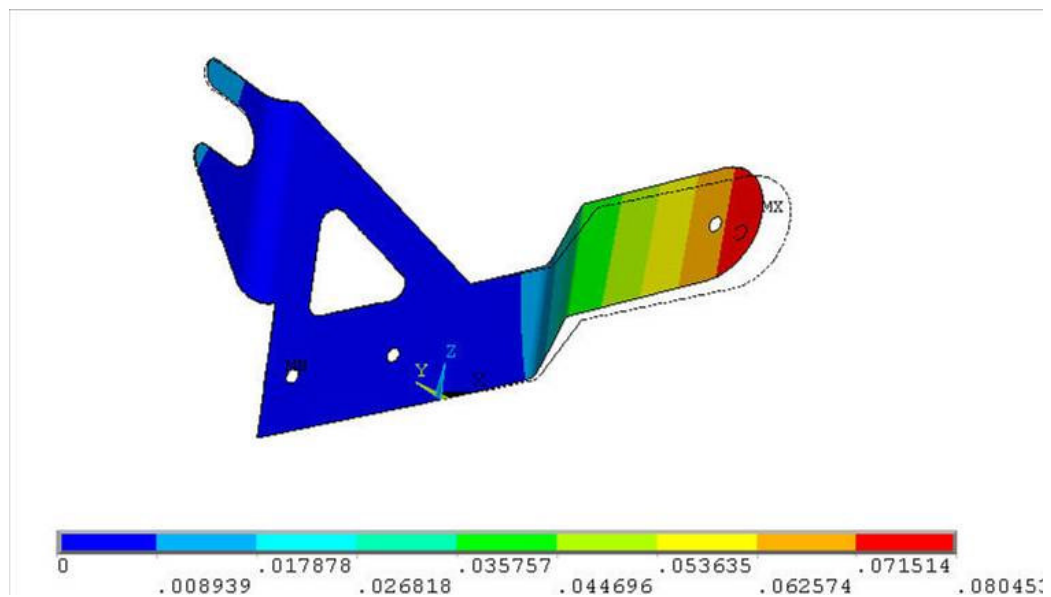
FIGURE 7 – Side Rail Deflection

4. PMA Development

The previous prototype had employed the use of one PMA centrally located. With the redevelopment of the prototype, the PMA structure was relocated to the sides of the device with the PMA count increased to two, the device still had to be capable of developing enough loading to counter the joint motion and to provide full range of

motion. Due to the physical configuration of the device, a normal range of motion constituted 0 to 120 degrees with zero being full extension.

An iterative map of pneumatic muscle actuator sizes and lengths was created to determine the required PMA diameter and resulting driving force and extension curves at constant pressure for a specified length. Alternatively, the driving force curves were compiled for isometric operation for changes in pressure within the PMA. Using a similar procedure as shown in research (Caldwell 1995, Caldwell 2000), the driving forces and the geometric changes in the PMA were calculated across a range of pressures and lengths to obtain full extension. A copy of the iterative map has been included as an appendix.

Because the PMA would be fed from a bottle storage container, the air consumption was determined to track how many full PMA evacuations the tank storage would accommodate. This requirement behind the calculation yielded the required tank size in order to obtain a device with the capacity of more than 100 full evacuations which would more than accommodate the leakage associated with the variable control of the PMA as it adapted to the changing states of the joint. The final bottle fed air supply specified for the device package included a 3000 psig tank with volume of 116 cubic inches capable of supplying 218 full evacuations of the device until the tank reaches 161.3 psig. A fixed pressure regulating valve is used to limit the maximum pressure inlet to the control valve is no higher than 150 psig. For the ease of equipping the device and service, a MK-1 first stage valve was used with the 13 cubic foot diving air tank with a first stage relief valve of 150 psi in case the seals within the first stage regulator fail. The charge life of the tank is shown in Figure 8.
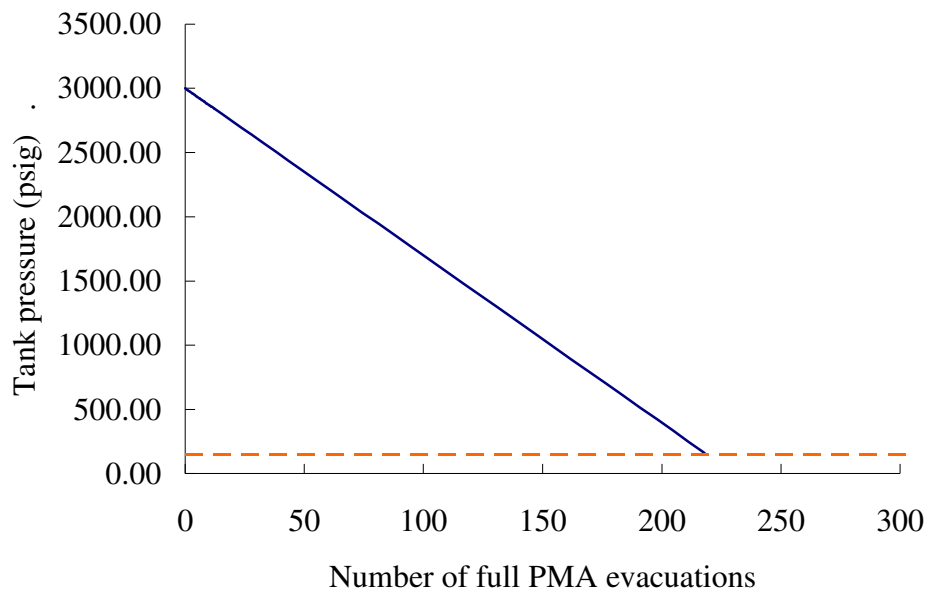
FIGURE 8 – Charge Life of PMA Supply Configuration.

Even though full range of motion was achieved with the use of one single PMA per side of the device, this configuration required the use of the PMA through the slack region where it is inflated below 30 psi. Due to the change in the requirements necessary to control the PMA through this range, a lower pressure limit of 30 psi has been included to preserve the dynamic stability and control of the device. An upper pressure limit of 80 psi equivalent to 6.3 bar was utilized to preserve the integrity of the elastic tubing inner liner of the PMA to prevent against blowouts at the end bushing barbs.

This additional configuration required the optimization of the PMA length to the full extension while sacrificing full flexion of the joint. In addition, existing clinical work with passive devices has been used to reduce the severity of the contracture to within 10 degrees of full extension. The initialization of treatment occurs when the contracture has reached the extent of a 25 degree flexion contracture for typical stroke victims. For severe contractures, an iterative array of PMA lengths was better suited to

managing the contracture without the requirement for recalibration of the device. This type of iterative map of PMA lengths would permit the use of the full developed PMA force for the more severe contractures where a single PMA would limit the actuating pressure in order to achieve the range of motion.

C. Joint Modeling

1. Muscle Modeling

The Hill model was developed as a means to mimic the various elastic responses of the human muscle. Included is a series elastic component to reflect the stiffness of the tendons and connective tissue for low loads and extensions beyond the neutral length. The parallel elastic component is significantly more stiff than the series elastic component and is neglected due to the high stiffness and associated parallel resistive force element for the low load and extension regions when considering the dynamic response of the joint. For loading that exceeds the elastic capacity of the series elastic element, the parallel elastic and resistive force elements are considered to contribute exclusively to the dynamic response of the joint. The parallel resistive force element mimics the damping found in the muscle group. For the isometric load case, where there is no joint motion to drive muscle load, the load generated is modeled using an active force generator element to mimic the twitch characteristics of the muscle group. An arrangement of the Hill Model with each component is shown in Figure 9.
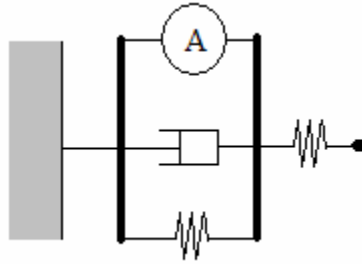
FIGURE 9 – Hill Model Arrangement of a Biceps muscle.

The stiffness elements are passive in nature and highly repeatable. Typically, the stiffness of the series and parallel elements is obtained experimentally through passive joint extension data under an increasing applied moment. A trial of passive joint extension data at an elbow joint, from a previous investigation (Quesada 2004) is shown in Figure 10. From previous research, the stiffness of an elbow joint has been obtained over a significant range to include both elastic elements. The passive extension curve is characterized by a low stiffness region reflecting the stiffness of the series elastic element and a high stiffness region reflecting the stiffness of the parallel elastic element. The transition point noticed at the knee of the curve is the observable point at which the series elastic element reaches its elastic capacity and the dynamic effects of the joint are carried by the parallel element. Through observation of the location of the transition point in sequentially collected passive extension data, a quantification of the degree of the contracture and the recovery process is obtained.
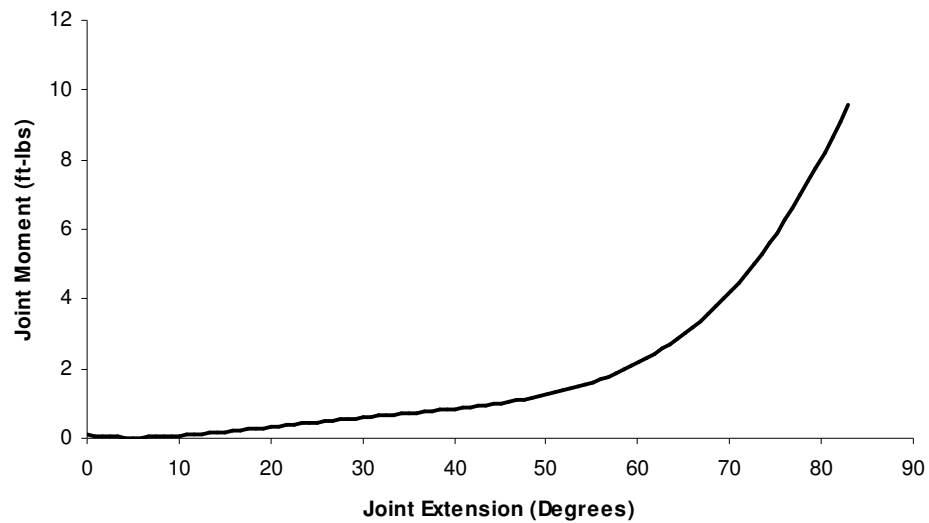
Figure 10 – Passive Joint Extension Curve for an Elbow Joint

The resistive force element provides a dynamic response based on the velocity at which the joint rotates. In order to obtain the damping coefficient required to define the response of this element, the time dependent force response of the joint is required. For the major muscle groups, the time dependent response was obtained through the use of EMG twitch data where the muscle was stimulated supramaximaly in order to develop tetanic tension as obtained by (Buchthal and Schmarlbruch 1970). The muscle force decay simulates an exponential decay characterized by a specific time constant. Of significance was that the time constant for the decay process was approximately twice that of the observed twitch time to tetanic tension (Shadmehr and Wise 2005). The damping coefficient was determined using the time constant and the elements' stiffness.

FIGURE 11 – EMG Trace of the Force Twitch Profile of the Biceps Muscle

2. PMA Modeling

From research into the mechanics of pneumatic muscle actuators, their behavior was determined to be non-linear over the inflation and deflation range. However, for the bulk of operation required for the device, the required adjustment range is small in relation to the overall range of motion and the model was linearized from a nominal pressure value for a mid range joint orientation typical for device operation. However, the different damping ratios for the PMA's in the inflation and deflation states remained valid due to the inflation against the dynamic pressure within the rubber liner and the deflation only against atmospheric pressure. Stiffness was calculated empirically and damping properties were obtained for a PMA using the correlations shown in research (Shadmehr and Wise 2005). A typical three element lumped parameter model of the PMA used to capture the dynamics of a single muscle is shown in Figure 12.
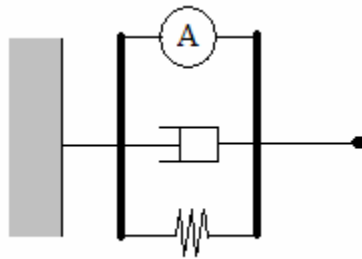
FIGURE 12 – Three Element Lumped Parameter PMA Model

3. Model Development

Due to the configuration of the joint and the elements involved, a second order single degree of freedom system was devised to characterize the response of the joint with the PMA driven LLPS device to counter the contracted state of the joint. The joint stiffness and damping components were arranged on the inside of the joint at a prescribed

offset from the joint center determined from anthropometric data (White 1990) in order to impart a restoring load intended to close the joint. The PMA stiffness and damping components were arranged on the outside of the joint at a constant offset from the joint as determined by the physical configuration of the device in order to impart a restoring load intended to open the joint. Because of the inclusion of the two PMAs, the stiffness and the damping coefficients have been accordingly adjusted. An arrangement of the model used for the combined joint and device is shown in Figure 13.
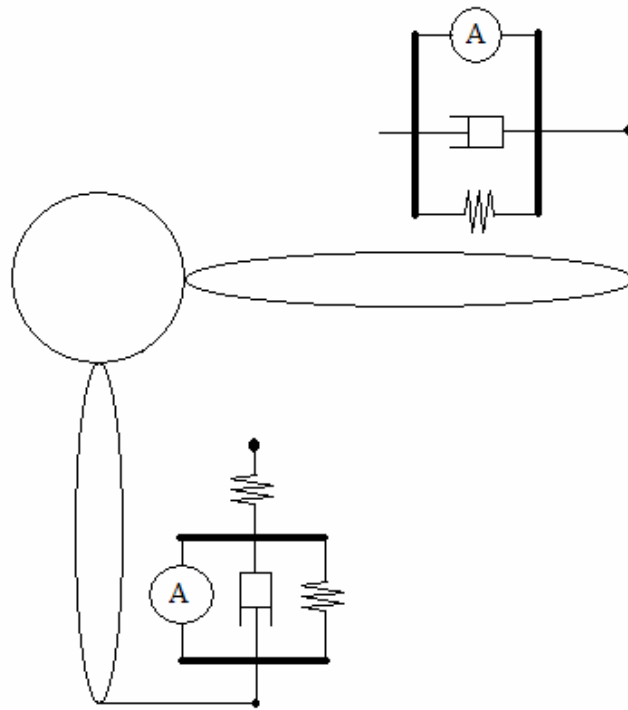
FIGURE 13 – Combined Joint and Device Model

The apparent translational inertial of the muscles actuating is overshadowed by the rotational inertia of the joint segments and the device segments. For the proximal and distal segments, the rotational inertia about the hinge joint was obtained from tabled anthropometric data (White 1990). Due to the faster response of the biceps brachii, the twitch response data was used to determine the damping at the physical joint and the

36

passive extension test data was used to determine the elastic components with an observed twitch time of 52 ms (Buchthal and Schmarlbruch 1970).

A nominal PMA pressure of 60 psi was used in order to determine the linearized components of the stiffness and damping coefficients. A linearized model was obtained in order to facilitate the use of a single input single output, single degree of freedom system. Due to the correlation between developed force and applied pressure within the PMAs, the dynamic changes associated with the physical parameters beyond the linearized value would be comprised by the applied force to the system at the PMA. The mass of the PMA was neglected due to its minimal effects in relation to that of the joint segments.

Included in Table I are the physical parameters associated with the joint model developed. The calculations used in order to obtain these parameters have been included as an appendix. In addition, the development of the transfer function used for each operating mode of the device was also included as an appendix.

TABLE I

PHYSICAL PARAMETERS FOR JOINT MODEL

Parameter Name (units)	Value
Proximal Rail length, a (m)	0.1134
Distal Rail length, c (m)	0.1134
Proximal Rail PMA Offset, b (m)	0.0508
Distal Rail PMA Offset, d (m)	0.0508
Proximal Arm Segment Inertia, I_{prox} (kg-m^2)	0.1005
Distal Arm Segment Inertia, I_{dist} (kg-m^2)	0.2417
Prototype Inertia, I_{prot} (kg-m^2)	0.02009
Muscle Series Element Stiffness, K_{se} (N/m)	6077
Muscle Parallel Element Stiffness, K_{pe} (N/m)	371200
Muscle Resistive Element Damping, b_m (N-s^2/m)	39240
PMA Stiffness, K_{pma} (N/m)	1417
PMA Damping, b_p (N-s^2/m)	1104

4. Model Considerations

There have been advances made in muscle modeling in order to include the histological response of the muscle to the histological chemical interactions that precipitate the moto-neural functions. However, the purpose of this research was not to consider the histological effects on muscle dynamics in precipitating the contractures, but rather the development of a device appropriate to mange the affects and respond to the dual state of the contractures and spasticity at the joints. Additionally, improvements have been observed in the development of force twitch trace mechanic replication with the use of PMAs acting as an exoskeletal muscle, yet, the intended use of the PMAs in this application are not intended to replace the exoskeletal muscle but rather respond to the changes incurred on the joint by the muscle system.

Those improvements were considered to be beyond the scope of the work. The dynamic response of the muscle mechanics has been shown to be reasonable approximated through the use of second order dynamic modeling techniques for both twitch mechanics and for isotonic and isometric muscle responses.

D. Control Algorithm

1. Primary Mode

The fundamental basis of the primary operational mode is to manage the extent of the joint contracture. To this end, the focus of the control algorithm is to maintain a set reference angular position for the dynamic joint in response to disturbances and joint softening. The primary degree of loading is generated through passive extension of the intended muscle or low level activation of the contractile components of the muscle group. Through the sequential adjustment of the desired angular position of the joint, the

joint is driven to the increased range of motion and the reduced joint stiffness as indicated through a higher threshold between the low stiffness and high stiffness regions obtained through passive extension.

In order to develop the function of the control algorithm, a negative feedback arrangement was used with the scaled difference between the desired angular position and the measured angular position taken to be the error in the system. Original configurations provided for an adjustable gain on the error along with the magnitude in the previously measured pressure within the PMA was used to determine a desired pressure within the PMA and input into the PID control sequence against the previously measured pressure. The PID controller for the auxiliary mode was used to control the primary control mode due to the reduced degree of disturbances required to be managed by the controller.

However, initial testing proved this configuration to be inherently unstable as the PID was controlled by an apparent quantity. In order to remedy this situation, the measured and desired joint angles were used as the inputs to the PID loop in order to improve the stability of the controller. Additionally, the measured joint angle was weighted against a gain factor and the desired angle in order to create a diminished apparent measured error in the system. The output of the PID loop was weighted to fall within the voltage ranges of the pressure regulator and subtracted from the existing voltage applied to the pressure regulator in order to determine a new set pressure in the PMAs. An error resulting from a measured angle greater than the desired angle will increase the pressure within the system in order to drive the joint to a reduced angle. The

schematic of the control diagram used for the primary joint angle control is shown in Figure 14.
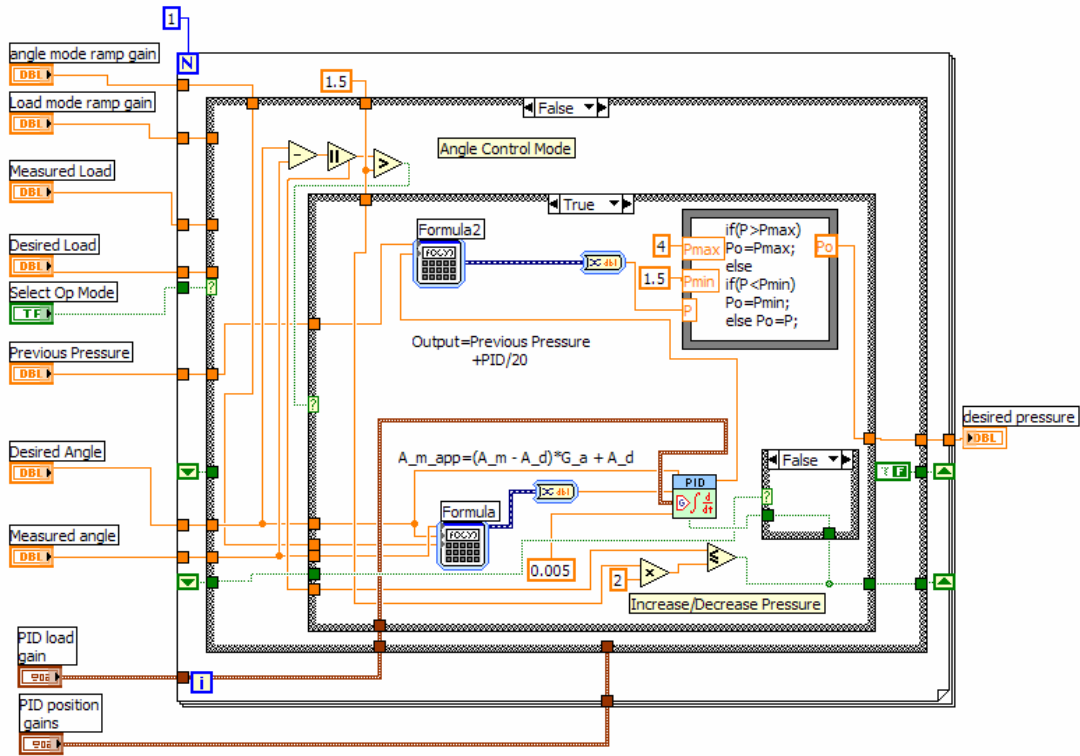
FIGURE 14 – Primary Control Mode Configuration

The use of the weighted measured process variable was utilized in order to provide control over the error input into the PID loop. With the high potential error, especially in the joint angle control mode, the use of the raw process error would provide for a high degree of overshoot and a fast rise time within the system that would lead to system wind-up. By providing a mechanism for control over an apparent system error, the characteristics of the system response can be adjusted without having to readjust the PID gains.

In contrast, the use of a weighted PID output was used to scale the PID outputs to a reasonable range of the voltage potential permitted across the pressure regulator. The PID loop in use is a process control PID control algorithm with a +/- 100 % output range

to dictate the necessary change on the output that had to be scaled to the 0-5 VDC signal. As opposed to the scaling of the measured error in order to obtain an apparent error, decreasing the scale of the PID output only serves to prolong the period of oscillation of the process under control and does not affect the output value of the PID output as would the scaling of the measured error. Thus, both techniques were utilized to provide a greater degree of control over the overall process.

The use of the same PID gains to control the primary and the auxiliary operating modes proved to be insufficient. Analysis of the response of the force and the joint angle measured within the system for step increases in pressure indicated the dependency nature of the system. This system response is demonstrated in Figure 15. The developed force occurred as a result of the developed pressure whereas the developed joint angle occurred as a result of the developed angle. This behavior provided for an inherent lag between each process. Additionally, the initial gains developed proved to be insufficient to provide an adequate response of the system and resulted in high overshoots and general instability of the system. A separate gain structure had to be developed for both the force and the joint angle dependent operating modes respective to their responses to changes in pressure within the system.
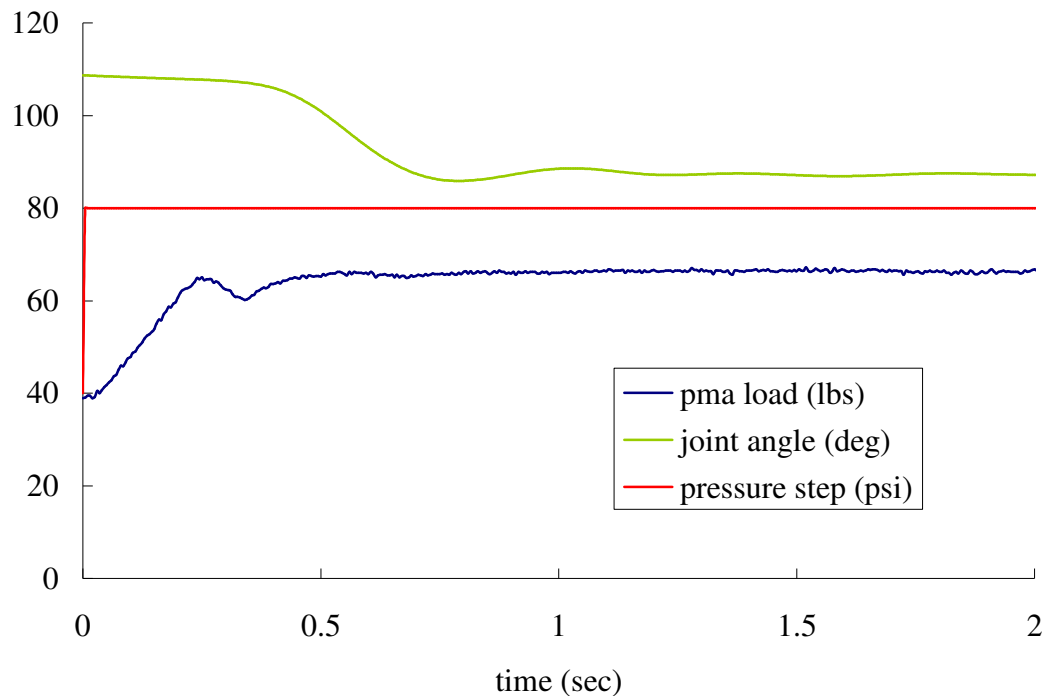
FIGURE 15 – System Lag Response for Force and Position

Additionally, the initial modeling of the system neglected the impact of the observed time delay in the system response between the developed force and the joint angle. Using the observed delay of 0.4 seconds, the model was adjusted appropriately using a (2,2) Padé approximation of the delay function. From the evaluation of the system using the SISO toolbox within Matlab, the original controller was proven to be unstable because of the effects of the delay and the noncompliance with the required discreet conversion for the continuous system using the Matched-Poles and Zeros method. The original response times were too short for the system to be capable of responding with a desired settling occurring before five samples have occurred. In practice, this controller was impractical. Revised controllers utilized significantly higher performance requirements had to be developed in order to appropriately regulate the operation of the device in light of the modified dynamics.

2. Auxiliary Mode

For the auxiliary operating mode, the intended focus is to manage the spastic activity episodes to minimize the risk of precipitation of a further complicated contracture. To achieve this functionality, the controller was designed to detect the onset and decline of the spastic activity episode and to maintain a critical load until the range of joint motion has returned to the desired angular position. From the passive extension data, a threshold level would be set at a level approximate of the threshold indicating the onset of the increased activity of the contractile element and a higher joint stiffness. Due to the arrangement of the PMA with the load cell, the determination of the threshold load level from the moment versus angle curve in the passive extension data is a routine calculation that does not require interpolation of calibration curves.

For the case of a load exceeding the threshold level, a buffer count was initially used to track how many successive intervals at which the threshold level of load had been exceeded. If the overload exceeded a prescribed overload limit then the algorithm called for the change in the operational modes to the auxiliary mode that required the difference in the measured load from the reference load value to be the error in the system. The time delay inputs the reference control mode on the main interface diagram that permits the device to operate in either the manual load control mode or a default autonomous mode that maintains the primary joint angle control mode except when the auxiliary load control mode is required. For every loop where the load does not exceed the prescribed overload limit including after a load excursion has subsided, the iteration count was maintained at zero. The non-overload configuration of the buffer is shown in Figure 16.

43
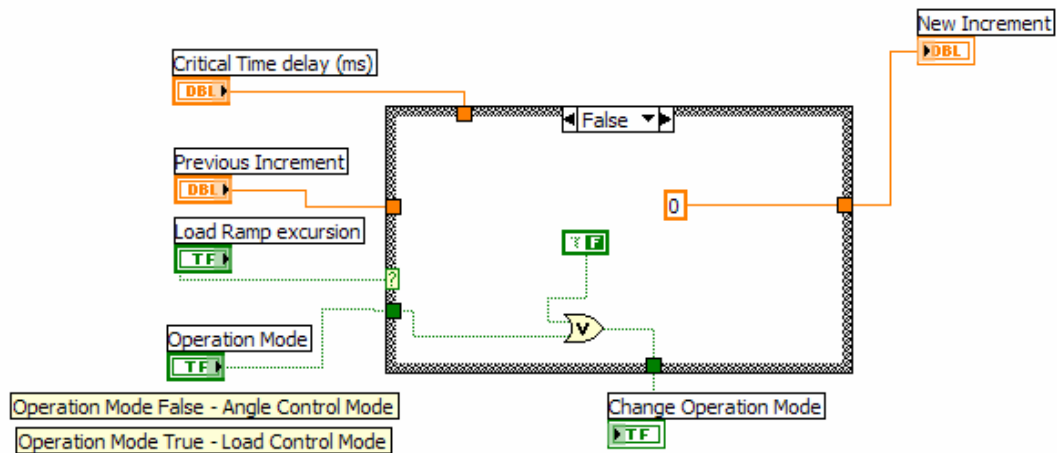
FIGURE 16 – Non-Overload Time Delay Configuration

For the loops where the load has exceeded the overload limit and the iteration count has not been exceeded, the iteration count is incremented by one. In the instance that the iteration count has been exceeded, a sub case structure ensures that the iteration count does not increment beyond the critical level which would result in high counts stored in a memory for prolonged load excursions. The overload time delay configuration is shown in Figure 17.
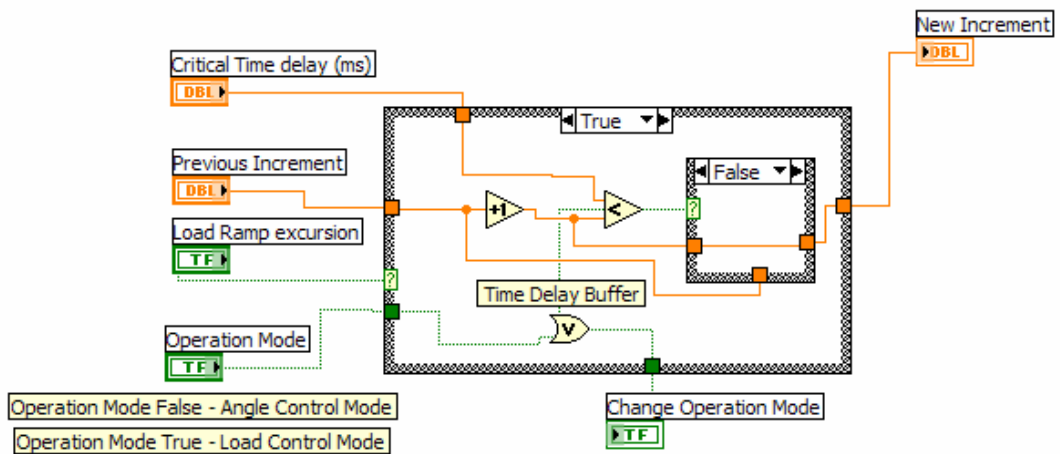
FIGURE 17 – Overload Time Delay Configuration

44

As was the case with the primary control mode, the initial controller depended upon an adjustable gain on the error with the previously measured pressure within the PMA was used to determine a desired pressure within the PMA. The desired pressure and the previously measured pressure were input into the PID controller such as to drive the pressure of the system lower for a higher load than desired and to increase the pressure of the system for a lower load than desired. The PID controller was designed to respond to the high magnitude dynamic changes in the loading observed by the onset of a spastic activity episode.

However, as with the primary control mode, this configuration proved to be unstable in the operation of the device. No range of gains on the error would eliminate the problems encountered with the lack of stability and high degree of overshoot beyond the desired load of the system. The controller was rewritten to include a weighted measured load by a gain factor and the desired load in order to create a diminished apparent error on the system. The PID loop was rewritten to utilize the desired and the apparent measured load directly rather than a scaled pressure dependent upon the previous set pressure and the system error in order to improve the internal stability of the pressure control loop. The desired voltage applied to the pressure regulator was set through the output of the PID controller scaled to the output ranges of the pressure regulator added to the previous set pressure.

This configuration provided for a direct control of the pressure dependent on only the measured and desired loads of the system. For a higher than desired measured load, the error will result in the pressure within the PMAs being decreased until an appropriate

pressure level is obtained. A schematic of the auxiliary control mode is shown in Figure 18.
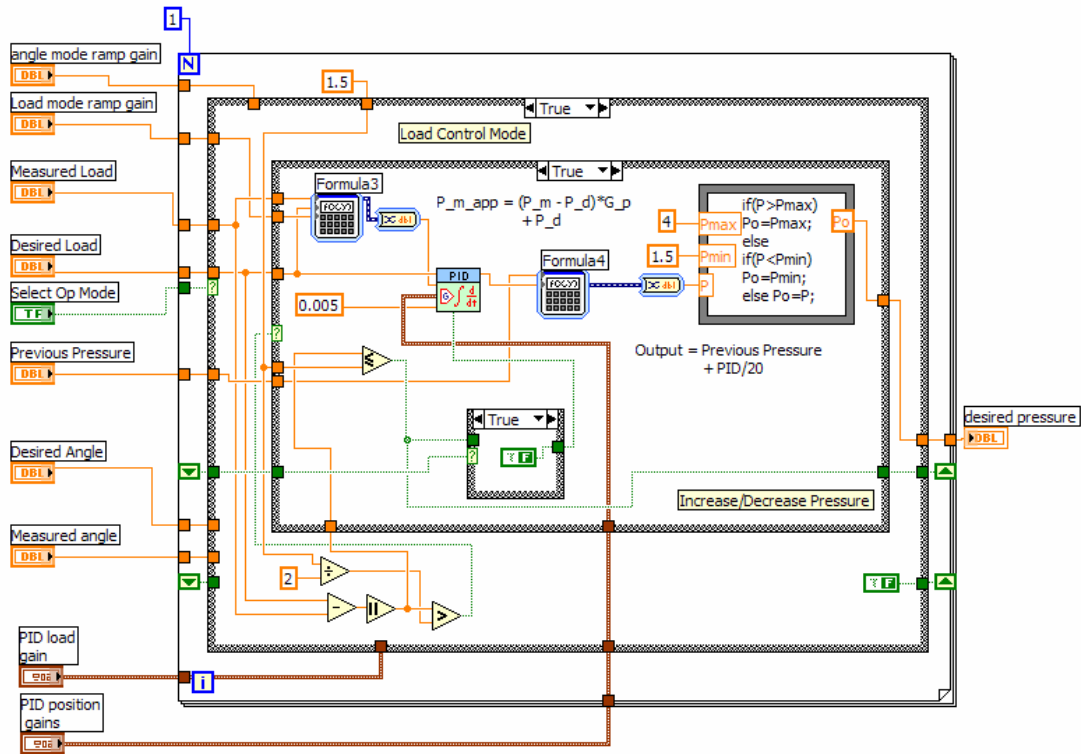
FIGURE 18 – Auxiliary Control Mode Configuration

The use of a time delay buffer proved problematic for the operation of the auxiliary load control mode. This mechanism, though intended to perform as a delay to ensure that a spastic activity episode had occurred, provided for peak overshoot of the desired maximum load. As a consequence as the controller responded to the high load by decreasing the pressure, the measured load fell below the critical level and reinitialized the buffer. This procedure resulted in a significant swing of the pressure within the PMA by the controller and the inability to properly switch control modes and maintain the load control mode. Essentially, the operation continuously alternated between the two controller modes while permitting unsafe and undesired joint moments excursions on the

46

patient to occur as the device tried primarily to seek a reference position. The only safe

operating mode capable was to include the critical time delay as zero ms negating the

effect of the buffer in practice. Thus, this feature was eliminated from the controller

except for the use of the manual load control mode.

In order to detect and reject the occurrence of the spastic activity episodes through

the use of the rotary potentiometer and the force transducer, an operational switch had to

be developed that would autonomously perform this function.   Initially, the load

switching subroutine was developed in a manner that was dependent only upon the

developed load within the force transducer, however this configuration would prove

troublesome in the rejection of the load control mode after the spastic activity episode has

subsided. As written, the detection sequence would issue a Boolean true command in the

event of a load excursion beyond the critically defined load and is shown in Figure 19.

However, in this instance the controller would self impose the restriction of maintaining

the peak load while extending the joint through and beyond the desired joint position.
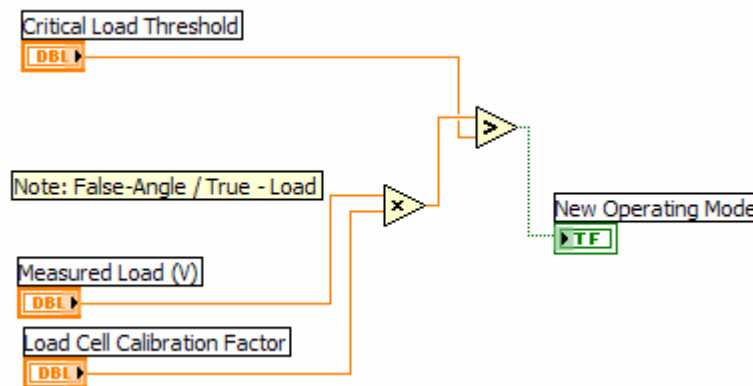
FIGURE 19 – Spastic Activity Detection Sequence

Thus a secondary condition was imposed as a rejection sequence that included the

measured joint angle as a parameter for determining the state of the contracture. If the

joint contracted beyond a certain error away from the desired position, then the rejection sequence would yield a Boolean true value. For the load switching subroutine to issue a change to the load control mode, both of the detection and rejection sequences were required to issue a Boolean true command. In the event that either fell false, then the control mode would switch to the joint position control mode. Bench-top and experimental testing has validated the function of the load switching subroutine. The rejection sequence is shown in Figure 20.
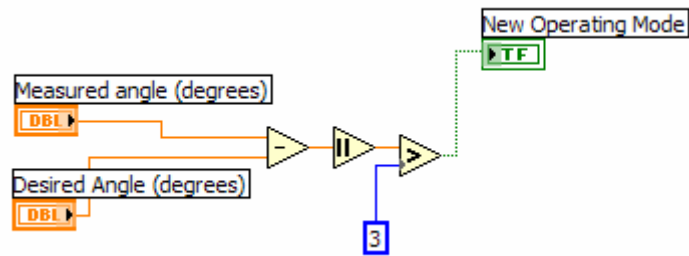
FIGURE 20 – Spastic Activity Episode Rejection Sequence

However, one failure mode of the switching mode as developed is the redetection of an assumed spastic activity for instances where the high load is maintained up to the rejection point due to the measured angle. In an instance such as this, it was determined that the load switching controller had the capability to switch back into load control mode and continue to stretch the joint beyond the desired joint position. This defect possessed the potential to place the patient at an undue risk of injury due to a prolonged higher load stretch beyond the load levels associated with the fundamentals of low load prolonged stretch.

This original load switch function also proved problematic for high grade and high velocity contractures. As the controller responded to the rapid increase in load, the decrease in set pressure required to provide the flexibility of the device, the load would

swing low for an intermittent period of time resulting in a rejection of the spastic activity regardless of joint angle. The high degree of error in the angle and the high joint stiffness proved to leave the controller unstable overall resulting in a rapid alternating behavior between load control and position control that no case was designed to respond to. Subsequently, the device exhibited a dangerous swing tendency that would fail the treatment procedure and require the removal of the device

In order to remedy these hazards, an extra condition was added through the use of a Boolean case structure that separated the load detection and rejection sequences to apply only to their respective functions. Thus, the detection sequence was only active if the previous loop of the controller operated in joint position control mode and the rejection sequence operated only if the controller operated in load control mode on the previous loop. Additionally, a second set of requirements on the detection sequence restricted the detection to loops where the joint position was higher than the permissible band of three degrees greater than the desired position.

This change prevented the rejection sequence from behaving as a detection sequence and changing the controller mode due to joint position alone permitting resistance to patient movement beneath the permissible load threshold. Accordingly, the recoded load switch controller prevented the detection sequence from behaving as a rejection sequence and prevented the problems as detailed above. The revised conditions are shown below for the detection sequence in Figure 21. The rejection sequence was maintained with the algebraic algorithm for calculating the measured load included for the operation of the overall control program.
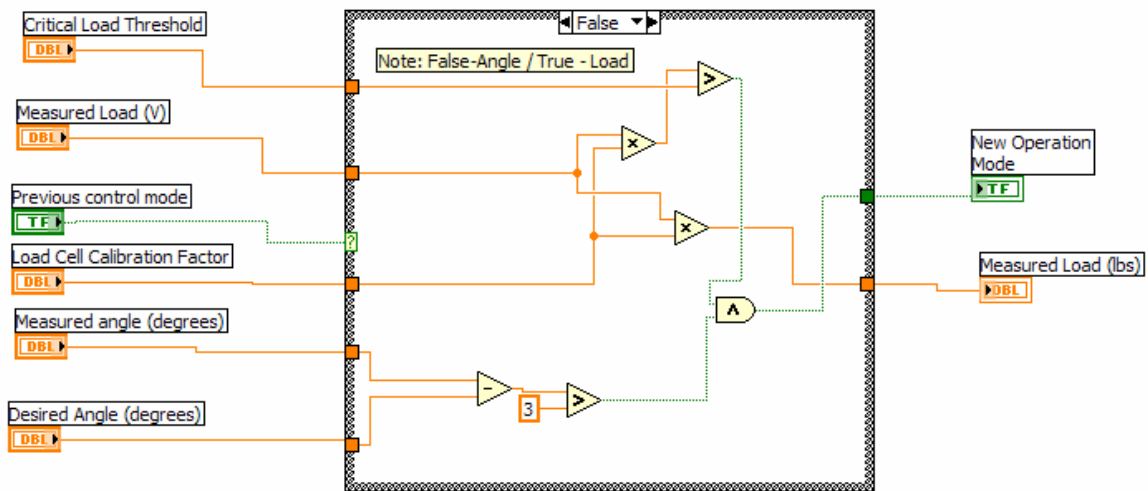
FIGURE 21 – Revised Detection Sequence

3. PID Controller Development

Before the use of a PID controller was devised, the premise of a more simple controller was evaluated. Proportional, proportional integral, and proportional derivative controllers were evaluated, yet the inherent shortcomings of each type limited their functionality for use in the final controller. Problems that arose included high steady state errors with the proportional difference controller, and high overshoot and settling time errors that were observed for the proportional integral and proportional derivative controllers. Each type was capable of stability, however, the response characteristics of each limited their use.

The proportional controller required high gains in order to reduce the settling time of the system, yet had a poor steady state error and poor response to input disturbances. For the bulk of the operation of the device, the primary function was determined to be disturbance rejection whether it occur as a result of tremor or spastic activity. The inclusion of the integral term to improve the steady state response came with a

consequence in system overshoot, which would provide significant problems where the device was required to maintain an approximate joint angle or joint load. The use of a derivative term alone with a proportional term provided for improved transient mechanics, however, there was no mechanism to eliminate step disturbance errors and results in a steady state error.

With the PID controller, as noted previously, a separate gain schedule had to be used for the primary joint angle control mode and the auxiliary PMA load control mode. This mechanism was required as a result of the inherent lag of the developed load behind the developed pressure and sequentially the developed joint angle behind the joint load. Additionally for PMAs, the behavior is approximately linear across the low stiffness range and across the high stiffness range. The crossover between the two stiffness ranges occurs where the PMA has become charged at above 30 psig (2 bar) and no longer exhibits the slack behavior attributed to the low stiffness range. If the PMA were to be operated across the full range, a pressure dependent gain schedule would have been required for both control modes. However, in the interest of the treatment procedures, the PMA will only be operated in the high stiffness range above 30 psi and below 80 psi. The upper limit range will provide for the safe operation PMAs to limit tubing failure at the bushings.

Response characteristics were limited to an overshoot to a step input, similar to the start up sequence of the device, of no more than 50 percent overshoot, with the settling time limited to fewer than two seconds. Due to the discreet digital control of the device, the rise time was required to be higher than six sample periods or 0.03 seconds, but for the purpose of practicality, was desired to be lower than 0.75 seconds. The time

constraints were approximately coincident to the observed joint angle and force behavior observed for a step input to the open loop system with consideration for the inherent lag within the system. The desired settling time to within 99% of the desired set value for each controller was desired to be less than 2 seconds. The Single-Input-Single Output (SISO) toolbox within Matlab 6.5 was utilized to optimize the desired controller dynamics after initial controller specification. A spreadsheet was used in conjunction in order to calculate the initial desired controller zero locations applicable for the desired response dynamics. A copy of the spreadsheet and associated coding is included as an Appendix. The final gains that were obtained are listed in Table II.

TABLE II

GAIN SCHEDULE OF PID CONTROLLERS

Gain Type	Angle Mode	Auxiliary Mode
K_A	1333	8.16
$T_I\,(s^{-1})$	1.14	0.05
$T_D\,(s)$	0.229	0.0125

The model that was developed lacked the characterization of the response of the angle with respect to the input pressure. Difficulty was encountered in establishing this transfer function that resulted in the residual instability of the controller.

As a comparison, the Ziegler-Nichols Step Response Tuning procedures for a Quarter-Decay Ratio were also performed on the system. The Ziegler-Nichols Tuning procedures is developed such that the transient response has a decay ratio of approximately 0.25 and is intended to provide a reasonable response between quick system response and stability margins. The tuning rules are shown in Table III along with the developed controller parameters obtained. For a step in the input controller

52

process, the desired PID coefficients were developed from the lag time, L, before the process reacts, and R, the response rate of the system. The step responses used for the Ziegler-Nichols Tuning procedures are included as an Appendix.

TABLE III

ZIEGLER-NICHOLS TUNING COEFFICIENTS

Gain Type	Angle Mode	Auxiliary Mode
K_A	0.0774	0.417
T_I (s^{-1})	0.8	0.05
T_D (s)	0.2	0.0125

From preliminary testing of the controller, a significant problem remained with instability on the overshoot of the desired joint angle. Investigation within the controller demonstrated that due to the high degree of initial error associated with a start up of the device or the inherent error associated with the self-rejection from the load sequence, the integral term dominated the output of the PID loop, resulting in a significant energy buildup within the controller that exceeded the capabilities of the proportional and derivative terms to dominate close to the desired joint angle. However, during low error configurations, the overshoot and precipitated instability was not apparent in the response of the controller. Any further scaling of the output of the PID controller would only prolong the period of oscillation of the unstable excursion, and the gain on the apparent error was suitable for the bulk of the operating region of the device.

In order to eliminate this wind-up problem with the controller, the controller was configured with an anti-windup arrangement. Within a prescribed error band on each side of the desired angle and load, the integral error was reinitialized to remove the extraneous energy from the controller and improve the stability of the system. To

prevent the controller within the error band from operating as a PD controller only, the re-initialization sequence was configured such that it was only applied on the loop following an excursion beyond the error band, thus preserving PID functionality within the error band. After a successful implementation with the joint angle control mode of the device, the anti-windup sequence was implemented with a smaller error band on the PMA load control mode.

Due to a constantly changing measured signal, the error associated with both operating modes would be variable throughout the operation of the device, leading to a continuously variable desired pressure within the PMAs. In order to preserve the air reserves and to eliminate un-necessary chattering of the valve and potential valve wear, a dead band was implemented into the control of the PMA driven device. Within a certain error band of accuracy on each side of the desired angle and load, the desired pressure would remain the same as was set on the previous loop. The error band size was determined through analysis of the self rejection routine limits and reasonable accuracy of the device. The angle dead band was set at +/- 1.5 degrees and the load error band was set at +/- 0.75 lbs. A schematic of the deadband and anti-windup configurations is shown in Figure 22.
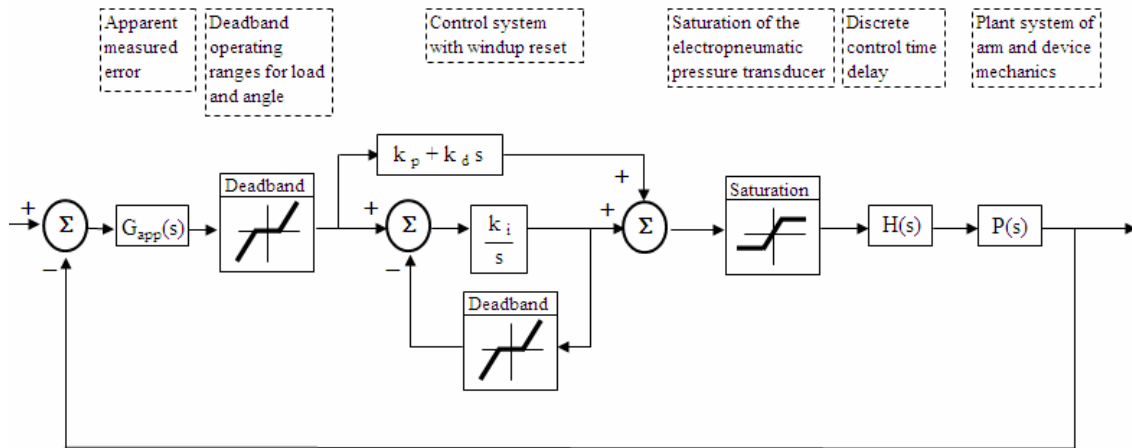
FIGURE 22 – Operating Range Schematic with Deadband and Anti-Windup

4. Patient Safety Logic

Maintaining the safety of the patient was a primary driving objective behind the development of the use of PMA driven LLPS devices. In accordance with this governing objective, several features were intentionally included in the design of the controller. Internal limits on the desired loads and the desired angles of the device were intentionally included to prevent an overload of the PMAs and to prevent the over travel of the device due to potential controller excursions. In order to maintain a factor of safety in the operation of the device, the load limit and the maximum angular displacement limits are not set at the peak permissible level and are restricted within the code to prevent tampering at the interface. The peak loads permitted was set at 60 lbs and the peak joint angle was set at 100 degrees. The safe range limits arrangement is shown in Figure 23.
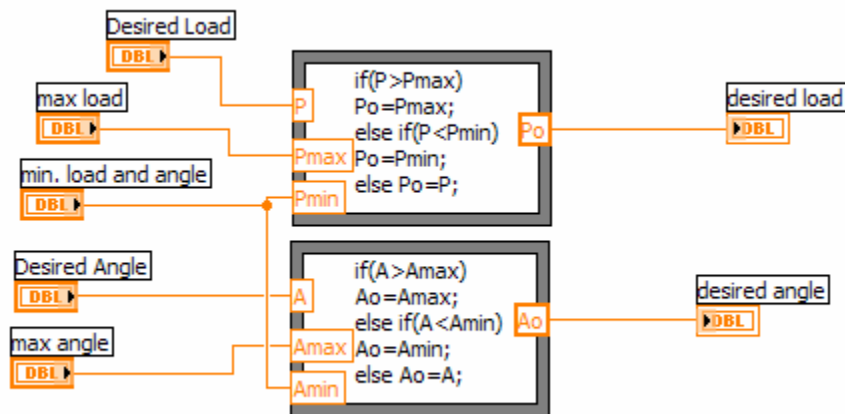
FIGURE 23 – Safe Operating Range Limits

A dual mode shut off logic was devised to function simultaneously from inputs from the patient controlled shut-off switch and the software shut-off switch. During operation of the device, both are capable of ceasing the operation of the control algorithm in a manner that actively protects the patient by unloading the internal charge within the PMAs before stopping the algorithm. The original revision of the controller did not consider the hold configuration of the output tables of the controller such that a stop signal would maintain the last previously stored desired pressure within the PMA, maintaining the device in the malfunctioned or injurious state. The developed logic ensures that the pressure in the PMAs is driven to zero psig through a reverse bleed before the controller operation is terminated with a warning light engaged on the master control panel.

In the development of a patient controlled shut-off circuit, the ability to detect a positive signal from the activation of a switch was required in order to input the mode of the signal into the logic of the controller. An excitation channel referenced to ground and a measured channel referenced to ground were used in conjunction with a momentary

normally open switch. This configuration would provide a dead channel with a voltage value of approximately zero during the normal function of the device which would be considered the low state of the switch. During the activation of the switch and the engagement of the channel, the voltage measured across the channel would peak to a value approximate of that of the excitation channel, which would be considered the high state of the switch. In order to differentiate between the two states of the switch, an intermediate voltage value was utilized as a threshold in order to activate the Boolean sequence that tied into the normal software shut off logic. A rolled sheet aluminum grip was used with a successfully large handle to ease the process of the patient actuating the switch. The dual mode shut-off logic is demonstrated schematically in Figure 24.
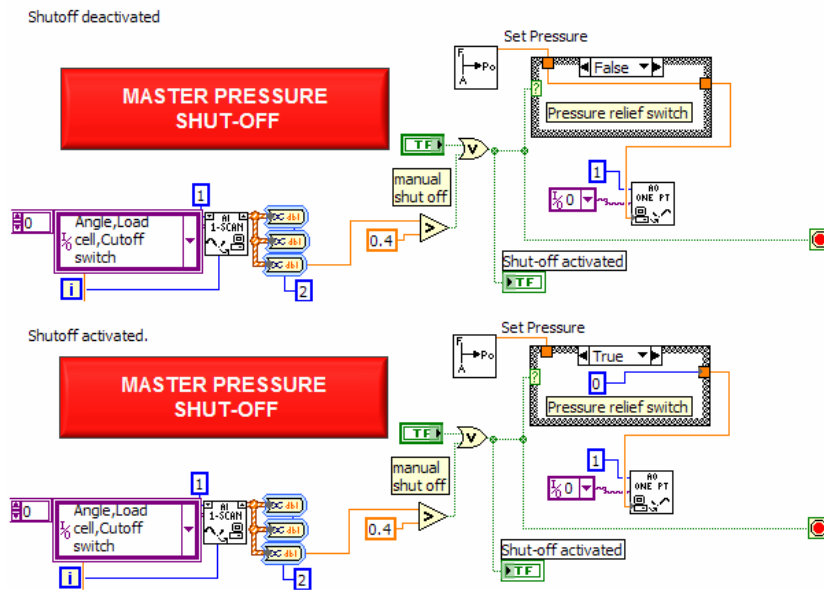
FIGURE 24 – Dual Mode Shut-Off Logic

In the event of a serious device malfunction that resulted in a pressure increase excursion, the control of the device was written so to provide an integral autonomous shut-down feature to preserve the patient safety. The back-up safety logic is intended to operate upon loss of the patient controlled shutoff mechanism and an uncontrolled

excursion which would increase the load experienced by the patient. At a threshold level of force, with the elastic properties of the PMA considered, the device would trip automatically and vent the charge within the PMAs. This software mechanism would trip at the extreme load level of 75 lbs.

5. Data Logging

The data logging requirements were coupled with the controller function in order to reduce component requirements and to streamline the function of the controller. With the control logic operated from a laptop PC with the data scaled internally for engineering units before processing, the data from each acquisition loop is stored sequentially with the current time of the loop into an array on the hard drive of the PC. This layout permits data processing on the same platform as the signal acquisition and device control after the session has been completed. Inputs were included within the device interface for the patient identification in addition to a trial number that are internally concatenated to create a unique file name for each patient and trial.

All data is stored as a text file on the hard drive where each iteration of the controller loop representing one row in the data. The purpose for storing each iteration at the time of sampling rather than to buffer a sample and write the data at once or in smaller segments was to minimize any lag associated with the memory resources required for writing to the file. For the 8 hour trials with the device, the file size would be approximately 500 MB with 23.04 million data points logged. Due to the high sample rate and the relatively large quantity of data points that required logging, efforts were made to minimize the required file size through the optimization of the file write technique in conversion directly to a text string and through the limitation on the

precision of the written values of the values of the developed PMA load, joint angle, and set pressure within the PMAs.

The required degree of precision to the five thousandth of a second was determined not to be necessary when determination of the spastic activities only required the capability of knowing the second in which the activity began and subsided as determined by the controller. Thus, the data write portion of the code was reconfigured to write on every 200th iteration of the loop corresponding to every 1 second of operation using a case structure activated by an iteration count that initialized at the validity of the count. This change reduced required file size significantly by eliminating the bulk of the data that was to have been logged. The eventual file size for an eight hour trial was reduced to approximately 2.5 MB permitting ease of data processing. The time of the loop acquisition was included with the file write portion of the code in order to minimize the data that had to be acquired and the processor requirements of the code for most iterations of the controller. The file write code is shown in Figure 25. For all cases where the count is less than the maximum count, the case structure adds one to the count.
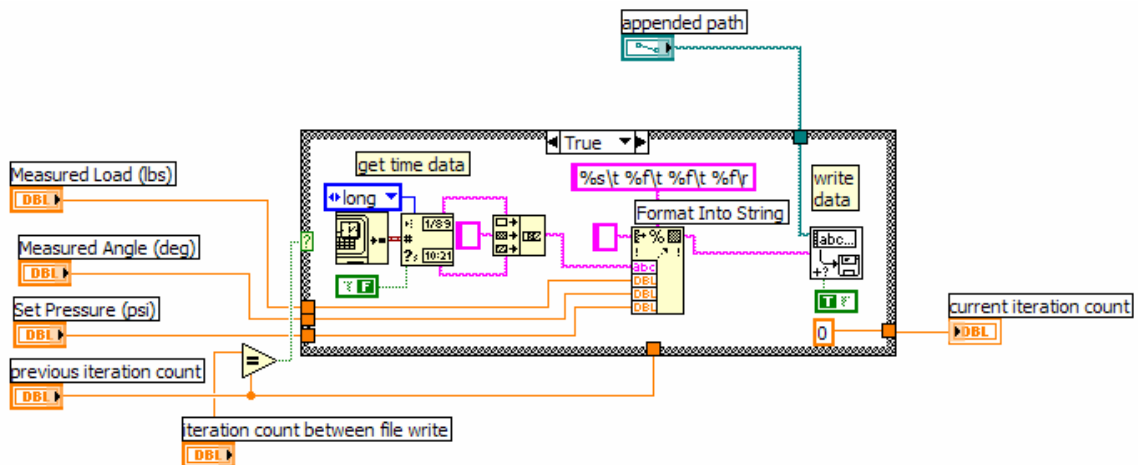
FIGURE 25 – File Write Arrangement

59

6. Device Interface

The input panel for the device interface has been divided into three sections. One section for engineering controls including sampling frequency, critical switchover load, the control mode error gains, and the PID controller gains for the separate control modes. Another section has been provided for the therapist or patient controls including a software shut down button, primary mode desired angle and auxiliary mode desired loading. The therapist controls have been maintained in as graphical a form as possible to permit ease of operation and comprehension, whereas the engineering controls are set through the device development prior to the therapist operation of the device.   The third section of the interface panel includes two graphical indicators to display the current device angle and the current developed load within the PMAs.

The calibration of the rotary potentiometer used to measure the joint angle is performed through a text prompt sequence at the beginning of each section. A two position calibration was envisioned that did not require the device to be set to zero degrees while fixtured to the patient in order to determine an offset voltage. Instead, the quotient of the differences in the two joint angles and the two corresponding voltages was used to develop the calibration constant for the slope of the calibration curve. Then using a linear function with one of the two initial joint angles and corresponding voltages, the subsequent joint angles for each loop were calculated from the measured voltage. The calibration sequence has been included as an appendix.

This sequence permitted the use of the device on patients with severe grades of contractures without having to arbitrarily add a scalar to the angular measurements due to the lack of flexibility of the patient in determining an offset voltage. This calibration

sequence is to be executed at the greatest attainable extension and contraction positions while the device is fitted to the patient in order to provide for interpolation of the joint angle within the flexibility range and to minimize effects of extrapolation beyond the flexible range. For patients with extremely severe contractures with range of motion at less than 30 degrees, the applying physician must take great care with measurement of the joint orientation with a goniometer to minimize the error perceived by the controller during extension.

In order to provide for unique file names for each patient and trial, a name and trial number section is included at the top of the interface menu for the therapist to enter for the patient. The device interface is shown in Figure 26.
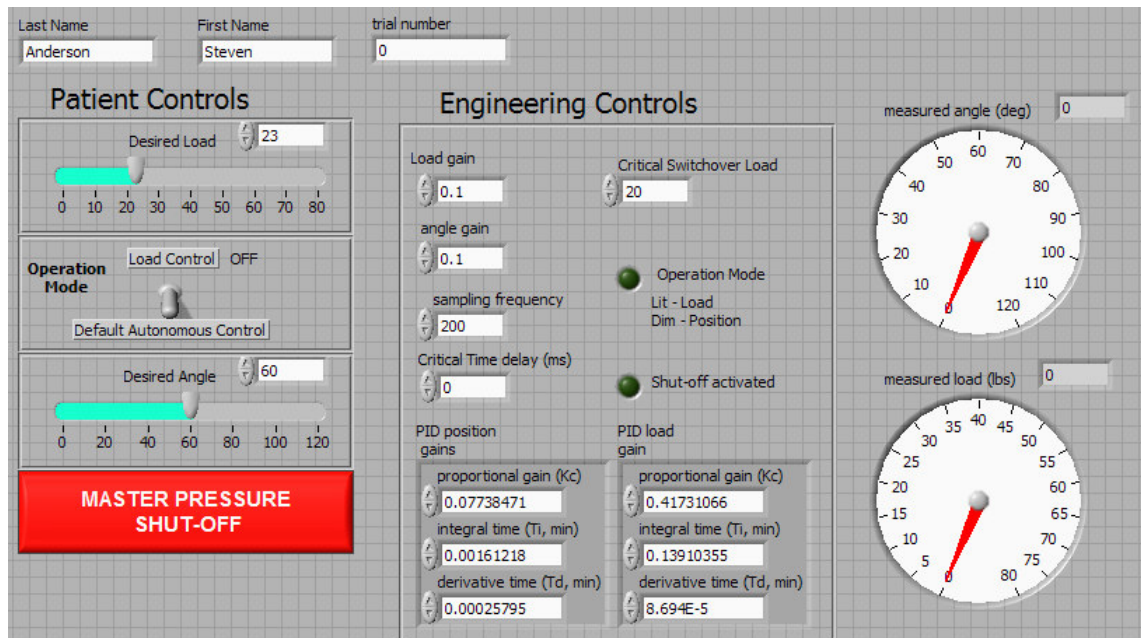
Figure 26 – Active LLPS Device Interface

7. Joint Stiffness Measurement

An additional controller has been devised in order to obtain the passive joint extension data using the prototype as the vehicle for data collection. The control

algorithm is a simplified form of the auxiliary controller with the pressure required in the PMA successively increased in order to create an increasing applied joint moment. The time of the collection for each loop, the current angle position and the current force measured in the PMA is logged for each loop of the controller. Due to the high data collection rate of 1000 Hz required for the passive joint extension data, the logic has been simplified significantly to suit the demands of the application. The threshold determined from the passive joint extension data determines the threshold level used for determining the onset of the spastic activity for the patient.

E. Sensor Technology

Due to the environment and the type of patients for which the device is intended, the data collection, signal conditioning, device controller, and sensor package had to remain relatively light and compact in order to permit the portability of the package. For the purpose of mass production, commercially available sensors and signal conditioning packages were considered.

The signal conditioning system was selected such that the size was small enough to be portable, yet the bulk of the required components were contained within one easily accessible housing. This desired configuration eliminated the need for multiple assemblies in order to handle the different analog input and output signals and would improve the portability of the system for ambulatory patients. The signal conditioning panellettes for the analog inputs had to maintain the functionality of an easily adjustable gain control and the full bridge load cell signal conditioning panellette had to maintain control for offset and gain control. This would permit the customization of the input

signals in order to reduce the effects of noise and dc offset that would require handling within the control algorithm and sacrifice crucial computing power and time.

Thus the choice of a laptop sized signal conditioning carrier with customizable panellettes was chosen to provide the signal conditioning for the system. A 12 bit data acquisition card (Daqcard-6062E) from National Instruments was purchased with both voltage analog input and analog output capabilities. This card accommodated a total of 16 channels AI channels and 2 AO channels and provided 5V excitation voltage for each of the sensors. The signal conditioning board is a SCC-2345 carrier with customizable panelettes for each signal type. Included are two AI modules, one full bridge strain gage module, and two feed through modules to permit AO control of the pressure regulator and the excitation of the devices. The board layout and channel schematic of the signal conditioning system is shown in Figure 27.
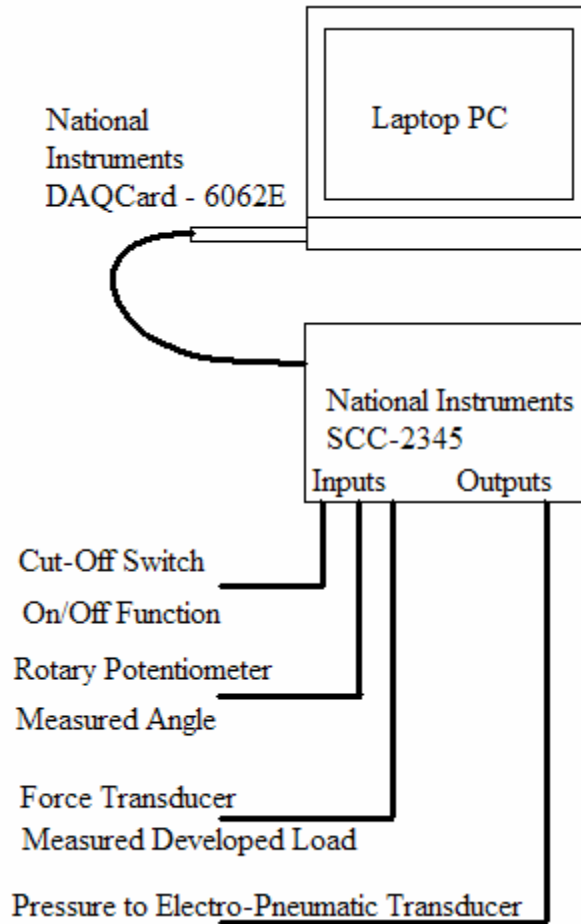
FIGURE 27 – Signal Conditioning System Arrangement

The use of a packaged flexible signal conditioning system was preferred over an industrial multi piece configuration due to the size and the relative cost to the option chosen. The field ready modules provided limited channels per package and required an independent power supply and connection to the main process controller. In addition, the industrial units required an additional device interface with a cost approximate to that of commercial laptop pc without the same degree of functionality. An additional data logger would have required more physical space and more power. Another option that involved a PLC control circuit would have provided neither the flexibility of the data processing within the controller nor signal conditioning flexibility while requiring PID

control using the raw measured signals. The increased cost and physical requirements of the other available options relegated the chosen option as the most flexible and the most cost effective without having to successively burn the logic onto hardware chips during the design development phase.

The current configuration consists of a signal conditioning carrier that fits within the footprint of a laptop pc. The significance of this benefit is that both components can be readily fit within the space of a messenger bag with a stackable rack to support both devices. The remainder of the extraneous equipment, sans prototype device, can fit within the confines of the bag. Thus bulk portability is obtained through this configuration.

The requirements of the load cell were deconstructed from the available passive extension data previously collected for elbow joints using a Biodex machine. Joint stiffness measurements would produce the peak loads that would be experienced by the device. Because of the relatively slowly changing and relatively static loads anticipated to be experienced by the device, a strain gage based load cell was determined to be necessary in order to appropriately measure the experienced load on the device by the PMA. Using the measured data, a peak load of 100 lbs was determined to be adequate to reflect the expected joint moments.

To facilitate load transfer from the PMA to the load cell, several configurations were examined however, a type with threaded studs located co-linear with the axis of the load cell was selected. This configuration would ensure good load transfer at the PMA and the device flange, low cross sensitivity to uneven loading as would be experienced by a circular type through-hole load cell, and ease of assembly for either side of the device.

A custom ring type load cell with strain gages mounted on the internal surface was also considered, however, presented significant issues related to the size of the ring cell required as well as accuracy over the low load regions. The overall compliance of the cell was also considered suspect due to the potential for a high degree of dynamic loading and its high degree of cross sensitivity and lack of stability against out of axis loading. A strain gaged plug type custom load cell was also considered, but the accuracy of the unit was determined to be suspect over the low load range.

An ELFM-2TE load cell was purchased from Entran, a subsidiary of Measurement Specialties, Inc. This load cell has a range of 5 lbs to 100 lbs and can measure loads in both tension and compression. The load cell operates in a full bridge configuration with a calibrated sensitivity of 7.35 mV at FSO.

For detection of the angular displacement of the side rails, a sensor had to be capable of responding appropriately to both static angular displacements and dynamic angular velocities. Two types of sensors were considered including a rotary potentiometer and a Hall effect sensor, which creates a linear voltage output from a rotational displacement of an element through a magnetic field. However, the Hall effect sensor required a constant physical offset and space constrictions within the side rails of the device and had been used previously in robotics with constantly moving arms. For the stability of the joint, product availability and the relatively static angular displacements exhibited during the bulk of the required activity of the device, a rotary potentiometer was selected as the choice for determining the angular displacements.

In the operation of the rotary potentiometer, the rotation of the sensor must not limit the operation of the device, thus a configuration with a 5000K resistance with

multiple turn capabilities was selected. The potentiometer was set at the midrange of the rotation limit before installation. However, for each assembly or disassembly, the sensor must be recalibrated for the given initial rotation of the wiper. A windowed average routine was originally used to eliminate the effects of the wiper crossing the internal windings of the rotary potentiometer which resulted in a high degree of noise. However, this routine proved ineffective and was replaced with a second order Butterworth Low-pass Digital filter with a cutoff frequency of 2 Hz. This change in the filtering technique permitted the minimization of the noise in the measured angle of the device to within +/- 0.5 degrees. All Digital Butterworth coefficients have been included as an appendix for review.

The rotary potentiometer has to be recalibrated upon reassembly for the offset voltage and the range of the scale in order to translate the measured voltage into angular displacement measurements. Within the signal conditioning system, the analog input channel used for the rotary potentiometer has been scaled and amplified across the measured voltage range through the range of motion of the device. This procedure improved the accuracy of the measured voltage signal and maximized the signal to noise ratio to eliminate consequential and dangerous effects of noise in the operation of the device.

For the purpose of controlling the pressure within the PMAs, there were a few configurations that were available. The typical arrangement noted in the research (Caldwell, 1990) consisted of a PMA constructed with two air lines with one supplying air to the muscle and one as a vent line. Electro-mechanical servo valves were located on lines with a pressure transducer on either line. However, this arrangement required the

use of the open and close functionality of several servo valves and the management of the non-linear action of each in order to adequately regulate the pressure within the PMA. This configuration permitted only discrete steps in the desired pressure dependent upon the number of valves used. Another significant drawback of this configuration was a significantly reduced life of a bottle fed air charge and required dual output control from the PID structure to regulate each valve as required. Additionally, this would require several output channels and an input channel on the data acquisition system requiring more system resources and increased system power requirements.

More recently, the development of linearly proportional electro-pneumatic transducers have permitted the capability to supply a pressure that is proportional across a voltage scale as applied to the regulator. The only calibration of the regulator is the balance the zero offset and the scale of the valve to the required range. This configuration required only one analog output channel to regulate the process pressure as opposed to the three channels required for the conventional configuration. However, due to the physical configuration of the system, there is a degree of inherent delay as the internal components trim to stabilize the backpressure through the valve to ensure a proportional output. However, this delay is inconsequential as the inherent delay of the developed force and the developed joint position dominate the system.

For the prototype device, a model TD6000 linearly proportional pressure regulator was purchased from Fairchild Industrial Products, Inc. The valve has a permissible input pressure range of 0-150 psig and a permissible linear output range of 0-120 psi. This regulator may be wired in either the forward bias configuration providing highest accuracy at the highest pressures or the reverse bias configuration providing

68

highest accuracy at the lowest pressures. Due to the requirements to maintain an extended joint configuration and to counter the developed load within the joint at this extended position, the controller would frequently have to maintain a higher pressure within the PMAs. Additionally, the low pressure region of the PMA operation was excluded. As a result, the regulator was wired in the forward bias configuration. The variable regulation range additionally prevents valve chatter possible with the operation of the two servo valves in a variable control state of the joint. A curve of the developed electropneumatic transducer pressure against the output voltage across it is shown in Figure 28.
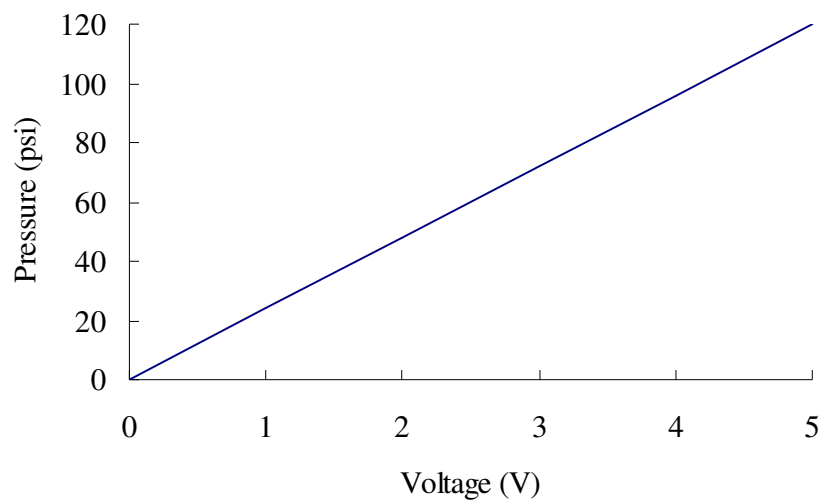
FIGURE 28 – Electro-Pneumatic Transducer Pressure Linearity

Also included is a high relief capability with a back feed vent. This configuration eliminates the need of a second valve in order to release the process pressure. The net cost of the electro-pneumatic transducer is high, however, considering the cost of the several servo valves and suitable pressure regulator in addition to the higher required degree of control required for the conventional configuration, the packaged assembly is cost competitive.

III.   DESIGN EVALUATION

A. Test Program

1. Overview

To evaluate the performance of the device, healthy human subjects were used. The required joint states were simulated through submaximal stimulation across the biceps brachii in order to activate and recruit the muscle fibers. Through the variation in the voltage applied across the brachii, the grade of the spatial recruitment level varied. Low level stimulations were used to simulate the contracted state of the joint through the inherent imbalance in the antagonistic function of the joint. Increased pulse stimulations were used in order to simulate the onset and prevalence of a spastic activity episode.

The built in data logging functionality of the PMA driven LLPS device was used relative joint data and the activity of the joint as the joint is excited through a series of simulated contractures. With the LLPS prototype device, the threshold load level was set from the evaluation of the coinciding load at the instance of activity.

2. Objectives

Each subject was fitted with stimulation pads, and the prototype device. A total of ten human subjects were used for the evaluation of the device. Each subject was tested in a blind configuration where the data was collected and segregated from the subject's identifying information prior to submission. The identification of each subject was maintained separate from the test data for each subject. The three primary objectives of the human subject testing involved the three primary functions of the prototype device. The device must maintain a prescribed joint angular position set beyond the grade of the

contracted state of the joint as simulated through the low grade excitation of the biceps brachii. At the onset of spastic activity episode, as triggered by the stimulation pads and determined through analysis of the data to detect the episode, the device must be capable of detecting the onset of the activity. Upon detection of the activity, the device must alternate from a joint angular position reference to a developed PMA load reference and maintain the reference developed PMA load until the activity has subsided. At the time of decline of the activity, as activated through the stimulation pads, the device must reject the spastic activity episode. Upon rejection, the device must seek a return to the joint angle reference position and maintain the prescribed joint angle reference position.

In addition to the functionality of the device in controlling the state of the joint, the functionality of the device controls must be validated. A change in the reference position must be followed by a measured change in the joint angle. A change in the reference developed PMA load during the load control mode must be followed by a measured change in the developed PMA load. The three function stop feature must be capable of stopping the operation of the device only after de-energizing the PMA circuits. The stop functions include the software stop button, the patient controlled stop button, and the internal overload stop button.

3. Methods

For the evaluation, the use of ten healthy subjects was utilized such that the control of the device would coincide with the applied stimulation across the joint. The subjects were required to be free from central nervous system or other neurological disorders that possessed the potential for extraneous signal generation across the actuated muscle fibers. Included disorders were multiple sclerosis, cerebellar ataxias, traumatic

brain injuries, spinal cord injuries, cerebral palsy, myocardial infarctions, or cerebro-vascular accidents. In addition, other health aspects evaluated included overall general health at the time of evaluation to ensure the correlation of the data.

Each subject will wear the device for a minimum of 10 episodes. Each subject shall be educated on the importance of the proper fit of the device. Upon application of the device, the fit will be inspected for critical features including proximity of the elbow joint to the coincident device joint, distal cuff angle, and the overall compliance of the cuff strap fit and the elbow saddle. The elbow saddle must be tight in order to limit the internal movement of the patient within the device which will render the joint angle tracking mode of the device ineffective.

The trial shall commence with a joint stiffness routine with the low grade contracture simulated with the stimulation pads. Through the range of motion the change from the passive elastic range to the active contraction range of the joint muscle will be evaluated through analysis of the data. This event will signify the onset of the activation of the contractile elements of the biceps brachii and the commencement of the high joint stiffness region. The measured load corresponding to this event will be noted and will be recorded within the PMA controller. The software control stop feature will be used in order to stop the call of the joint stiffness measurement routine.

During the course of the evaluation period of the PMA driven LLPS prototype device, the patient shall experience a minimum of 10 series of simulated spastic activity episodes with duration of at least 5 seconds for each one with a delay period of at least 5 seconds between each episode. This program shall permit the response of the device to respond to the state of the joint sufficiently.

The stop functionality of the shut off switch shall be used in order to terminate the function of the final program call.

Each subject was evaluated during the evaluation period for any physical responses to the applied electrical stimulation of the biceps that was considered to be of consequence.

B. Results

The bulk of the collected data is included as an appendix for each subject. For one specific test subject, the joint angle, load, and PMA pressure are shown below in Figure 29 over the course of the test evaluation. The spikes indicate the times at which the affected muscle was stimulated to simulate an episode.
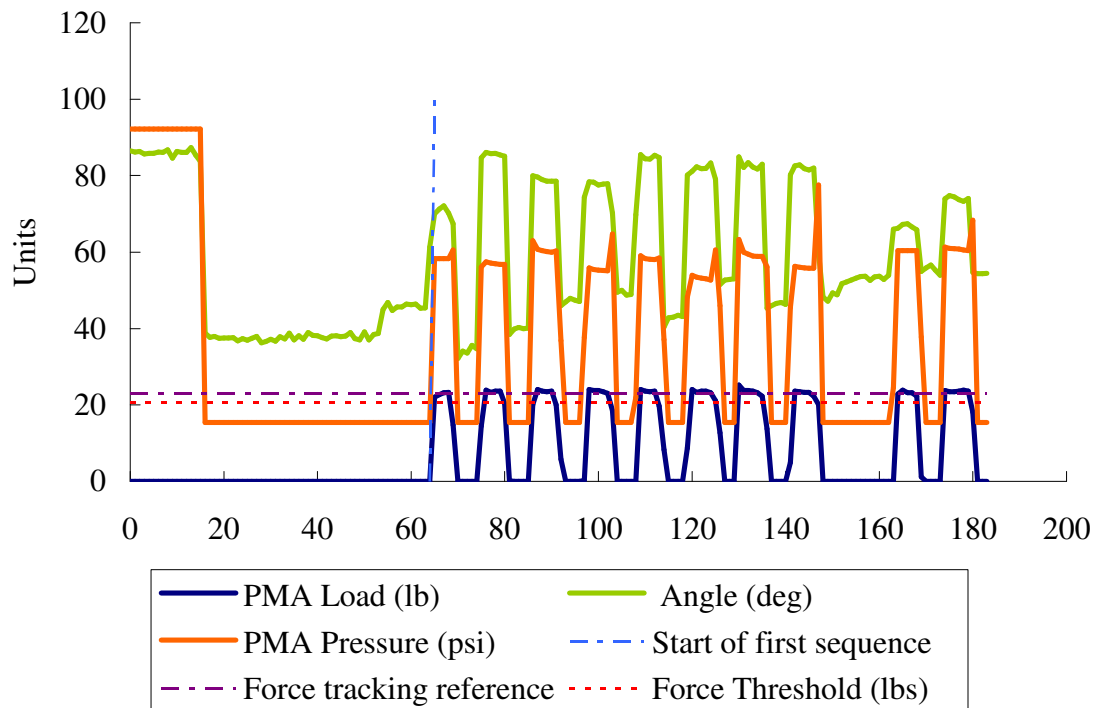
FIGURE 29 – Joint Trace Data

From the data, it is evident that there are two distinct regions to the evaluation. The first 60 seconds of the evaluation was directed towards evaluation of the angular position tracking capability of the device. From the data, there were three distinct joint positions that were evaluated over the course of the first 1 minute at 85 degrees, 37 degrees and 45 degrees. There is some degree of deviation from the desired joint set-point, however the joint position is returned to the desired set-point. Additionally, the time required for the device to achieve the new joint position is within 2 seconds of the activation of the position change during the strictly position tracking mode.

The switchover threshold between the Position-tracking (Primary) mode and the Force-tracking (Auxiliary) mode was set to 20 lbs force. The desired joint load was set to a value 3 lbs above the threshold at 23 lbs force. The distance between the threshold and the desired load was intentionally set to eliminate the risk of oscillating the operation of the device due to a successive change in load states at the threshold.

From the data in Figure 29, the force tracking increases at the onset of spastic activity to the threshold at which time the operation of the device is alternated to the joint load tracking mode. Leading the load increase is a demonstrated increase in the developed pressure within the PMAs designed to counter the load increase to maintain joint position. At the time that the threshold is reached, the pressure increase ramp-up is halted as the device seeks to stabilize the joint load using the PMA developed pressure. The cessation of the pressure increase permits the joint angle to collapse to a higher value than what was maintained before the onset of the activity to allow the device to maintain the joint load.

For each episode, the load ramp up and the ramp down are coincided with significant changes in the joint relative change in position within a second of the state of the joint crossing the threshold. An algorithm was applied to the data collected by the device to identify the instances in which the threshold has been reached and to identify the coinciding peaks in joint position rate of change and was included as an appendix. From this analysis, the peaks in the joint position rate of change and the threshold instances for the force trace were coincided within a second for each instance. This relationship is illustrated in Figure 30.
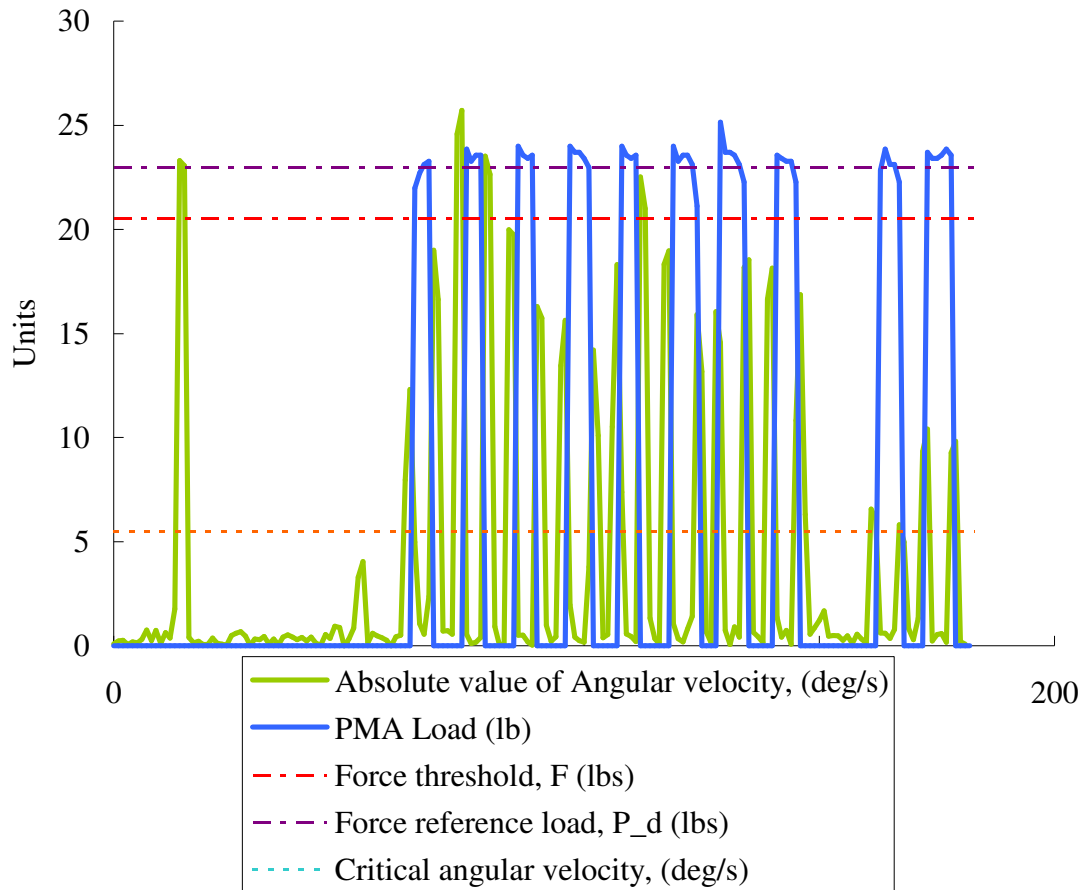
FIGURE 30 – Device Crossover Detection

The algorithm applied to the logged data also included an evaluation of the force tracking and the position tracking capability of the device. The deviation from the mean for the force trace beyond the threshold was calculated and evaluated as a sample size greater than 30 permitting the use of a normalized distribution in the evaluation. Each of the force trace data points with the exception of two points at the threshold change-over point were within a 98% interval around the joint load desired load at +/-1.093 lbs force. Including these instances at the thresholds, the 98% interval around the joint load desired load was determined to be +/- 1.443 lbs force. Some of the outlying data that affects the 98% interval may be attributable to the transition period between the position tracking and the joint load tracking modes, hence why they only occur on the ramp up and ramp down process of the force trace. With the transition periods excluded, the maximum error in the joint load maintained was within +/-4.5% of the desired joint load. The theoretical percentage error for the confidence interval was calculated to be 6.3%

In a similar manner, the joint position tracking capability of the device was evaluated using an algorithm to calculate the deviation away from the desired joint angle. The initial joint angle evaluation period from 18 seconds to 55 seconds where the joint angle was maintained constant was used given its larger sample size and the stretch of unbroken data due to transition periods. The deviation between each data point and the mean was calculated and evaluated using a normal distribution due to the sample size of greater than 30. The tracking capability of the device as indicated by the joint angle trace data fell entirely within the 98% window of +/- 1.59 degrees. Of note, in relation to the magnitude of the angles across which the device was evaluated, the accuracy on the joint

angle tracking mode of the device is within a desirable range of less than +/- 4% of the desired joint position.

For the joint tracking mode only, the time required to stabilize at the new position is negligibly small from the data shown above where the device is capable of settling at the new joint angle with minimum overshoot of the desired joint angle within 2 seconds for major and minor joint angle changes as demonstrated in Figure 31 where the device was changed from a joint angle of 85 degrees to a joint angle of 37 degrees and then from 37 degrees to 45 degrees.

For the transition period from the joint load tracking mode to the joint position tracking mode however appears to require a significantly higher amount of time to settle, although without significant overshoot of the desired joint position. As noticed from the data between excitations 1 through 8, the small duration between the excitations does not permit enough time for the device to return to the neutral joint angle position. However, the joint position collapses as the next excitation begins to occur before having fully restored from the previous excitation. Of note is the duration between the excitations 8 and 9. The settling of the joint position occurs within an eight second range which is longer than the five seconds between the excitation periods preceding the gap.

The remainder of the data for the above listed trace has been included in the appendix. The data and the curves for the other test subjects have also been included as a reference in the appendix.

IV. CONCLUSION

In evaluation of the device, the function has been validated to confirm that the basic requirements that were established have been met. The device, as shown through the evaluation, was capable of maintaining a prescribed relative joint position. Upon detecting the onset of the simulated spastic activity, the device was capable of distinguishing between the higher and lower grade activity. For activity that produced joint loads beyond the established threshold, the device changed from using the pressure to counteract the joint moment to permitting the joint to collapse and maintain the prescribed joint load. At the recession of the activity, the device was capable of self-rejection of the activity once the threshold for the loading has been achieved and the joint position has been re-established. At this time the device was capable of altering its operation mode to maintain the original prescribed joint relative position.

However, with the design of the device, the capability of the device to use pressure to counteract the lower grade contractures has proven to be difficult through analysis of the test data where the device collapsed by a significant portion of the range of motion even though the loading had not exceeded the threshold. Reducing the threshold would only serve to increase the frequency at which the device would incidentally be activated into the auxiliary joint load tracking mode. Further evaluation of the size of the PMAs used on the sides of the device would need to be pursued to ensure that the device is capable of adequately responding to the lower grade activations of the joint without permitting the device to collapse when it is not required.

Additionally, with the programming of the controller established, efforts would be well suited to converting the code to a format that would be more conducive to operating on a more trimmed package. Possible options include a stand alone signal conditioning board with a PLC coded algorithm to control the logic of the program. This would provide a more capable packaging that would increase the mobility of the patients when in a clinical setting and when the device left beyond a clinical setting.

The primary limit to the mobility of the developed device is the strong dependency upon a ready air supply. Even with measures taken to reduce the consumption of the air supply through dead-bands within the control logic of both operational modes, the device will still require more than 13 cubic feet of air to sustain an episode exceeding 10 minutes in duration. This volume of air is equivalent to the volume contained within a pony sized diving air tank at 3000 psi.

Initial design attempts had been focused on providing a portable air supply, however this strong dependency of the device on having a capable and reliable supply would limit the functionality and mobility of the device. The most probable result will be that the use of the device will be limited to the most in need who are found within an organized assisted living arrangement or in a therapy session type of arrangement where a form of a house air supply may be used.

REFERENCES CITED

Akima, H., Y. Kawakami, et al. (2000). "Effect of short-duration spaceflight on thigh and leg muscle volume. ." Medicine & Science in Sports and Exercise 32(10): 1743-1747.

Anderson, J., B. Snow, et al. (1988). "Efficacy of soft splints in reducing severe knee-flexion contractures." Developmental Medicine and Child Neurology 30(4): 502-508.

Blanton, S. and S. Grissom (2002). "Use of a sstatic adjustable ankle-foot orthosis following tibial nerve block to reduce plantar-flexion contracture in an individual with brain injury." Physical Therapy 82(11): 1087-1097.

Booth, J., M. Doyle, et al. (1983). "Serial casting for the management of spasticity in the head-injured adult." Physical Therapy 63: 1960-1966.

Braun, R. and M. Botte (1999). "Treatment of shoulder deformity in accquired spastiity." Clinical Orthopaedics & Related Research 368: 54-65.

Buchthal, F. and H. Schmalbrauch (1970), "Conraction times and fibre types in intact human muscle," Acta Physiologica Scandinavica 79:435-452,

Caldwell, D., G. Medrano-Cerda, et al. (1993). Braided pneumatic muscle actuator control of a multi-jointed manipulator. IEEE SMC Conference, Le Touquet, France.

Caldwell, D., G. Medrano-Cerda, et al. (1995). Control of pneumatic muscle actuators. IEEE Control Systems Magazine.

Caldwell, D., A. Razak, et al. (1993). Braided pneumatic muscle actuators. IFAC Conference on Intelligent Autonomous Vehicles, Southampton, UK.

Chou, C.-P. and B. Hannaford (1994). Static and dynamic characteristics of mckibben pneumatic artificial muscles. IEEE Robotics and Automation Conference.

Corry, I., A. Cosgrove, et al. (1998). "Botulinum toxin A compared with stretching casts in the the treatment of spastic equinus: a randomised prospective trial." Journal of Pediatric Orthopedics 18(3): 304-311.

Dylan, M., A. Sherman, et al. (1998). "Factors associated with contractures in acute spinal cord injury." Spinal Cord 36(6): 405-408.

Ferido, T. and M. Habel (1988). "Spasticity in head trauma and CVA patients: etiology and management." Journal of Neurosciences and Nursing 20(1): 17022.

Fernandex-Palazzi, F. and L. Battistella (1999). "Non-operative treatment of flexion contracture of the knee in haemophilia." Haemophilia 5 Supplement 1: 20-24.

Fitts, R., D. Riley, et al. (2000). "Microgravity and skeletal muscle." Journal of Applied Physiology 89: 823-839.

Flett, P., L. Stern, et al. (1999). "Botulinum toxin A versus fixed cast stretching for dynamic calf tightness in cerebral palsy." Journal of Pediatrics and Child Health 35(1): 71-77.

Gilbert, M. and T. Radomisli (1999). "Management of fixed flexion contracture of the elbow in haemophilia." Haemophilia 5 Supplement 1: 39-42.

Gracies, J., E. Elovic, et al. (1997). "Traditional pharmacological treatments for spasticity. Part I: Local Treatments." Muscle and Nerve 6 Supplement 1: 61-91.

Grissom, S. and S. Blanton (2001). "Treatment of Upper Motoneuron Plantarflexion contractures by using an adjustable ankle-foot orthosis." Archives of Physical Medicine & Rehabilitation 82: 270-273.

Grover, J., H. Gellman, et al. (1996). "The effect of a flexion contracture of the elbow on the ability to transfer in patients who have quadriplegia at the sixth cervical level." Journal of Bone & Joint Surgery - American Volume 78(9): 1397-1400.

Jansen, C., J. Windau, et al. (1996). "Treatment of a knee contracture using a knee orthosis incorporating stress-relaxation techniques." Physical Therapy 76(2): 182-186.

Kitahara, A., T. Hamaoka, et al. (2003). "Deterioration of muscle function after 21-day forearm immobilization." Medicine & Science in Sports & Exercise 35(10): 1697-1702.

Light, K., S. Nuzik, et al. (1984). "Low-load prolonged stretch vs. high-load brief stretch in treating knee contractures." Physical Therapy 64(3): 330-333.

MacKay-Lyons, M. (1989). "Low-load prolonged stretch in treatment of elbow flexion contractures secondary to head trauma: a case report." Physical Therapy 69(4): 292-296.

McPherson, J., A. Becker, et al. (1985). "Dynamic splint to reduce the passive component of hypertonicity." Achives of Physical Medicine, & Rehabilitation 66(4): 249-252.

Moseley, A. (1997). "The effect of casting combined with stretching on passive ankle dorsiflexion in adults with traumatic head injuries." Physical Therapy 77(3): 240-247.

Mosley, A. (1997). "The effect of casting combined with stretching on passive ankle dorsiflexion in adults with traumatic head injuries." Physical Therapy 77(3): 240-247.

Noritsugu, T. and T. Tanaka (1997). Application of Rubber Artifical Muscle Manipulator as a Rehabilitation Robot. IEEE/ASME Transactions on Mechatronics. 2.

Nuismer, B., A. Ekes, et al. (1998). "The use of low-load prolonged stretch devices in rehabilitation programs in the Paciific northwest Comment in." American Journal of Occupational Therapy 52(9): 770.

Otis, J., L. Root, et al. (1985). "Measurement of plantar flexor spasticity during treatment with tone-reducing casts." Journal of Pediatric Orthopedics 5: 682-686.

Pohl, M., S. Ruckriem, et al. (2002). "Effectiveness of serial casting in patients with severe cerebral spasticity: A comparison study." Archives of Phsical Medicine & Rehabilitation 83(784-90).

Prosser, R. (1996). "Splinting in the management of proximal interphalangeal joint flexion contracture." Hand Therapy 9(4): 378-386.

Quesada, P.M. 2004. Control of LLPS, J.B. Speed School of Engineering, University of Louisville.

Repperger, D., K. Johnson, et al. (1999). Nonlinear Feeback Controller Design of a Pneumatic Muscle actuator System. 1999 American Control Conference, San Diego, CA.

Repperger, D., C. Phillips, et al. (1997). A Study of Pneumatic Muscle Technology for Possible Assistane in Mobility. 19th Annual International conference on the IEEE Engineering in Medicien and Biology Society, Chicago, IL.

Roper, B. (1987). "The orthopedic management of the stroke patient." Clinical Orthopaedics & Related Research 219: 78-86.

Schulte, H. (1961). The Characteristics of the McKibben Artificial Muscle. The Application of External Power in Prosthetics and Orthotics. Washington, DC, National Academy of Sciences, National Research Council.

Shadmehr, R. and S. Wise, "A Simple Muscle Model." *Internet Source.* 1 January 2005. http://webhost5.nts.jhu.edu/reza/book/musclemodel.pdf,. 8 July 2006,

Stap, L. and P. Woodfin (1986). "Continuous passive motion in the treatment of knee flexion contractures. A case report." Physical Therapy 66(11): 1720-1722.

Steffen, T. and L. Mollinger (1995). "Low-load prolonged stretch in the treatment of knee flexion contractures in nursing home residents." Physical Therapy 75(10): 886-895.

Tardieu, C., A. Lespargot, et al. (1988). "For how long must the soleus muscle be stretched each day to prevent contracture?" Developmental Medicine and Child Neurology 30(1): 3-10.

Vattanasilp, W., L. Ada, et al. (2000). "Contribution of thixotropy, spasticity, and contracture to ankle stiffness after stroke." Journal of Neurology, Neurosurgery, and Psychiatry 69(1): 34-39.

Widrick, J., S. Trappe, et al. (2002). "Unilateral lower limb suspension does not mimic bed rest or spaceflight effects on human muscle fiber function." Journal of Applied Physiology 93: 354-360.

Yarkony, G. and V. Sahgal (1987). Contractures. A major complication of craniocerebral trauma. Clinical Orthopaedics. 219: 93-96.

APPENDIX I: SCAFFOLD LOAD MAPPING

Schematic of the Scaffold Loading Array was developed in order to analyze the

mechanical design of the scaffold elements including specifically the side rails.
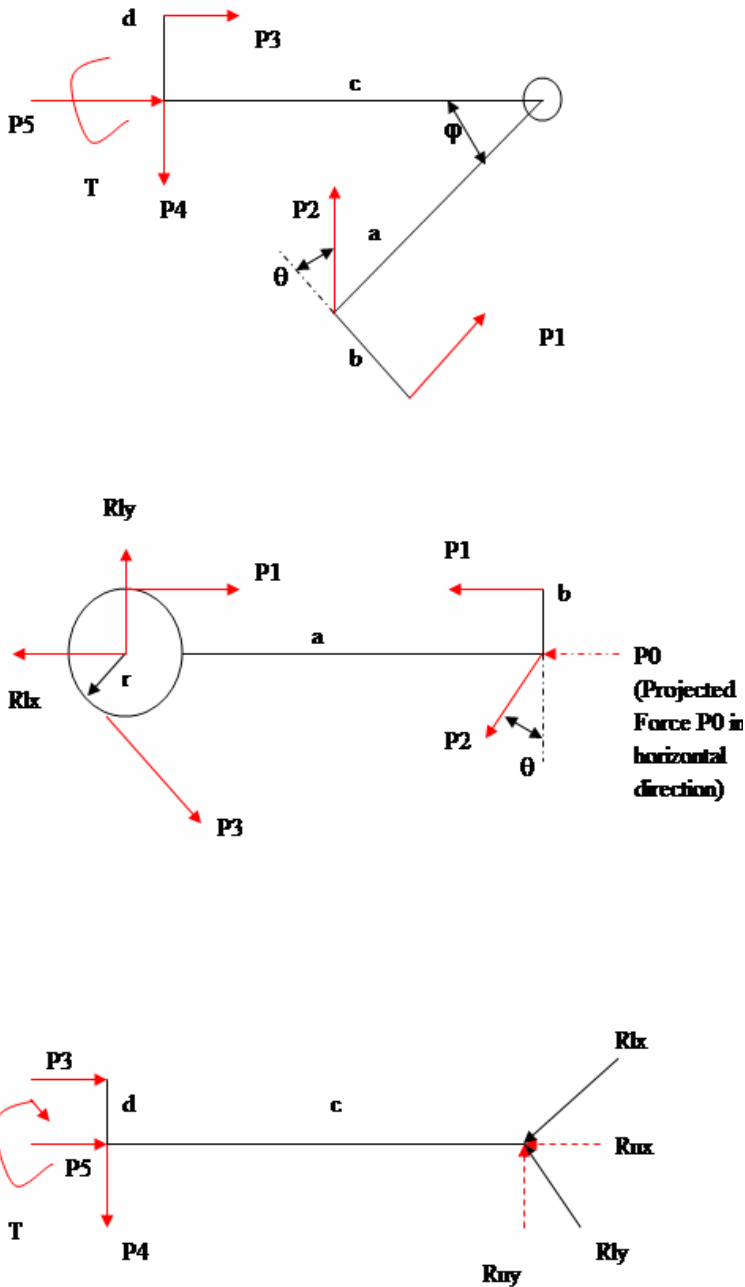
FIGURE 31 – Scaffold Load Array

The subsequent relationships for each of the loads identified in the preceding load array were derived through the use of matrix analysis software using Matlab 6.5. For the horizontal reaction force, Rlx, on the lower scaffold having side length a, two cases were developed whether P2 is measured or not measured directly. Where P2 is not measured, Rlx is given by

$$Rlx = P3 \cdot \left(\cos \varphi - \frac{b}{a} \tan \theta \right) \tag{1}$$

where P2 is the applied force on the saddle of the scaffold, P3 is the developed PMA load, a is the side rail length, b is the side rail PMA offset distance, θ is the load angle from normal to the side rail, and φ is the joint angle where 180 degrees is full extension.

When P2 is measured directly, Rlx is given by

$$Rlx = P3 \cdot \left[\frac{a \cdot \cos \theta}{b} \left(\cos \varphi - \frac{b}{a} \tan \theta \right) \right] \tag{2}$$

Subsequently, there are two cases developed for determining the vertical reaction force on the lower scaffold, Rly. When the applied saddle load, P2, is not known and measured, the reaction force is given by

$$Rly = P3 \cdot \left(\frac{b}{a} + \sin \varphi \right) \tag{3}$$

Otherwise, when the applied saddle load, P2, is known and measured, the reaction force is given by

$$Rly = P2 \cdot \cos\theta \cdot \left(1 + \frac{a}{b}\sin\varphi\right) \qquad (4)$$

The magnitude of the reaction force is given by

$$R = \sqrt{Rlx^2 + Rly^2} \qquad (5)$$

where R is the reaction force magnitude, and Rlx and Rly are the horizontal and vertical reaction forces, respectively.

The angle of the reaction load was determined with respect to the schematic shown for the lower scaffold where the 0 degree orientation commences from the distal end of the rail and radiates toward the coincident joint. This reaction angle is given by

$$\psi = \arctan\left(\frac{Rly}{Rlx}\right) \qquad (6)$$

where ψ is the reaction angle, and Rlx and Rly are the horizontal and vertical reaction loads, respectively.

The projected saddle load in the horizontal direction, P0, is given by

$$P0 = P2 \cdot \sin\theta \qquad (7)$$

86

The reaction load on the scaffold flange, P1, is given by

$$P1 = P3 \qquad (8)$$

where P1 is the scaffold flange load, P3 is the developed PMA load.

Where the developed PMA load is not measured directly, the scaffold flange load is determined by

$$P1 = P2 \cdot \frac{a}{b} \cos\theta \qquad (9)$$

where P1 is the scaffold flange load, P2 is the projected saddle load, a is the side rail length, and b is the PMA side rail offset and θ is the load angle from normal to the side rail.

Where P2 is not measured directly, it can be calculated using the developed PMA load using

$$P2 = P3 \cdot \frac{b}{a \cdot \cos\theta} \qquad (10)$$

where P2 is the saddle load, P3 is the developed PMA load, a is the lower side rail length, b is the side rail PMA offset, and θ is the load angle from normal to the side rail.

For the upper side rail, the translated horizontal reaction force on this side rail is given by

$$Rux = Rly \cdot \sin \varphi + Rlx \cdot \cos \varphi \qquad (11)$$

where Rux is the horizontal reaction load on the upper saddle, Rlx and Rly are, respectively, the horizontal and vertical reaction loads on the lower saddle, and φ is the joint angle.

The translated vertical reaction force on the upper side rail is given by

$$Ruy = Rly \cdot \cos \varphi - Rlx \cdot \sin \varphi \qquad (12)$$

The vertical component of the upper saddle reaction force is given by

$$P4 = Ruy \qquad (13)$$

where P4 is the vertical saddle reaction force and Ruy is the vertical reaction force on the upper saddle.

The horizontal component of the upper saddle reaction force is given by

$$P5 = Rux - P3 \qquad (14)$$

where P5 is the horizontal saddle reaction force, Rux is horizontal reaction load on the upper saddle, and P3 is the developed PMA load.

Because the upper saddle is pinned to prevent rotation of the saddle, a torque is developed at the upper saddle-upper side rail interface that is given by

$$T = P3 \cdot d + P4 \cdot c \tag{15}$$

where T is the developed torque, P3 is the developed PMA load, P4 is the vertical reaction from the upper saddle, d is the upper side rail PMA offset, and c is the upper side rail length.

The upper rail transverse torque developed across the upper rail due to the lateral offset in the side rail is given by

$$T_{u,trans} = Rux \cdot f \tag{16}$$

where $T_{u,trans}$ is the upper rail transverse torque, Rux is the horizontal reaction force on the upper side rail, and f is the lateral offset.

The upper rail axial torque developed across the upper rail due to the width of the saddle is given by

$$T_{u,axial} = P4 \cdot g \tag{17}$$

where $T_{u,axial}$ is the upper rail axial torque, P4 is the vertical reaction force at the upper saddle, and g is the upper saddle radius.

The lower rail transverse torque developed across the lower rail due to the lateral offset in the side rail is given by

$$T_{l,trans} = Rlx \cdot f \tag{18}$$

where $T_{l,trans}$ is the lower rail transverse torque, Rlx is the horizontal reaction force on the lower side rail, and f is the lateral offset.

The lower rail axial torque developed across the lower rail due to the width of the saddle is given by

$$T_{l,axial} = P2 \cdot h \cdot \cos\theta \tag{19}$$

where $T_{l,axial}$ is the lower rail axial torque, P2 is the reaction force at the lower saddle, θ is the load angle from normal to the side rail, and h is the lower saddle radius.

APPENDIX II: DEVICE DRAWINGS

Component Draft Documents
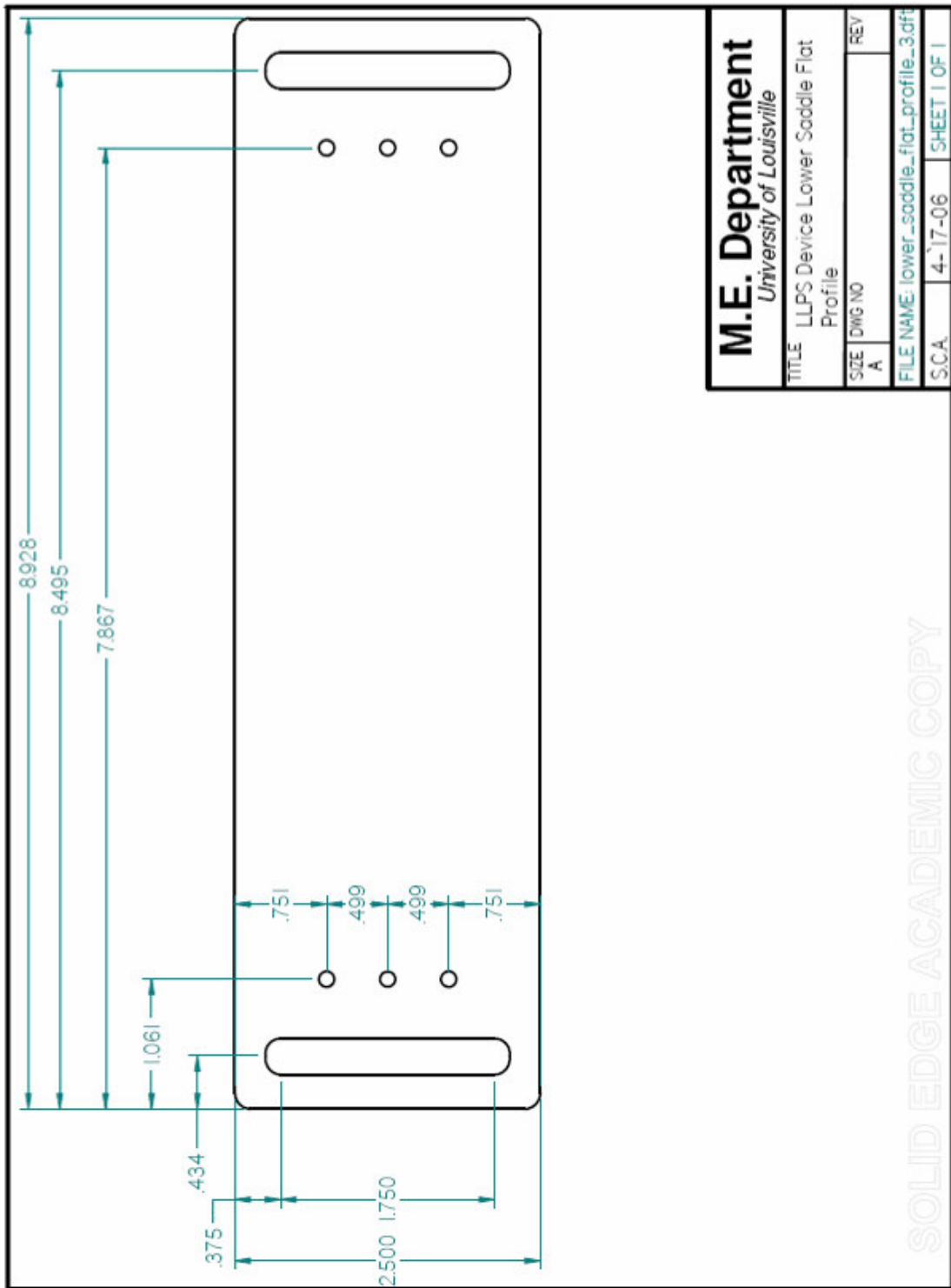
FIGURE 32 – Lower Saddle Flat Profile

M.E. Department
University of Louisville

TITLE LLPS Device Lower Saddle

SIZE A | DWG NO | REV

FILE NAME: lower_saddle_r3.dft

S.C.A. | 4-17-06 | SHEET 1 OF 1

R 2.250

R 2.125

.125
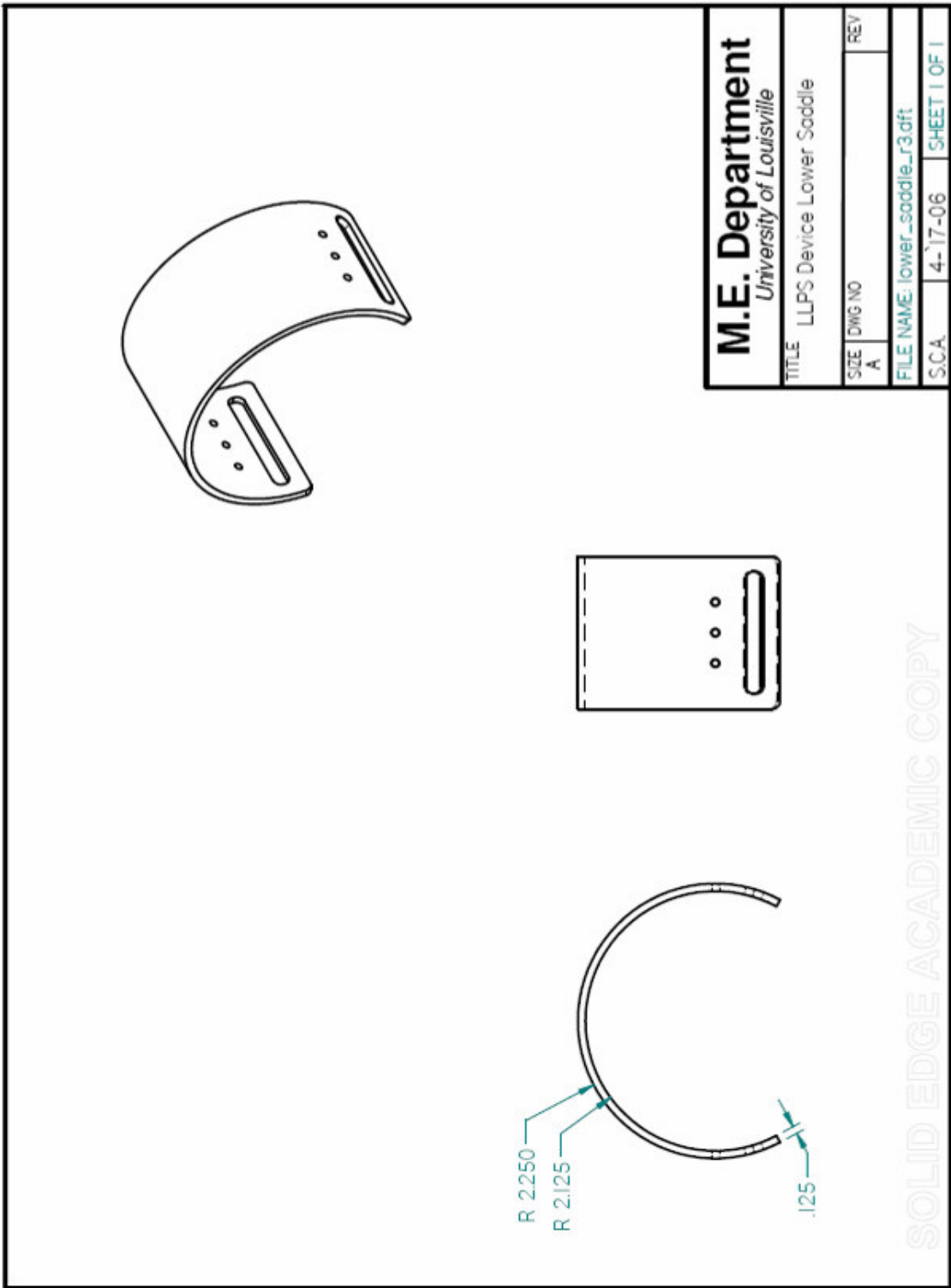
FIGURE 33 – Lower Saddle Profile

The drawing title block reads:

M.E. Department
University of Louisville

TITLE: LLPS Device Lower Side Rail

SIZE: A
DWG NO
REV

FILE NAME: lower_side_rail_r3.dft
S.C.A.   4-17-06   SHEET 1 OF 1

Dimensions shown: .750, 6.000, 3.908, 2.800, 37°, .125, 1.125
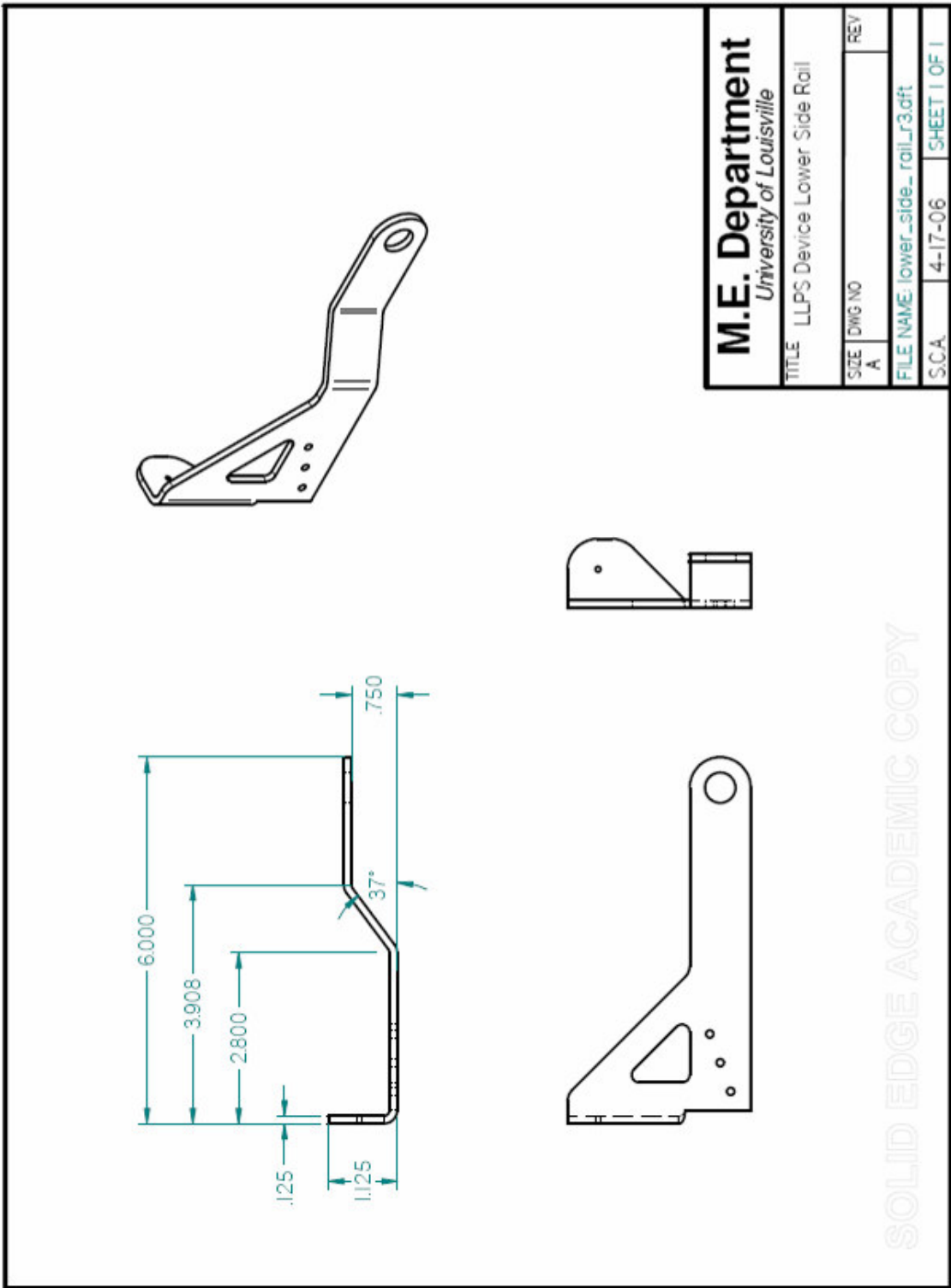
FIGURE 34 – Lower Side Rail Profile

94

FIGURE 35 – Lower Side Rail Flat Profile

FIGURE 36 – Radial Guide

R 2.250
R 2.375
.125

M.E. Department
University of Louisville
TITLE   LLPS Device Upper Saddle
SIZE DWG NO
A
FILE NAME: upper_saddle_r3.dft
S.C.A.   4-17-06   SHEET 1 OF 1
REV
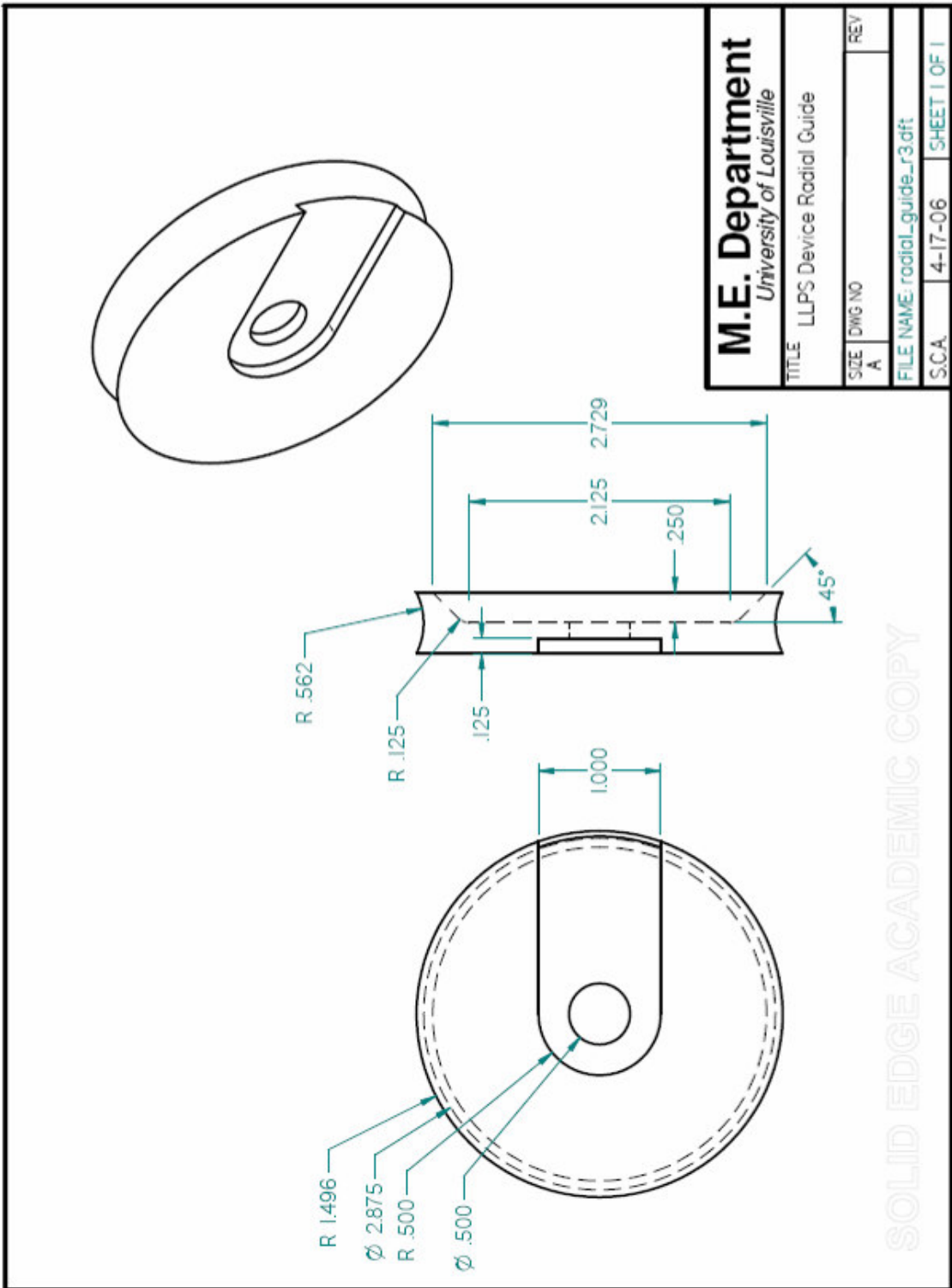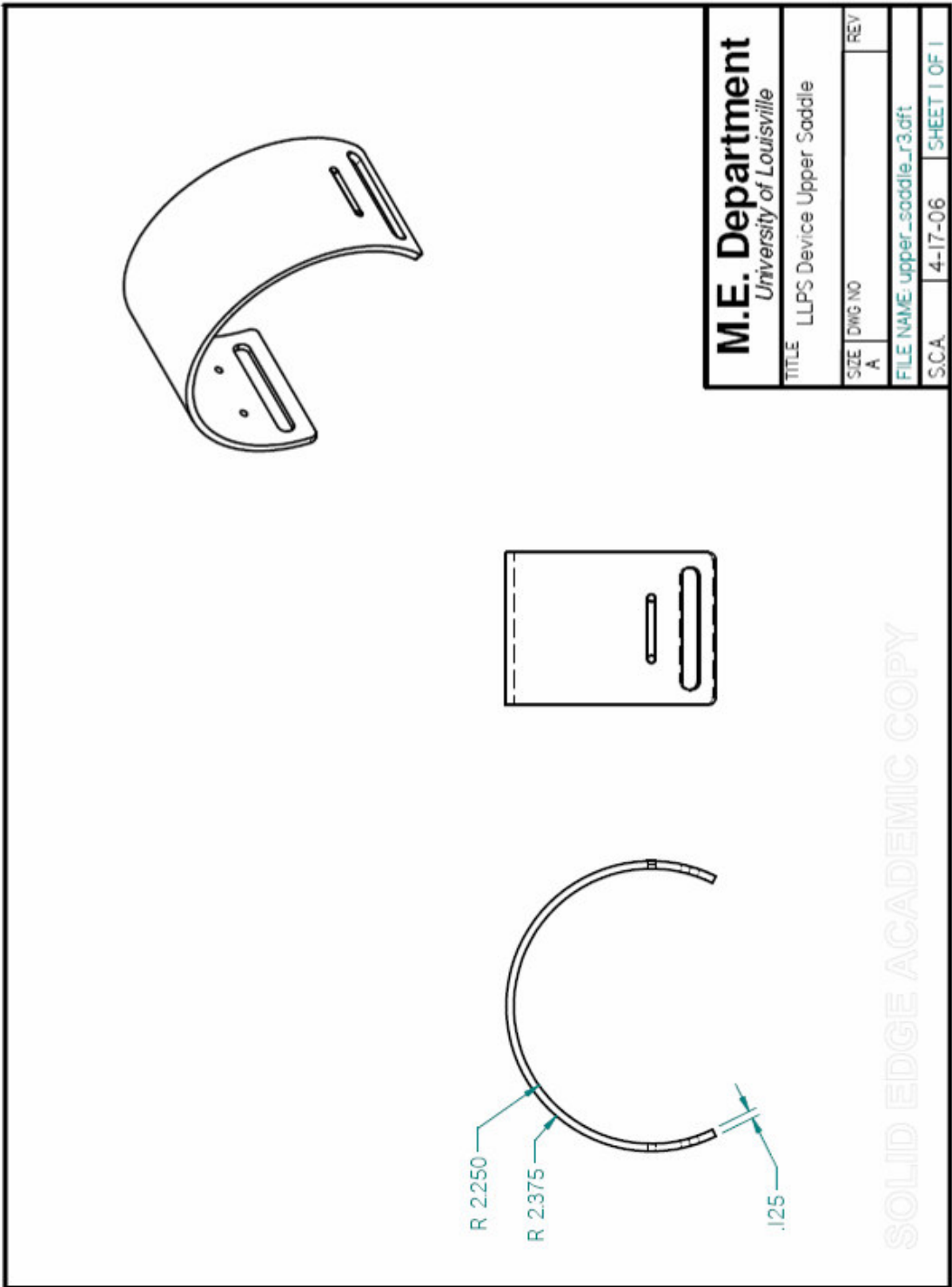
FIGURE 37 – Upper Saddle Profile
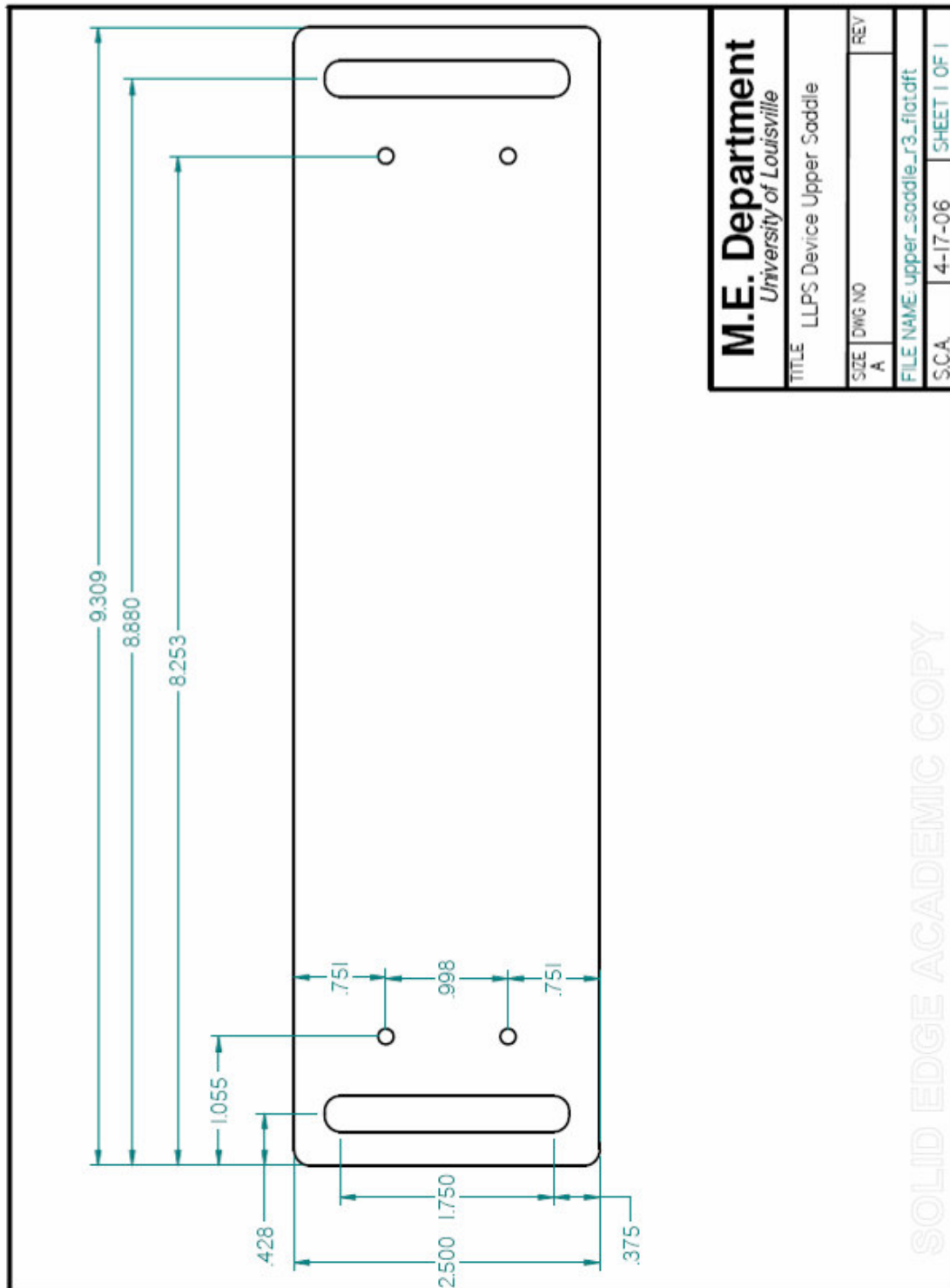
FIGURE 38 – Upper Saddle Flat Profile
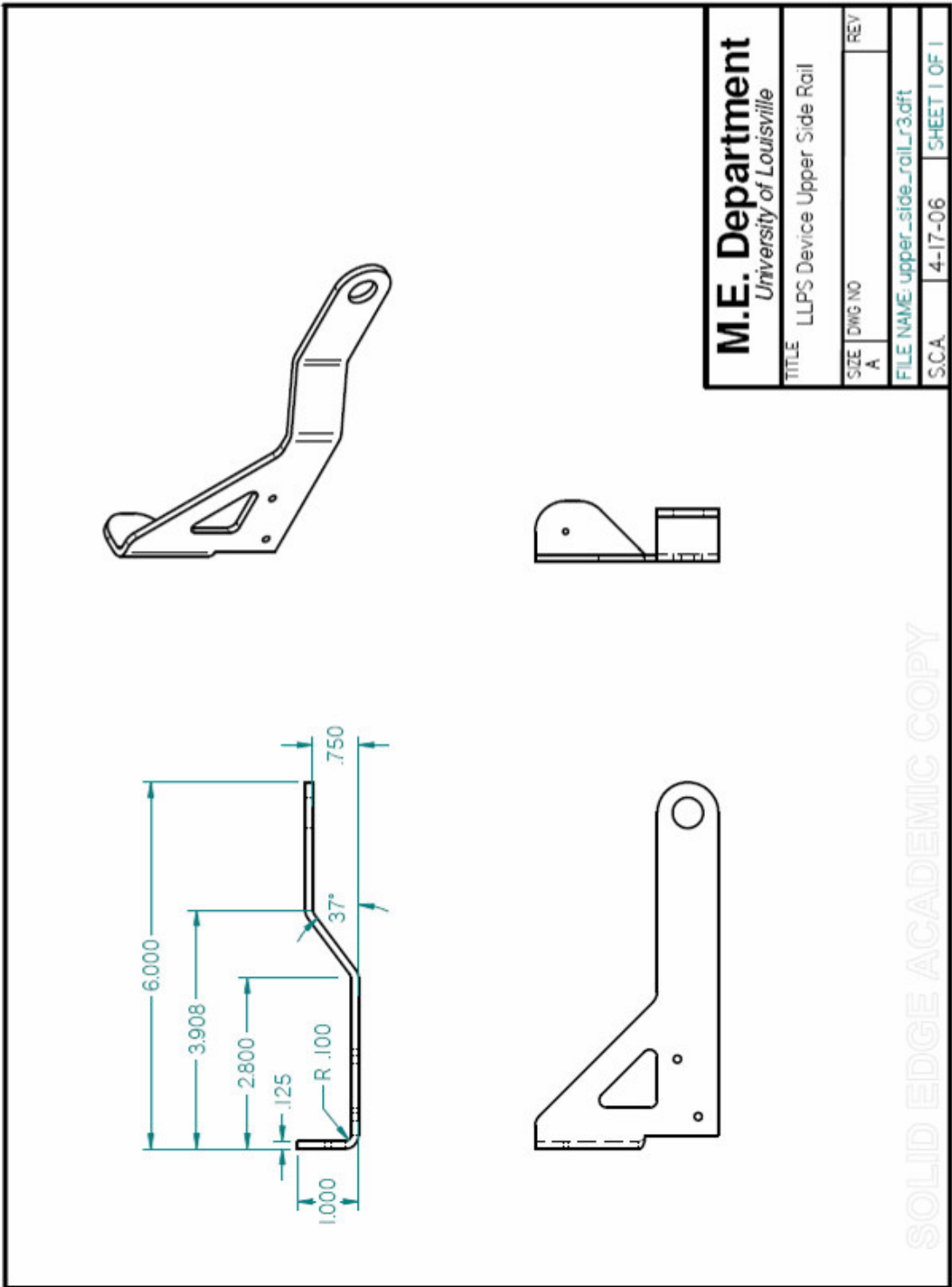
FIGURE 39 – Upper Side Rail Profile
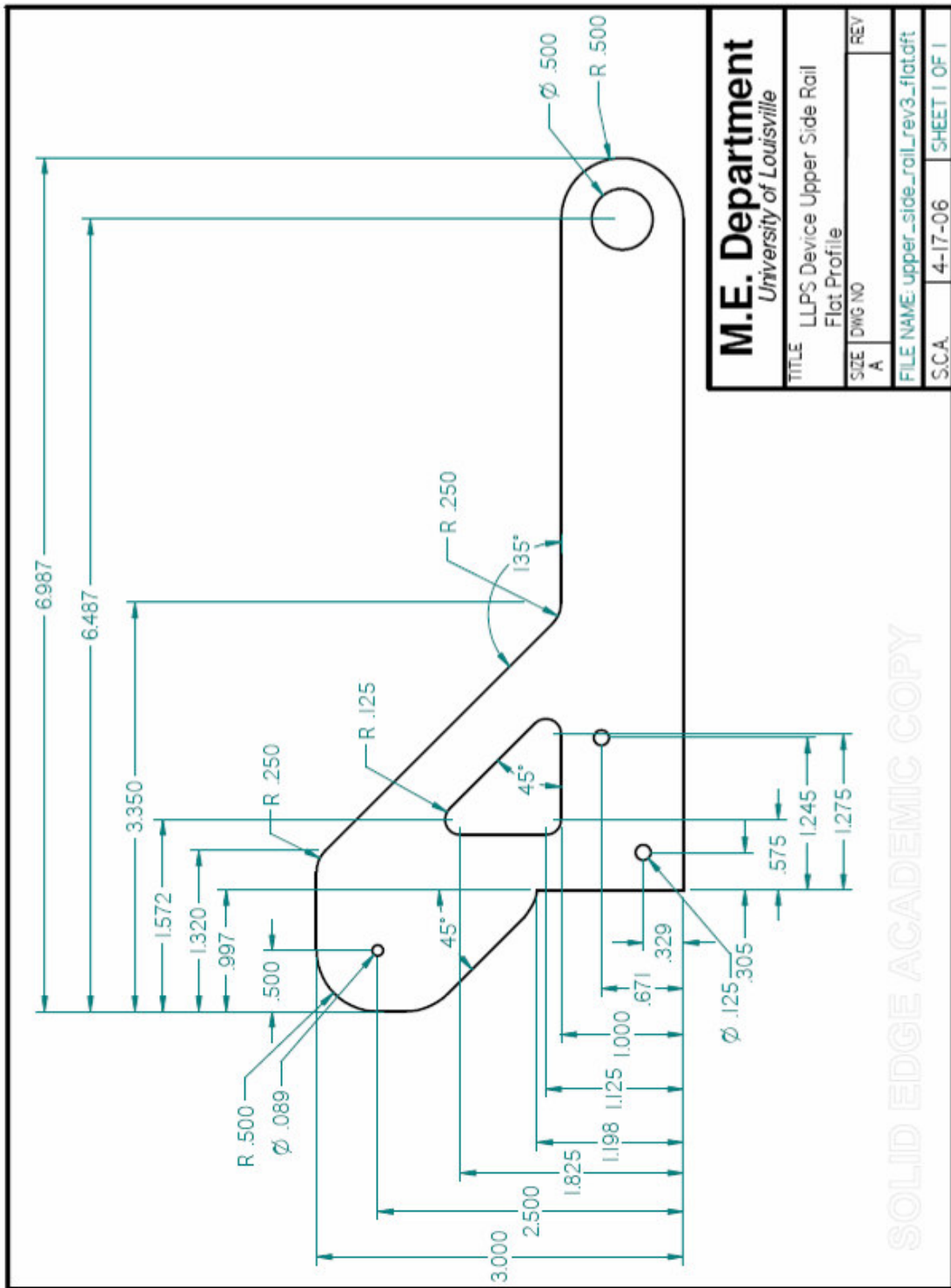
FIGURE 40 – Upper Side Rail Flat Profile

APPENDIX III: PMA MECHANICS

For an initial PMA, the constant parameters include the initial diameter d_0, initial length, L_0, the initial fiber interweave angle, θ_0 and the other defining parameters including the helix fiber length and the diametric distance parameter.

The helix fiber length is calculated using

$$h = \frac{L_0}{\cos \theta_0} \qquad (20)$$

where h is the helix fiber length, L_0 is the initial length, and θ_0 is the initial fiber interweave angle.

The diametric distance parameter is calculated using

$$f = \frac{d_0}{\sin \theta_0} \qquad (21)$$

where f is the diametric distance parameter, d_0 is the initial diameter of the PMA, and θ_0 is the initial fiber interweave angle.

Using this original information, the new fiber angle at a new PMA length is calculated using

$$L' = h \cdot \cos \theta \qquad (22)$$

where L' is the new length, and h is the helix fiber length, and θ' is the new fiber angle.

From the new fiber angle, the new PMA diameter was calculated using a modified form of the diametric distance parameter from above where

$$d' = f \cdot \sin \theta \tag{23}$$

where d' is the new diameter of the PMA, f is the diametric distance parameter, and θ' is the new fiber angle.

For the iterative mapping of the PMA length in order to determine the appropriate PMA size, the force, pressure and interweave properties were analyzed. For the level of the calculations required, the work and energy force relationship developed by Schulte in 1962 sufficed in order to approximate the calculations and provide suitable optimization and selection. The high pressure region of PMA optimization was excluded removing the direct need for the higher accuracy predictions available (Caldwell, 2000) to rectify the errors present in this higher pressure region.

The force generated by the PMA at a given position and pressure is given by

$$F = \frac{\pi \cdot P \cdot d_0^2}{4} \left(3 \cdot \cos^2 \theta - 1\right) \tag{24}$$

where F is the force, P is the pressure, d_0 is the original diameter, and θ is the current interweave angle.

To determine the length and the diameter of the PMA at a given force and pressure, the previous relationship is rearranged for θ as shown below.

$$\theta = \arccos\left[\sqrt{\frac{1}{3}\cdot\left(\frac{4\cdot F}{\pi\cdot P\cdot d_0^2}+1\right)}\right] \tag{25}$$

The helix fiber length and the diametric distance parameters are used to calculate the new length and diameter, respectively, for the new interweave angle as shown below.

$$L = h\cdot\cos\theta \tag{26}$$

$$d = f\cdot\sin\theta \tag{27}$$

The optimization curves for length and force at different pressures dependent upon force are shown in Figures 41 and 42.
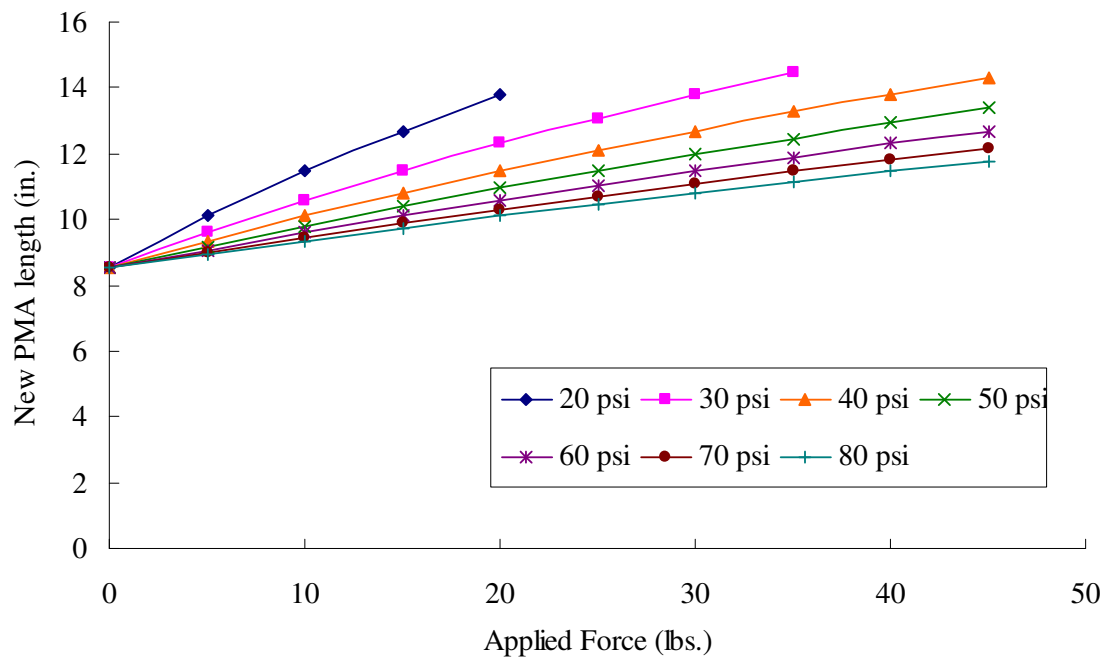
FIGURE 41 – PMA Length Versus Force Metrics
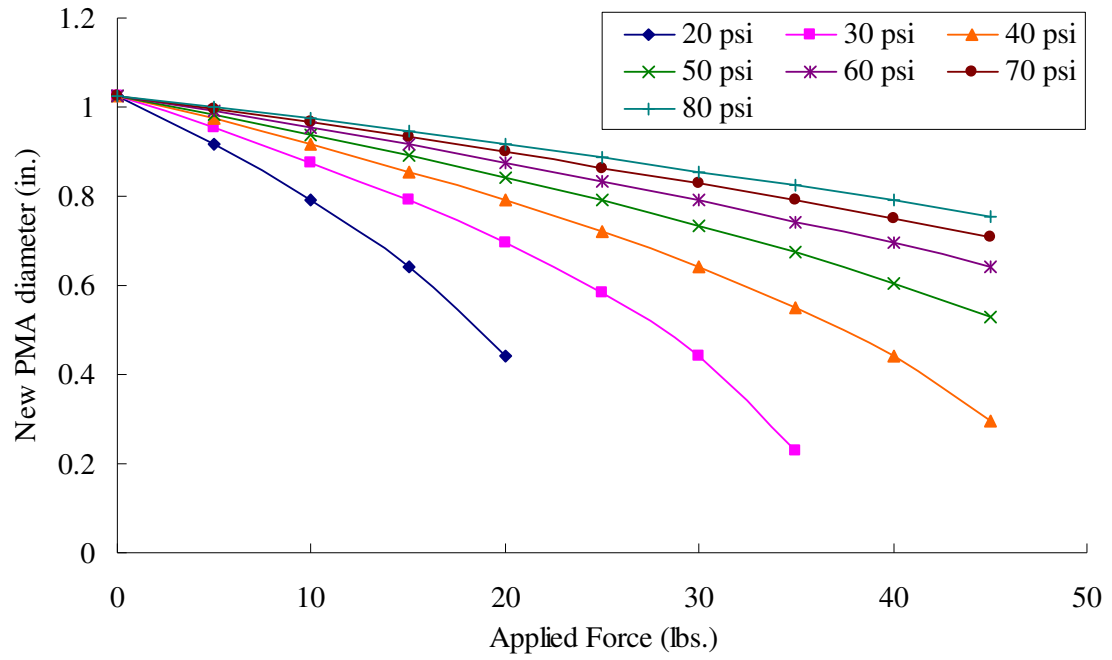
FIGURE 42 – PMA Diameter Versus Force Metrics

APPENDIX IV: JOINT MODELING PARAMETERS

From the Scaffold Load Array, the prototype constants are known. The proximal and distal side rail lengths are each the same. The proximal and distal side rail PMA offset lengths are each the same. The prototype rotational inertia was calculated using a solid modeling program with the density of aluminum known. The constants were converted from English standard units to SI units for the purpose of modeling and are listed below in the Table 4.

TABLE IV

PROTOTYPE PARAMETERS

Parameter Name	English Units	SI units
Side Rail Length, a and b	4.5 in	0.1143 m
Side Rail PMA offset length, c and d	2 in	0.0508 m
Prototype Rotational Inertia, I_{prot}	68.66 lb_m-in^2	0.02009 kg-m^2

The rotational inertia of the proximal and distal arm segments were tabulated from tabled data available (Winters, 1990) for a typical human subject of mass 79.4 kg and height of 1.78 m. The rotational inertial of the human subject was calculated from the mass and radius of gyration of the patient and is shown in Table V in SI units.

Using Joint Extension Data shown in Figure 10 for measured joint moment versus joint extension in degrees, the series elastic stiffness and parallel elastic stiffness elements were obtained. The series elastic element stiffness was obtained from the slope of low stiffness region of the curve and the parallel elastic element stiffness was obtained from the slope of the high stiffness region of the curve. The knee of the curve was established as a reference to distinguish between the high and low stiffness regions. All

stiffness data was converted from English Standard units to SI units for the purpose of the model.

The parallel resistive force element (damping coefficient) of the elbow joint was obtained from the EMG trace data obtained by (?) for the biceps muscle. With a twitch time of 52 ms for the biceps brachii, the resistive force element was obtained using

$$b = \frac{2\tau}{K_{SE} + K_{PE}} \tag{28}$$

where b is the resistive force element, K_{SE} and K_{PE} are the series and parallel element stiffnesses, respectively, and τ is the twitch time of the biceps brachii in seconds. The elbow joint and associated muscles were used for the model because of its faster response time compared to that of the knee joint.

TABLE V

SUBJECT PARAMETERS

Parameter Name	SI units
Proximal Arm Segment Inertia, I_{prox} (kg-m^2)	0.1005
Distal Arm Segment Inertia, I_{dist} (kg-m^2)	0.2417
Muscle Series Element Stiffness, K_{SE} (N/m)	6077
Muscle Parallel Element Stiffness, K_{PE} (N/m)	371200
Muscle Parallel Element Damping Coef., b_m (N-s^2/m)	39240

The PMA stiffnesses and inflation and deflation dynamics were obtained from the empirical relationships using a force and extension curve for the PMA to determine elastic stiffness in the low stiffness region similar in process to that used to evaluate for the muscle elastic elements through calculating the slope. The PMA damping coefficient

was determined through the twitch time in a manner similar to that used to calculated the

damping coefficient for the muscle parallel resistive element.

APPENDIX V: JOINT MODELING PROCEDURE

TABLE VI

PHYSICAL PARAMETERS FOR JOINT MODEL

Parameter Name (units)	Value
Proximal Rail length, a (m)	0.1134
Distal Rail length, c (m)	0.1134
Proximal Rail PMA Offset, b (m)	0.0508
Distal Rail PMA Offset, d (m)	0.0508
Proximal Arm Segment Inertia, I_{prox} (kg-m^2)	0.1005
Distal Arm Segment Inertia, I_{dist} (kg-m^2)	0.2417
Prototype Inertia, I_{prot} (kg-m^2)	0.02009
Muscle Series Element Stiffness, K_{se} (N/m)	6077
Muscle Parallel Element Stiffness, K_{pe} (N/m)	371200
Muscle Resistive Element Damping, b_m (N-s^2/m)	39240
PMA Stiffness, K_{pma} (N/m)	1417
PMA Damping, b_p (N-s^2/m)	1104

The Proximal and Distal Rail lengths, a and c, respectively, were defined within the original structure design at 113.4 mm in length for both arms. The Proximal and Distal Rail PMA Offsets, b and d, respectively, were defined within the original structure design at 50.8 mm in length for both arms segments.

The Prototype Inertia was calculated for the combined assembly of the brace structure about the coincident joint between the proximal and distal segments as I_{prot} with a mass moment of inertia of 0.02009 kg-m^2. The inertia for the upper arm and the fore arm and hand segments at the elbow joint were calculated using the segment mass and the length for each to calculate the radius of gyration and the inertia about the center of gravity of each segment. For the purpose of the calculations, a person of 177.8 cm in height and with a mass of 80 kg was used. The anthropometric data was obtained from

tabled data (Plagenhoef and Patterson 1971, and Lea and Febiger, 1973) for each segment.

The radius of gyration was given by

$$I_J = m_S \left(L_S r_{SL} \right)^2 \tag{29}$$

where r_{SL} is the radius of gyration segment length ratio, I_J is the mass moment of inertia about the joint, m_S is the segment mass and L_S is the segment length.

The segment length was obtained using

$$m_S = M_{SL} m \tag{30}$$

where m_S was the segment mass, M_{SL} was the patient segment mass ratio, and m is the patient body mass.

The segment length, L_S, was obtained using

$$L_S = L_{SL} L \tag{31}$$

where L is the overall patient height and L_{SL} was the segment length ratio.

From the Hill model and the Joint Extension Curve, the series elastic element stiffness, parallel elastic element stiffness, and the muscle resistive element damping was determined. For the low activation region, the series elastic element stiffness was obtained by calculating the slope of the region using

$$K_{SE} = \frac{M_2 - M_1}{\theta_2 - \theta_1} \qquad (32)$$

where K_{SE} is the series element stiffness, M_1 and M_2 are the moments measured at locations 1 and 2, respectively, and θ_1 and θ_2 were the angles at where the moments were measured at locations 1 and 2, respectively.

For the high activation region, the parallel elastic element stiffness was obtained by calculating the slope of the region using

$$K_{PE} = \frac{M_4 - M_3}{\theta_4 - \theta_3} \qquad (33)$$

where K_{SE} is the series element stiffness, M_3 and M_4 are the moments measured at locations 3 and 4, respectively, and θ_3 and θ_4 were the angles at where the moments were measured at locations 3 and 4, respectively.

Using the EMG twitch time, the resistive element damping was obtained using

$$b_m = \frac{2\tau}{\left(K_{SE} + K_{PE}\right)} \qquad (34)$$

where b_m was the resistive element damping, τ was the twitch time for the muscle and K_{SE} and K_{PE} were the elastic elements for the series and parallel elements, respectively.

Using a single degree of freedom system to model the system degrees of freedom for the joint angle motion, transfer functions were developed for each load case of the joint whether it would require the primary mode for maintaining joint position or the auxiliary mode for maintaining joint load. The model is shown in Figure 43.
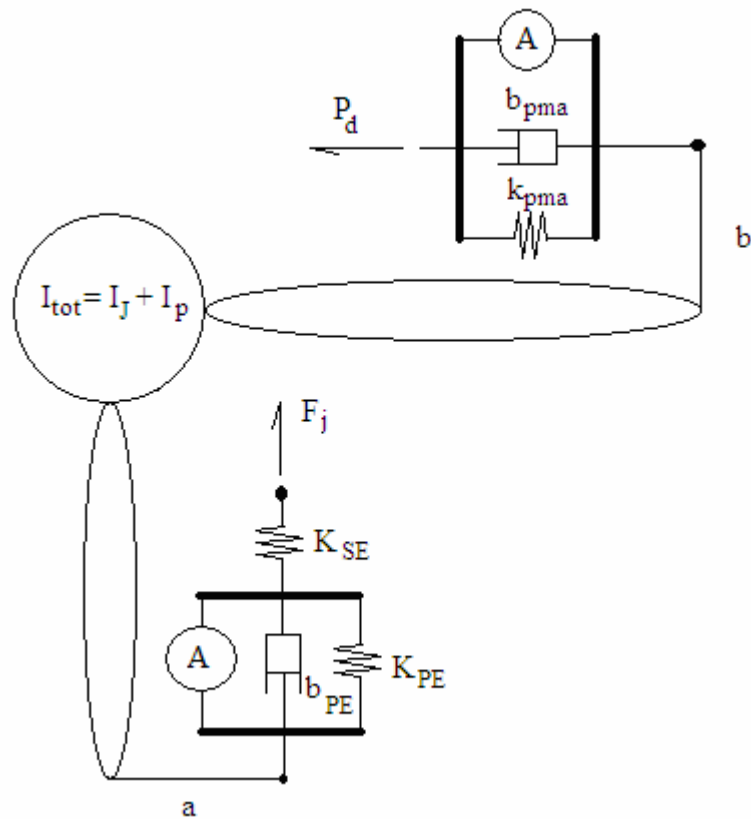
FIGURE 43 – Combined Joint and Device Model

For the Primary Mode for maintaining joint position, the assumptions were made that the resistive element on the joint muscle minimizes the effects of the parallel elastic element to a negligible effect and thus the effects of both of the parallel elements can be neglected. Additionally, the developed force of the PMA as a result of the required angle is approximately linear for the narrow range over which the device will operate within this mode. For the small deviations in the joint angle, the relative motion of the elastic

and resistive elements was approximated about the center of the joint to angular relative displacements.

The joint moments were summed about the elbow joint such that

$$\Sigma M_o = -aF_J + bF_{pma} = I_{tot}\alpha \tag{35}$$

where F_J was the force exerted by the muscle, F_{pma} was the force exerted by the PMA, and I_{tot} was the total rotational inertia of the joint and the prototype. The force exerted by the muscle could be expanded to the force due to the extension or contraction of the series elastic element given by

$$F_J = K_{SE}\left(x_1 - x_1^*\right) \tag{36}$$

where K_{SE} is the elastic stiffness of the series element and x and x* are the initial and new positions of the element. For small angles, the relative change in the elastic element was approximated as the angular displacement, θ, as given by

$$\left(x_1 - x_1^*\right) = a\theta \tag{37}$$

where θ is the angular displacement and a is the approximate offset of the muscle from the joint. Accordingly, the rate of change in the elastic element position is given as below.

$$\dot{x} = a\dot{\theta} \tag{38}$$

In a similar manner, the reactive force due to the PMA was given by the expansion of its components of

$$F_{pma} = b\left[K_{pma}\left(y_1 - y_1^*\right) - b_{pma}\dot{y} + P_d\right] \tag{39}$$

Where K_{pma} is the stiffness of the PMA element, b_{pma} is the resistive damping element of the pma, P_d is the force due to the change in pressure of the PMA, b is the offset of the PMA on the brace structure, and y and y* are the initial and the stretched lengths of the PMA. In a similar manner to the series elastic element for the muscle, the small deflections of the element deflections can be resolved at the joint to angular displacements and angular velocities as a function of the offset distance from the joint center as shown below. The negative sign indicates that the change in angle is opposite that for the muscle elements.

$$\left(y_1 - y_1^*\right) = -b\theta \tag{40}$$

$$\dot{y} = -b\dot{\theta} \tag{41}$$

The force due to the pressure change was approximated by

$$P_d = k_p\theta \tag{42}$$

113

where P_d is the force due to the pressure change, k_p is the proportional constant on the pressure change and θ_d is the desired joint angle.

Thus, the resulting transfer function was determined to be as follows.

$$\frac{\theta}{\theta_d} = \frac{k_p b}{s^2 \left(I_{prot} + I_{dist} + I_{prox} \right) + s \left(b_{pma} b^2 \right) + \left(K_{SE} a^2 - K_{pma} b^2 \right)} \tag{43}$$

For the Auxiliary Mode for maintaining joint position, the assumptions were made that the series elastic element was stretched to full capacity and yielded no effect on the system and was considered negligible. Additionally, the developed force of the PMA as a result of the required angle is approximately linear for the narrow range over which the device will operate within this mode. For the small deviations in the joint angle, the relative motion of the elastic and resistive elements was approximated about the center of the joint to angular relative displacements.

The joint moments were summed about the elbow joint similar to the procedure for the primary mode such that

$$\Sigma M_o = -a F_J + b F_{pma} = I_{tot} \alpha \tag{44}$$

where F_J was the force exerted by the muscle, F_{pma} was the force exerted by the PMA, and I_{tot} was the total rotational inertia of the joint and the prototype. The force exerted by

the muscle could be expanded to the force due to the extension or contraction of the parallel elastic element and the resistive damping element of the muscle model given by

$$F_J = K_{PE}\left(x_1 - x_1^*\right) + b_m \dot{x}$$ (45)

where K_{PE} is the elastic stiffness of the parallel element, b_m is the resistive element damping, and x and x* are the initial and new positions of the element. For small angles, the relative change in the elastic element was approximated as the angular displacement, θ, as given by

$$\left(x_1 - x_1^*\right) = a\theta$$ (46)

where θ is the angular displacement and a is the approximate offset of the muscle from the joint. Accordingly, the rate of change in the elastic element position is given as below.

$$\dot{x} = a\dot{\theta}$$ (47)

In a similar manner, the reactive force due to the PMA was given by the expansion of its components of

$$F_{pma} = b\left[K_{pma}\left(y_1 - y_1^*\right) - b_{pma}\dot{y} + P_d\right]$$ (48)

115

Where K_{pma} is the stiffness of the PMA element, b_{pma} is the resistive damping element of the pma, P_d is the force due to the change in pressure of the PMA, b is the offset of the PMA on the brace structure, and y and y* are the initial and the stretched lengths of the PMA. In a similar manner to the series elastic element for the muscle, the small deflections of the element deflections can be resolved at the joint to angular displacements and angular velocities as a function of the offset distance from the joint center as shown below.

$$\left(y_1 - y_1^*\right) = -b\theta \tag{49}$$

$$\dot{y} = -b\dot{\theta} \tag{50}$$

Thus, the resulting transfer function was determined to be as follows.

$$\frac{\theta}{P_d} = \frac{b}{s^2\left(I_{prot} + I_{dist} + I_{prox}\right) + s\left(b_{pma}b^2 - b_m b^2\right) + \left(K_{PE}a^2 - K_{pma}b^2\right)} \tag{51}$$

The system delays for the angle tracking primary mode and the load tracking auxiliary mode were approximated using Pade (2,2) approximations given by

$$H(s) = Pade(2,2) = \frac{s^2\left(\frac{1}{12}\right)T_{dp}^2 - s\left(\frac{1}{2}\right)T_{dp} - 1}{s^2\left(\frac{1}{12}\right)T_{dp}^2 + s\left(\frac{1}{2}\right)T_{dp} - 1} \tag{52}$$

where T_{dp} is the delay in the open loop response of the displacement of the system to a change in pressure. For the position response, the delay was 0.4 seconds.

Similarly, the Pade (2,2) approximation for the force tracking mode using

$$H(s) = Pade(2,2) = \frac{s^2\left(\frac{1}{12}\right)T_{df}^2 - s\left(\frac{1}{2}\right)T_{df} - 1}{s^2\left(\frac{1}{12}\right)T_{df}^2 + s\left(\frac{1}{2}\right)T_{df} - 1} \qquad (53)$$

where T_{df} was the delay in the open loop response of the force developed by the PMA due to a step change in pressure. For the force response, the delay was 0.025 seconds. The system transfer functions for each operation mode are multiplied by the delay approximations in order to simulate the delay encountered in the system.

APPENDIX VI: PID CONTROLLER ALGORITHM

With the system transfer functions known, the system open loop roots were

established. The location for the PID zeros for prescribed overshoot, settling time, and

settling range were estimated using an algorithm to calculate the location of the controller

zeros.

From the desired overshoot percentage, the damping ratio of the desired pole for

the system operating point was determined using

$$\zeta = \sqrt{\frac{\left(\dfrac{\ln(0.01M_p)}{\pi}\right)^2}{1+\left(\dfrac{\ln(0.01M_p)}{\pi}\right)^2}} \qquad (54)$$

where ξ is the damping ratio, and M_p is the maximum prescribed overshoot percentage.

For the natural frequency of the first desired pole, the frequency is given by

$$\omega_n = \frac{\ln(0.01e_s)}{(-\zeta t_s)} \qquad (55)$$

where ω_n is the natural frequency, ξ is the damping ratio, t_s is the prescribed settling time,

and e_s is the settling range within the steady state value for the performance

characteristics.   The first zero was set beyond the range of influence of the existing poles

of the system to minimize the effects of the numerator dynamics. The phase condition is

used to estimate the location of the second point for the PID controller and that the characteristic equation of the PID controller is satisfied. The characteristic equation is given by

$$C(s) = K_A\left(1 + \frac{1}{T_I s} + T_D s\right)$$

(56)

where C(s) is the characteristic equation of the controller, T_D is the derivative gain, T_I is the integral gain, and K_A is the proportional absolute gain of the system required to approach the desired system operating pole.

APPENDIX VII: PID CONTROLLER TUNING

Orthotic Device Response to a step input
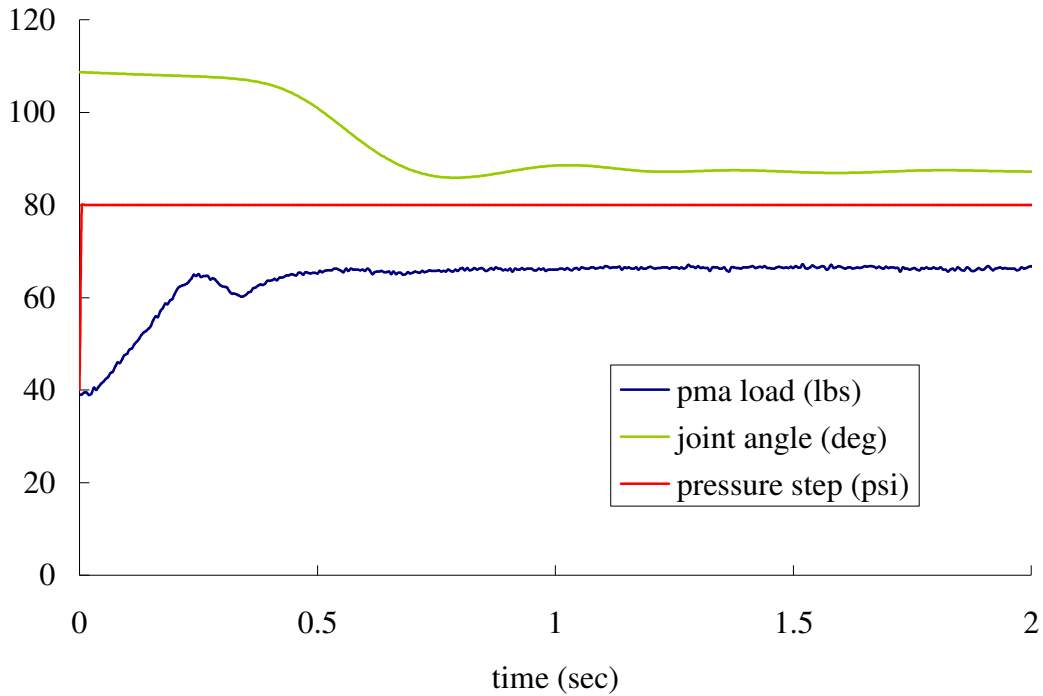
FIGURE 44 – Response of a Fitted Prototype Device to a Step Pressure Change

Using the rules outlined through Ziegler-Nichols for a Quarter Decay Ratio, the PID Proportional Gain, Integral Gain, and Derivative Gains were determined from three characteristics of the step response; the amplitude of the response time A, the lag time L and the process time constant τ.

The response rate was calculated as the slope of the rise or fall segments as shown appropriately for the force and angle changes in Figure 37 using

$$R = \frac{A}{\tau} \qquad (57)$$

where R is the rise rate, A is the amplitude of the response time, and τ is the process time constant.

The standard PID controller equations consist of the three terms. The standard form for the PID controller is shown as

$$C(s) = K_A \left(1 + \frac{1}{T_I s} + T_D s \right) \qquad (58)$$

where K_A is the proportional gain, T_I is the integral gain, and T_D is the derivative gain and all gains are given in terms of seconds.

The alternative form of the equation uses a factored form of the preceding controller form except that all gains are given in terms of minutes as shown as

$$C(s) = K_A + \frac{K_I}{s} + K_D s \qquad (59)$$

where K_A is the proportional gain, K_I is the integral gain, and K_D is the derivative gain and all gains are given in terms of minutes.

For the step response characteristics for a PID controller, the rules were developed as shown in Table VII.

TABLE VII

ZIEGLER-NICHOLS PID TUNING RULES

Gains Parameters	Gain Rule (seconds)	Gain Rule (minutes)
Proportional	$\dfrac{1.2}{RL}$	$\dfrac{1.2}{RL}$
Integral	$2 \cdot L$	$\dfrac{1}{100 \cdot R \cdot L^2}$
Derivative	$0.5 \cdot L$	$\dfrac{1}{120 \cdot R}$

APPENDIX VIII: ROTARY POTENTIOMETER CALIBRATION SEQUENCE

A two point calibration sequence is used to capture the joint angles and voltages at two distinct locations in the joint range of motion. To correlate the joint angle to the measured voltage, a scalar calibration factor relates the difference in joint angle to the difference in measured voltage through

$$\theta_1 - \theta_0 = K(V_1 - V_0) \tag{60}$$

where K is the calibration factor, V_0 and V_1 are the measured voltages at joint angles, θ_0 and θ_1.

Rearranging the relationship for the scalar calibration coefficient, a calibration factor was obtained.

$$K = \frac{(\theta_1 - \theta_0)}{(V_1 - V_0)} \tag{61}$$

In order to correlate measured voltage from the rotary potentiometer to obtain a measured angle, one distinct calibration point of angle and voltage and the calibration factor are used through a rearrangement of the calibration factor relationship as shown below.

$$\theta_m = \theta_1 - K(V_1 - V_m) \tag{62}$$

where K is the calibration factor, V_m and V_1 are the measured voltages at joint angles, θ_m and θ_1.

APPENDIX IX: ROTARY POTENTIOMETER LOW PASS FILTER

For a Low-Pass Digital Butterworth Filter, the filtered output data was obtained through

$$x'_n = a_0 x_n + a_1 x_{n-1} + a_2 x_{n-2} + b_1 x'_{n-1} + b_2 x'_{n-2} \tag{63}$$

where x'_n is the filtered data at time n, x_n is the raw data at time step n, x_{n-1} is the raw data at time step n-1, x_{n-2} is the raw data at time step n-2, and constants $a_0 - a_2$ and $b_1 - b_2$ are the weighting constants.

The first and third weighting constants, a_0 and a_2, respectively, were obtained using

$$a_0 = a_2 = \frac{\varpi_C^2}{\left(1 + \sqrt{2}\varpi_C + \varpi_C^2\right)} \tag{64}$$

where ω_c is the cutoff frequency ratio, and C is the filter order correction factor.

The second weighting factor, a_1, was obtained as twice the value of a_0.

$$a_1 = 2a_0 \tag{65}$$

The weighting factor for the previous filtered value was obtained using

$$b_1 = -\frac{2\varpi_C^2}{\left(1 + \sqrt{2}\varpi_C + \varpi_C^2\right)} + \frac{2}{\left(1 + \sqrt{2}\varpi_C + \varpi_C^2\right)} \tag{66}$$

where a_0 is the first weighting factor on the current raw data value, and ω_c is the cutoff frequency ratio for the filter.

Where the constants $a_0 - a_2$ and $b_1 - b_2$ are weighting factors, the weighting factor for the filtered value from two steps previous, b_2, was given as found below.

$$b_2 = 1 - a_0 - a_1 - a_2 - b_1 \tag{67}$$

The cutoff frequency ratio, ω_c, was determined using

$$\omega_C = \frac{\tan\left(\pi \dfrac{f_C}{f_S}\right)}{C} \tag{68}$$

where f_c is the cutoff frequency selected, f_s is the sample frequency for the raw data, and C is the correction factor for the filter order. For a second order filter, C is equal to 2.

126

APPENDIX X: TEST DATA

The data set that was used to evaluate the functionality of the device is shown

below in Figure 45.
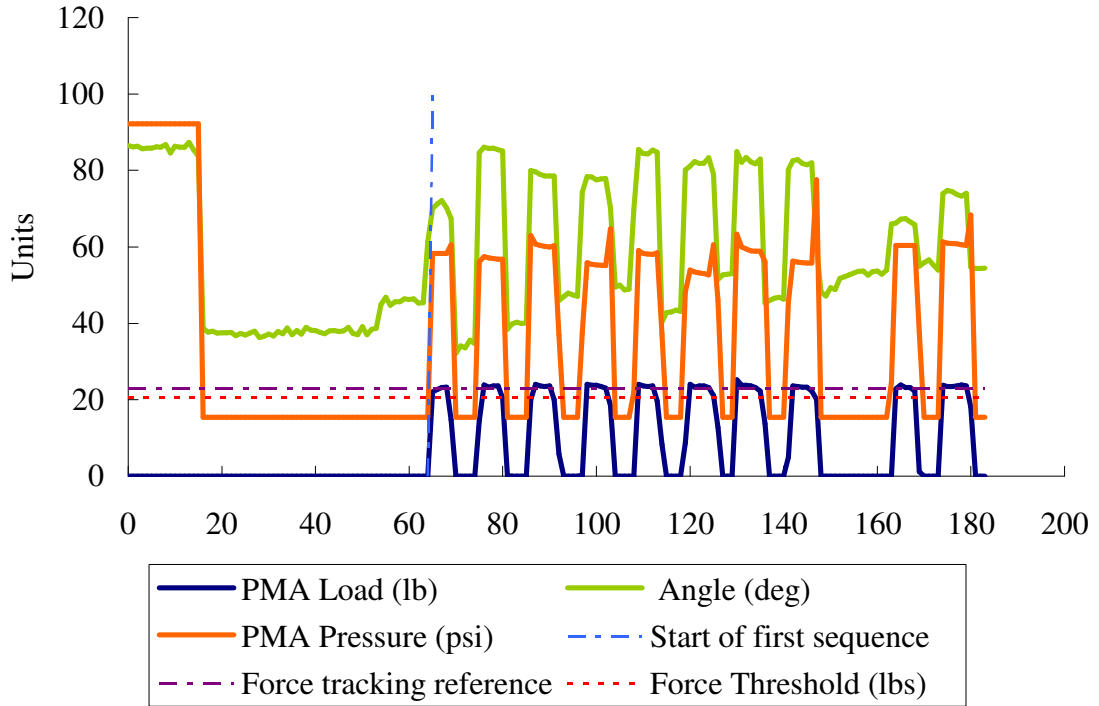
FIGURE 45 – Sample Data Set of Device Performance

To determine the locations of the joint collapsing, the discrete time derivative of

the joint angle was calculated using

$$\dot{\theta} = \frac{\theta_{i+1} - \theta_{i-1}}{2\Delta t} \tag{69}$$

where $\dot{\theta}$ is the discrete time derivative, θ_{i+1} and θ_{i-1} are the joint angles at the time intervals immediately following and preceding, respectively, the sample i, and Δt is the discrete time interval between samples.

For identifying the values of the force trace while the device was operating in the force tracking mode, a Boolean operator was used to select only the samples that exceeded the 20 lb force cross-over threshold force level. Beyond this load, the device should permit the joint to collapse and the edges of these sample subsets should align with the high values for the joint angular velocity. Thus a load trace was created to identify the locations where the force was in excess where

$$P_d < 20 \tag{70}$$

where P_d is the developed PMA load in lbs. The load trace and the absolute value of the angular velocity were used to create the device crossover detection illustrated in Figure 46 below and Figure 30 in the Design Evaluation.
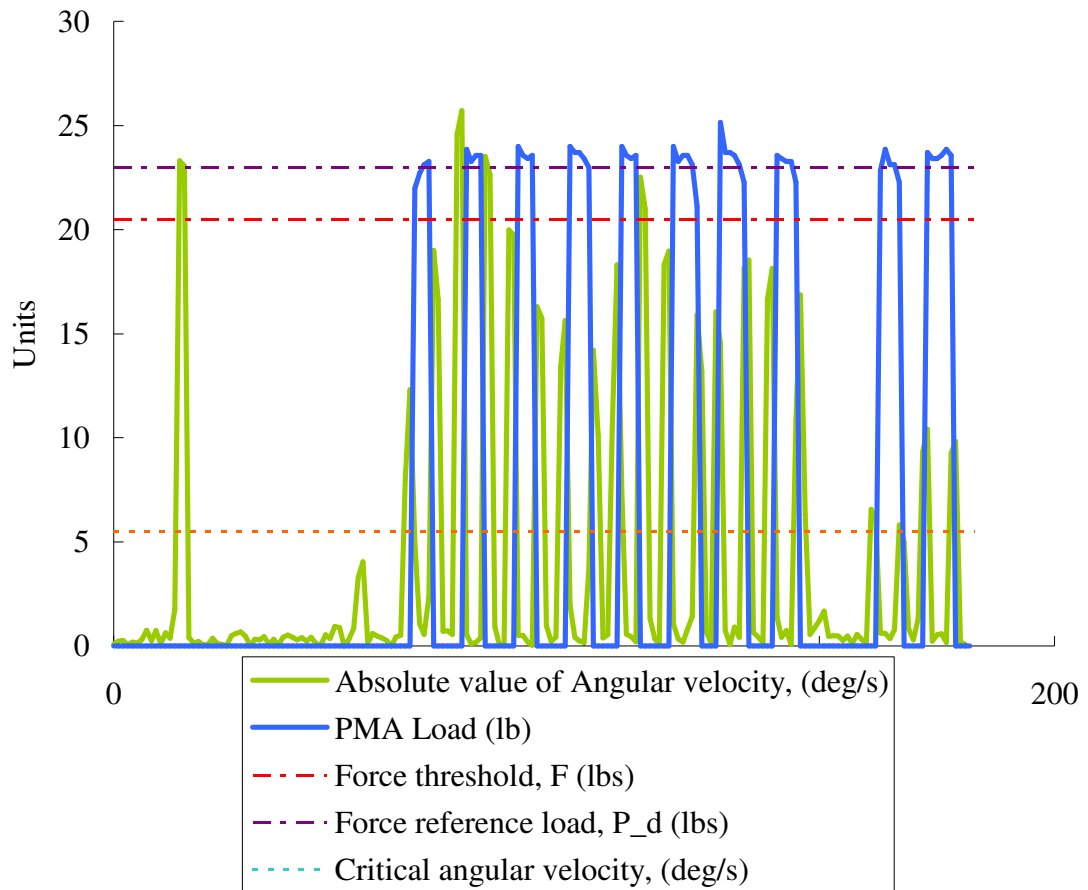
Figure 46 – Load Detecting and Rejecting Data Trace

To evaluate the deviation of the tracking of the joint position, the percent error was calculated with respect to the desired joint position and was calculated using

$$E_p = 100 \cdot \frac{\theta_i - \theta_d}{\theta_d} \tag{71}$$

where E_p is the percent error of the joint position, θ_i is the current joint angle, and θ_d is the desired joint angle.

Additionally, a 98% confidence interval was calculated for the ability of the controller to maintain the joint position. With a sample size of more than 30 seconds, sampled at each second, the sample was evaluated as a normally distributed population. The confidence interval was calculated for where 1% of all samples would fall beyond the interval and was calculated using a z-value of 2.3 corresponding to a proportion of the cumulative distribution exceeding the value of 0.01. The confidence intervals were created using

$$98\% \ CI = \theta_d \pm n\sigma \qquad (72)$$

where θ_d is the desired mean joint position, n is the z-value for the corresponding interval, and σ_p was the standard deviation of the samples for the joint position data.

Similar to the joint position tracking, the same procedure was used to calculate the percentage error and 98% CI for the developed joint load, P_d.

The test data for the curve used within the design evaluation is listed in Table VII below.

TABLE VIII

TEST DATA

Sample Time	PMA Load (lb)	Joint Angle (deg)	PMA Pressure (psi)
Wednesday, January 10, 2007 10:50 AM	0	86.52679	92.25
Wednesday, January 10, 2007 10:50 AM	0	86.17685	92.25
Wednesday, January 10, 2007 10:50 AM	0	86.35759	92.25
Wednesday, January 10, 2007 10:50 AM	0	85.71233	92.25
Wednesday, January 10, 2007 10:50 AM	0	85.84265	92.25
Wednesday, January 10, 2007 10:50 AM	0	85.84431	92.25
Wednesday, January 10, 2007 10:51 AM	0	86.21393	92.25
Wednesday, January 10, 2007 10:51 AM	0	86.13199	92.25
Wednesday, January 10, 2007 10:51 AM	0	86.83291	92.25
Wednesday, January 10, 2007 10:51 AM	0	84.61626	92.25
Wednesday, January 10, 2007 10:51 AM	0	86.35033	92.25
Wednesday, January 10, 2007 10:51 AM	0	86.10387	92.25
Wednesday, January 10, 2007 10:51 AM	0	86.14425	92.25
Wednesday, January 10, 2007 10:51 AM	0	87.37129	92.25
Wednesday, January 10, 2007 10:51 AM	0	85.39443	92.25
Wednesday, January 10, 2007 10:51 AM	0	83.83147	92.25
Wednesday, January 10, 2007 10:51 AM	0	38.76357	15.375
Wednesday, January 10, 2007 10:51 AM	0	37.71365	15.375
Wednesday, January 10, 2007 10:51 AM	0	37.97852	15.375
Wednesday, January 10, 2007 10:51 AM	0	37.44115	15.375
Wednesday, January 10, 2007 10:51 AM	0	37.54988	15.375
Wednesday, January 10, 2007 10:51 AM	0	37.5532	15.375
Wednesday, January 10, 2007 10:51 AM	0	37.66669	15.375
Wednesday, January 10, 2007 10:51 AM	0	36.81756	15.375
Wednesday, January 10, 2007 10:51 AM	0	37.416	15.375
Wednesday, January 10, 2007 10:51 AM	0	36.98596	15.375
Wednesday, January 10, 2007 10:51 AM	0	37.47217	15.375
Wednesday, January 10, 2007 10:51 AM	0	37.96502	15.375
Wednesday, January 10, 2007 10:51 AM	0	36.27636	15.375
Wednesday, January 10, 2007 10:51 AM	0	36.61326	15.375
Wednesday, January 10, 2007 10:51 AM	0	37.21229	15.375
Wednesday, January 10, 2007 10:51 AM	0	36.67937	15.375
Wednesday, January 10, 2007 10:51 AM	0	37.87071	15.375
Wednesday, January 10, 2007 10:51 AM	0	37.26148	15.375
Wednesday, January 10, 2007 10:51 AM	0	38.77026	15.375
Wednesday, January 10, 2007 10:51 AM	0	37.08509	15.375

131

Wednesday, January 10, 2007 10:51 AM	0	38.11403	15.375
Wednesday, January 10, 2007 10:51 AM	0	37.18938	15.375
Wednesday, January 10, 2007 10:51 AM	0	38.94918	15.375
Wednesday, January 10, 2007 10:51 AM	0	38.22562	15.375
Wednesday, January 10, 2007 10:51 AM	0	38.12172	15.375
Wednesday, January 10, 2007 10:51 AM	0	37.63511	15.375
Wednesday, January 10, 2007 10:51 AM	0	37.30905	15.375
Wednesday, January 10, 2007 10:51 AM	0	38.08556	15.375
Wednesday, January 10, 2007 10:51 AM	0	38.13194	15.375
Wednesday, January 10, 2007 10:51 AM	0	37.84696	15.375
Wednesday, January 10, 2007 10:51 AM	0	38.07725	15.375
Wednesday, January 10, 2007 10:51 AM	0	38.93637	15.375
Wednesday, January 10, 2007 10:51 AM	0	37.36382	15.375
Wednesday, January 10, 2007 10:51 AM	0	37.07165	15.375
Wednesday, January 10, 2007 10:51 AM	0	39.10971	15.375
Wednesday, January 10, 2007 10:51 AM	0	37.08035	15.375
Wednesday, January 10, 2007 10:51 AM	0	38.45322	15.375
Wednesday, January 10, 2007 10:51 AM	0	38.75713	15.375
Wednesday, January 10, 2007 10:51 AM	0	45.01163	15.375
Wednesday, January 10, 2007 10:51 AM	0	46.82037	15.375
Wednesday, January 10, 2007 10:51 AM	0	44.7226	15.375
Wednesday, January 10, 2007 10:51 AM	0	45.62322	15.375
Wednesday, January 10, 2007 10:51 AM	0	45.68608	15.375
Wednesday, January 10, 2007 10:51 AM	0	46.39562	15.375
Wednesday, January 10, 2007 10:51 AM	0	46.22281	15.375
Wednesday, January 10, 2007 10:51 AM	0	46.38498	15.375
Wednesday, January 10, 2007 10:51 AM	0	45.36015	15.375
Wednesday, January 10, 2007 10:51 AM	0	45.36993	15.375
Wednesday, January 10, 2007 10:51 AM	0	61.30266	15.375
Wednesday, January 10, 2007 10:52 AM	21.97506	69.99747	58.26915
Wednesday, January 10, 2007 10:52 AM	22.69792	71.26479	58.30636
Wednesday, January 10, 2007 10:52 AM	23.13164	72.12338	58.30636
Wednesday, January 10, 2007 10:52 AM	23.27621	70.16944	58.29958
Wednesday, January 10, 2007 10:52 AM	14.74642	67.39926	60.50558
Wednesday, January 10, 2007 10:52 AM	0	32.16839	15.375
Wednesday, January 10, 2007 10:52 AM	0	34.1386	15.375
Wednesday, January 10, 2007 10:52 AM	0	33.57931	15.375
Wednesday, January 10, 2007 10:52 AM	0	35.58613	15.375
Wednesday, January 10, 2007 10:52 AM	0	34.69929	15.375
Wednesday, January 10, 2007 10:52 AM	14.45728	84.73831	56.12753
Wednesday, January 10, 2007 10:52 AM	23.8545	86.14148	57.42022
Wednesday, January 10, 2007 10:52 AM	23.27621	85.79953	57.08196
Wednesday, January 10, 2007 10:52 AM	23.56536	85.91442	56.94057
Wednesday, January 10, 2007 10:52 AM	23.56536	85.46256	56.77999
Wednesday, January 10, 2007 10:52 AM	20.38476	85.11923	56.77517

Wednesday, January 10, 2007 10:52 AM	0.144573	38.42852	15.375
Wednesday, January 10, 2007 10:52 AM	0	39.85211	15.375
Wednesday, January 10, 2007 10:52 AM	0	40.2753	15.375
Wednesday, January 10, 2007 10:52 AM	0	39.97071	15.375
Wednesday, January 10, 2007 10:52 AM	0	40.11063	15.375
Wednesday, January 10, 2007 10:52 AM	20.09561	79.93026	62.98374
Wednesday, January 10, 2007 10:52 AM	23.99908	79.56834	60.71925
Wednesday, January 10, 2007 10:52 AM	23.56536	78.93253	60.36305
Wednesday, January 10, 2007 10:52 AM	23.42079	78.54025	60.09507
Wednesday, January 10, 2007 10:52 AM	23.56536	78.56013	59.93439
Wednesday, January 10, 2007 10:52 AM	19.95104	78.48426	60.30211
Wednesday, January 10, 2007 10:52 AM	5.78291	45.95923	36.9058
Wednesday, January 10, 2007 10:52 AM	0	46.99237	15.375
Wednesday, January 10, 2007 10:52 AM	0	47.9379	15.375
Wednesday, January 10, 2007 10:52 AM	0	47.43187	15.375
Wednesday, January 10, 2007 10:52 AM	0	47.08244	15.375
Wednesday, January 10, 2007 10:52 AM	0.289146	74.31771	37.67327
Wednesday, January 10, 2007 10:52 AM	23.99908	78.36139	55.8946
Wednesday, January 10, 2007 10:52 AM	23.70993	78.23643	55.42736
Wednesday, January 10, 2007 10:52 AM	23.70993	77.53811	55.24644
Wednesday, January 10, 2007 10:52 AM	23.42079	77.73881	55.18315
Wednesday, January 10, 2007 10:52 AM	22.98707	77.88354	55.12434
Wednesday, January 10, 2007 10:52 AM	18.50531	70.18743	64.69112
Wednesday, January 10, 2007 10:52 AM	0	49.47572	15.375
Wednesday, January 10, 2007 10:52 AM	0	50.00099	15.375
Wednesday, January 10, 2007 10:52 AM	0	48.71354	15.375
Wednesday, January 10, 2007 10:52 AM	0	48.92275	15.375
Wednesday, January 10, 2007 10:52 AM	0	69.74788	21.9168
Wednesday, January 10, 2007 10:52 AM	23.99908	85.54924	59.0093
Wednesday, January 10, 2007 10:52 AM	23.56536	84.49557	58.25208
Wednesday, January 10, 2007 10:52 AM	23.42079	84.40471	58.13227
Wednesday, January 10, 2007 10:52 AM	23.56536	85.37954	58.06439
Wednesday, January 10, 2007 10:52 AM	19.6619	84.79901	58.42373
Wednesday, January 10, 2007 10:52 AM	8.240647	40.36213	37.15949
Wednesday, January 10, 2007 10:52 AM	0	42.81317	15.375
Wednesday, January 10, 2007 10:52 AM	0	42.98978	15.375
Wednesday, January 10, 2007 10:52 AM	0	43.50057	15.375
Wednesday, January 10, 2007 10:52 AM	0	43.15964	15.375
Wednesday, January 10, 2007 10:52 AM	8.674365	80.14866	48.28341
Wednesday, January 10, 2007 10:52 AM	23.99908	81.09648	53.91903
Wednesday, January 10, 2007 10:52 AM	23.27621	82.25617	53.4057
Wednesday, January 10, 2007 10:52 AM	23.56536	81.76015	53.14668
Wednesday, January 10, 2007 10:52 AM	23.56536	81.8958	53.0031
Wednesday, January 10, 2007 10:52 AM	23.13164	83.34672	52.68747
Wednesday, January 10, 2007 10:53 AM	21.10762	79.05702	60.5788

Wednesday, January 10, 2007 10:53 AM	12.7224	51.51418	45.99226
Wednesday, January 10, 2007 10:53 AM	0	52.71443	15.375
Wednesday, January 10, 2007 10:53 AM	0	52.83068	15.375
Wednesday, January 10, 2007 10:53 AM	0	52.98274	15.375
Wednesday, January 10, 2007 10:53 AM	25.15566	84.92877	63.29092
Wednesday, January 10, 2007 10:53 AM	23.70993	82.10474	59.97197
Wednesday, January 10, 2007 10:53 AM	23.70993	83.46912	59.43342
Wednesday, January 10, 2007 10:53 AM	23.56536	82.23668	58.96857
Wednesday, January 10, 2007 10:53 AM	23.13164	81.6676	58.87358
Wednesday, January 10, 2007 10:53 AM	22.2642	83.07717	58.83854
Wednesday, January 10, 2007 10:53 AM	13.73441	45.31661	56.07119
Wednesday, January 10, 2007 10:53 AM	0	46.00549	15.375
Wednesday, January 10, 2007 10:53 AM	0	46.61793	15.375
Wednesday, January 10, 2007 10:53 AM	0	46.86709	15.375
Wednesday, January 10, 2007 10:53 AM	0	46.32408	15.375
Wednesday, January 10, 2007 10:53 AM	4.915474	80.16225	45.54443
Wednesday, January 10, 2007 10:53 AM	23.56536	82.60915	56.24789
Wednesday, January 10, 2007 10:53 AM	23.42079	82.89091	56.00473
Wednesday, January 10, 2007 10:53 AM	23.27621	81.76563	55.85541
Wednesday, January 10, 2007 10:53 AM	23.27621	81.41064	55.80452
Wednesday, January 10, 2007 10:53 AM	22.2642	81.92516	55.81151
Wednesday, January 10, 2007 10:53 AM	20.09561	59.78004	77.49496
Wednesday, January 10, 2007 10:53 AM	0	48.20908	15.375
Wednesday, January 10, 2007 10:53 AM	0	47.15598	15.375
Wednesday, January 10, 2007 10:53 AM	0	49.31712	15.375
Wednesday, January 10, 2007 10:53 AM	0	48.87478	15.375
Wednesday, January 10, 2007 10:53 AM	0	51.74013	15.375
Wednesday, January 10, 2007 10:53 AM	0	52.20956	15.375
Wednesday, January 10, 2007 10:53 AM	0	52.65209	15.375
Wednesday, January 10, 2007 10:53 AM	0	53.18605	15.375
Wednesday, January 10, 2007 10:53 AM	0	53.59093	15.375
Wednesday, January 10, 2007 10:53 AM	0	53.70116	15.375
Wednesday, January 10, 2007 10:53 AM	0	52.62739	15.375
Wednesday, January 10, 2007 10:53 AM	0	53.4981	15.375
Wednesday, January 10, 2007 10:53 AM	0	53.7247	15.375
Wednesday, January 10, 2007 10:53 AM	0	52.86643	15.375
Wednesday, January 10, 2007 10:53 AM	0	53.97764	15.375
Wednesday, January 10, 2007 10:53 AM	0	66.002	24.49027
Wednesday, January 10, 2007 10:53 AM	22.8425	66.20264	60.36255
Wednesday, January 10, 2007 10:53 AM	23.8545	67.24493	60.35577
Wednesday, January 10, 2007 10:53 AM	23.13164	67.39841	60.34785
Wednesday, January 10, 2007 10:53 AM	23.13164	66.54676	60.34785
Wednesday, January 10, 2007 10:53 AM	22.2642	65.8367	60.36202
Wednesday, January 10, 2007 10:53 AM	1.156582	54.91402	37.79129
Wednesday, January 10, 2007 10:53 AM	0	55.86117	15.375

Wednesday, January 10, 2007 10:53 AM	0	56.57333	15.375
Wednesday, January 10, 2007 10:53 AM	0	55.28187	15.375
Wednesday, January 10, 2007 10:53 AM	0	53.92289	15.375
Wednesday, January 10, 2007 10:53 AM	23.70993	73.94947	61.30622
Wednesday, January 10, 2007 10:53 AM	23.42079	74.7337	60.98954
Wednesday, January 10, 2007 10:53 AM	23.42079	74.41729	60.88433
Wednesday, January 10, 2007 10:53 AM	23.56536	73.64983	60.76452
Wednesday, January 10, 2007 10:53 AM	23.8545	73.25556	60.57902
Wednesday, January 10, 2007 10:53 AM	23.56536	73.97606	60.40603
Wednesday, January 10, 2007 10:53 AM	18.07159	54.7103	68.29389
Wednesday, January 10, 2007 10:53 AM	0	54.32053	15.375
Wednesday, January 10, 2007 10:53 AM	0	54.31761	15.375
Wednesday, January 10, 2007 10:53 AM	0	54.4749	15.375

APPENDIX XI: CONTROL METHOD SCHEMATIC

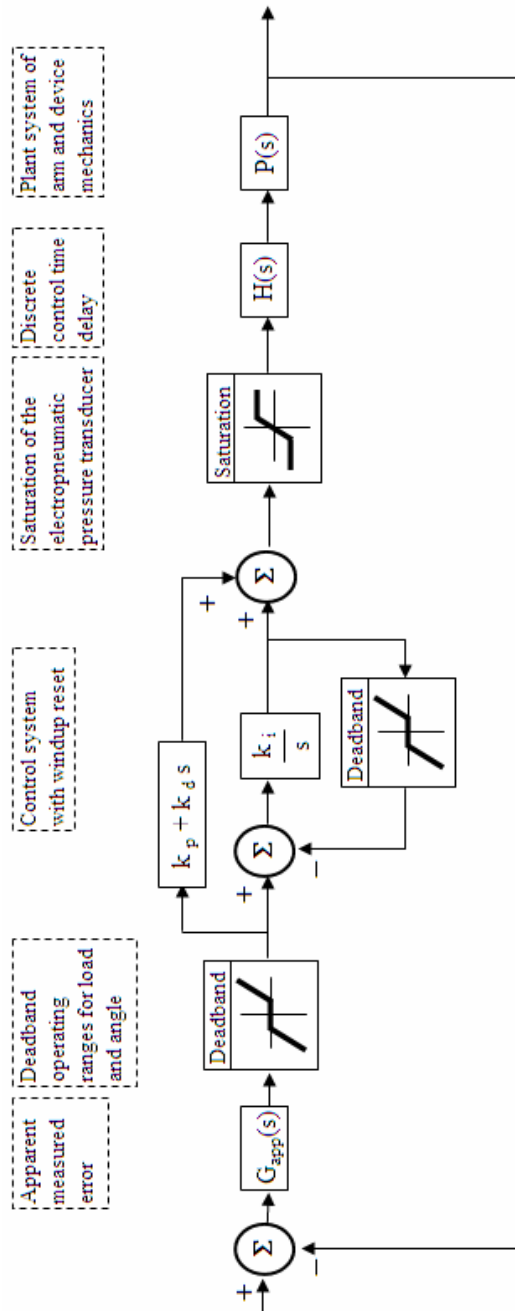A schematic of the control method including the anti-windup and dead-band systems are shown below in Figure 47.

FIGURE 47 – Control Method Schematic